The Structures and Properties of Pr/Nd-Fe-B-(Cu) Permanent Magnets and Alloys

Rubens N. Faria Jr.

A Thesis Submitted for the Degree of

Doctor of Philosophy

School of Metallurgy and Materials
Faculty of Engineering
University of Birmingham

April, 1993

ACKNOWLEDGEMENTS

The author would like to thank his supervisors Prof. I. R. Harris and Dr.J. S. Abell for their enthusiastic support, encouragement and guidance. The author is also grateful to Mr.N. Smith for his indispensable technical assistance, and members of the Applied Alloy Chemistry Group for their help with many areas of the research.

Many thanks are due to the Brazilian Government, in particular to the **CNPq** (Conselho Nacional de Desenvolvimento Científico e Tecnológico) and **CNEN** (Comissão Nacional de Energia Nuclear) for the provision of a research scholarship for the author. Thanks are due to the **SERC, EURAM** and **CEAM** (Concerted European Action on Magnets) for the support of the general research programme of which this work forms a part. Thanks are also due to **REP** (Rare Earth Products) for the provision of the alloys.

Thanks are also extended to other members of the School who have provided technical assistance and advice.

Finally, the author would like to express his gratitude and love to Marcia and his parents for their immense devotion and support.

SYNOPSIS

An investigation into the effect of directional solidification under controlled conditions on a range of Pr/Nd-Fe-B-(Cu) alloys has been undertaken. Cast permanent magnets have been prepared using alloys directionally solidified in moulds with different cooling rates. Heat treatment has subsequently been applied to the bulk alloys as a means of enhancing the magnetic properties.

Rods of cast alloys have also been directionally solidified under controlled conditions for diverse values of the temperature gradient/growth rate ratio G/R using a vertical floating zone (VFZ) technique. The effects of directional solidification processing on the microstructural and magnetic properties have been studied as a direct means of producing grain-aligned rods with enhanced hard magnetic properties.

Finally, successful attempts have been made to produce high quality sintered Pr-Fe-B-Cu permanent magnets using the hydrogen decrepitation (HD) process. Studies of post sintering heat treatment have been carried out on the HD sintered magnets prepared from the as-cast alloy and zoned materials.

Cast ingots, VFZ material and HD sintered magnets have been characterised by magnetic measurements and by optical and scanning electron microscopy. The former includes ferrofluid and Kerr-effect observations of the magnetic domains and the latter includes chemical analysis using EDX and WDX.

CONTENTS

CHAPTER ONE

INTRODUCTION

1.1 Brief Historical Introduction

Magnetic materials have a very ancient history. The earliest records were written in China around 2000 B.C. relating to magnetite, a naturally occurring magnetic rock (iron oxide). The word magnetism is derived from the word magnetite and it is believed that the origin of the word magnetite is because it was found at a place called Magnesia. The first practical use of magnetite, also known as lodestone, was the compass for navigation.

The first systematic experiments on magnetism were performed by William Gilbert, in about 1600 A.D. In his celebrated book, *De Magnete* , he described the properties of attraction and repulsion and loss of magnetic properties on heating magnetic materials, and also recognizing that the earth itself is a huge magnet. The scientific study of magnetism, which began with Gilbert, languished until the rapid succession of discoveries in the 19th century, starting with Oersted's observation of the magnetic field associated with an electric current in 1820. The development of permanent magnetic materials only began in the early 20th century when various magnetic steels replaced lodestone. The principal figure of merit for a magnet is expressed as the maximum energy product and for steels this is about 2.5 MGOe.

In the 1940's, steels were replaced by alloys of aluminium, nickel, cobalt and iron, called Alnico magnets, with a maximum

energy product of 5 MGOe. Twenty years later the maximum energy product of Alnicos had been improved to 10 MGOe (Ticonal magnets). These were also replaced by barium and strontium ferrite (about 5 MGOe) because the raw materials are much cheaper.

In the second half of the 1960's rare earth (RE) transition metal (TM) magnets were developed. Permanent magnets of $SmCo_5$, with a maximum energy product of about 20 MGOe, were the first generation, followed by 2/17-type magnets a decade later. The maximum energy product of these magnets was around 33 MGOe.

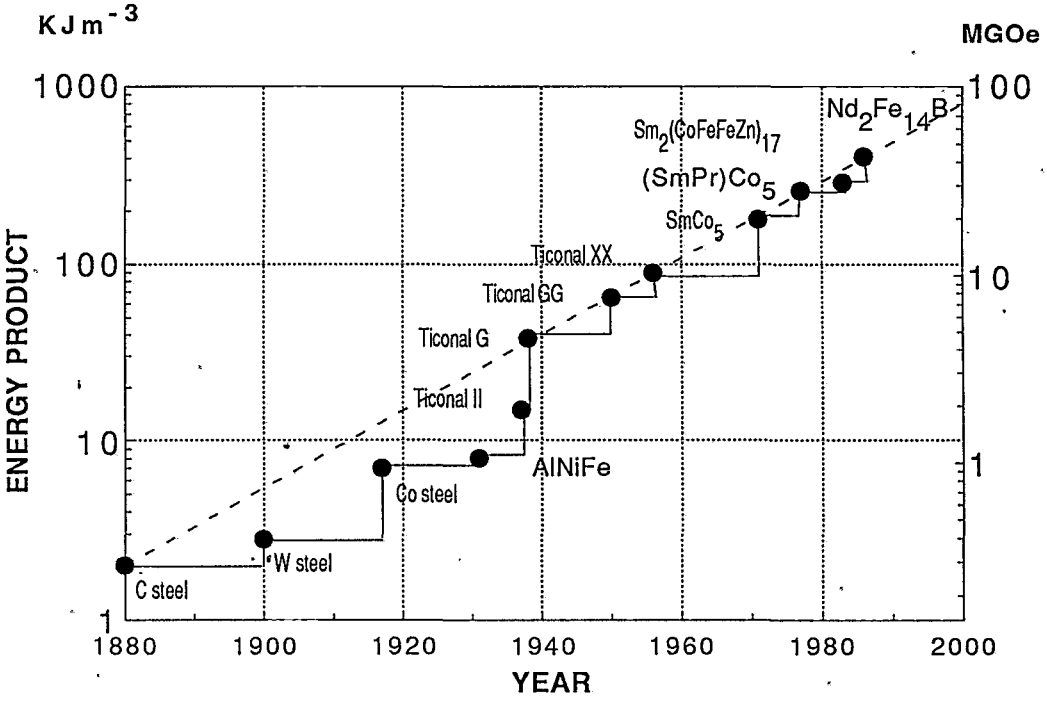

Fig.1.1.1 Historical trend of the maximum energy product.

In 1983 a new magnetic material based on the NdFeB alloy system was announced in Japan. Using a powder metallurgy route magnets were produced with a maximum energy product of 36 to 50 MGOe. Although these magnets have low Curie temperature (312°C), they are gradually replacing the Sm-Co magnets. To

illustrate the improvement in magnetic materials, the maximum energy product of various permanent magnets is shown in fig. 1.1.1.

1.2 Introduction to Present Work

Since the discovery of NdFeB permanent magnets there has been a considerable amount of research undertaken in an attempt to understand their magnetic properties, with a view to improving them. Recently great interest has arisen in PrFeB magnets due to the absence of a spin reorientation at lower temperatures when compared with NdFeB magnets and hence better magnetic characteristics at low temperatures. The addition of elements such as Cu, Ag or Pd has led to PrFeB alloys with good magnetic properties in the form of hot-pressed and cast magnets.

This thesis describes work carried out on PrFeB alloys with and without Cu substitution. When possible the investigations were extended to Nd-based magnets. The objective of the present work was to investigate the PrFeB alloys and magnets and to improve their magnetic properties. A further objective was to relate the final magnetic properties of the cast and the sintered magnets (via hydrogen decrepitation) with the initial state of the alloys.

Directional solidification using a vertical floating zone technique has been applied to the as-cast ingots as a controlled means of modifying the alloy microstructure. At the same time investigations of the cooling parameters of mould casting have also been carried out. The effect of composition, solidification behaviour and heat treatments on the magnetic properties has been investigated. Finally, an attempt to relate microstructure and magnetic properties has also been carried out.

CHAPTER TWO

MAGNETISM AND MAGNETIC MATERIALS

2.1 Magnetic Units

The study of magnetism is bedevilled by the existence of two different systems of units both currently in use, the S.I. and c.g.s. systems. The c.g.s. system of units has been generally accepted for over fifty years and is still very widely used because of the numerical equality between flux density, **B**, and magnetising field, **H**. This is not so for the S.I. system, however, there has been a movement to change to this system because of its wider use in engineering and technical areas. The results reported in this thesis are presented in the c.g.s. system since most of the publications on cast magnets are in this system, thus a comparison will be facilitated. Table 2.1.1 gives a summary of unit conversions.

Table 2.1.1 Units conversions

QUANTITY	S.I to C.G.S.
ϕ	1 Weber = 10^8 Maxwells
B	1 Tesla = 10^4 Gauss
H	1 KAm^{-1} = 12.57 Oersted
$\mu_0 H$	1 Tesla = 10^4 Oersted
(BH)max	1 KJm^{-3} = 0.1257 MGOe

2.2 Magnetic Quantities

The definitions of magnetic quantities and the general theory of magnetism and magnetic materials can be found in most texts on the subject, such as Bozorth (1959), Parker and Studders (1962), Cullity (1972), McCaig (1977), Zijlstra (1982) and Jiles (1991),

therefore only a brief summary will be included here.

The Sommerfeld system (SI) says that when a magnetic field, **H**, is applied to a material it may be considered to give rise to a magnetic induction, **B**, which is related to **H** by

$$\mathbf{B} = \mu_0 \ (\mathbf{H} + \mathbf{M}) \qquad 2.2.1.$$

M (or **I**) is the magnetization or the magnetic moment per unit volume of the material. **B**, **H**, and **M** are all vector quantities; μ_0 is the permeability of a vacuum, $4\ \pi \times 10^{-7}$ Hm^{-1}, though it is better to call it the magnetic constant. In the Kennelly system (SI), equation 2.2.1 may be written in terms of the magnetic polarization, **J** ($=\mu_0\mathbf{M}$):

$$\mathbf{B} = \mu_0\mathbf{H} + \mathbf{J} \qquad 2.2.2.$$

J is in tesla. Since **J** and **M** are the same quantity apart from the magnetic constant, the magnetization is equivalent to the magnetic polarization. In the c.g.s.- e.m.u. system, equations 2.2.1 and 2 are written as :

$$\mathbf{B} = \mathbf{H} + 4\pi\mathbf{M} \qquad 2.2.3$$

so that, in a vacuum, B and H are numerically equal, but in different units of gauss (G) and oersteds (Oe) respectively. The c.g.s. unit of magnetization is the gauss, but a factor of 4π is needed to convert this to magnetic induction, as shown by equation 2.2.3.

Using only magnitudes, dividing 2.2.1 by **H** gives: $\mathbf{B/H}=\mu_0(1+\mathbf{M/H})$ which can be written as:

$$\mu = \mu_0 \ (1 + \chi) = \mu_0 \ \mu_r \qquad 2.2.4$$

where μ is the magnetic permeability of the material, χ is its

magnetic susceptibility and μ_r is its relative permeability. In the c.g.s. system $\mu_0=1$ and $\mu=\mu_r$. The susceptibility is dimensionless in the S.I. system. The permeability of a material is not a constant, except under specific conditions of measurements. B is also referred to as the magnetic flux density, ϕ / A, where ϕ is the magnetic flux and A is the area normal to the flux.

2.3 Hysteresis

The most common manner to represent the behaviour of magnetic materials is by plotting **B** or **M** against **H** as illustrated in Fig.2.3.1. The effects of applied fields on a material are fundamental to the study of magnetism and magnetisation curves are a clear representation of the characteristics of these materials.

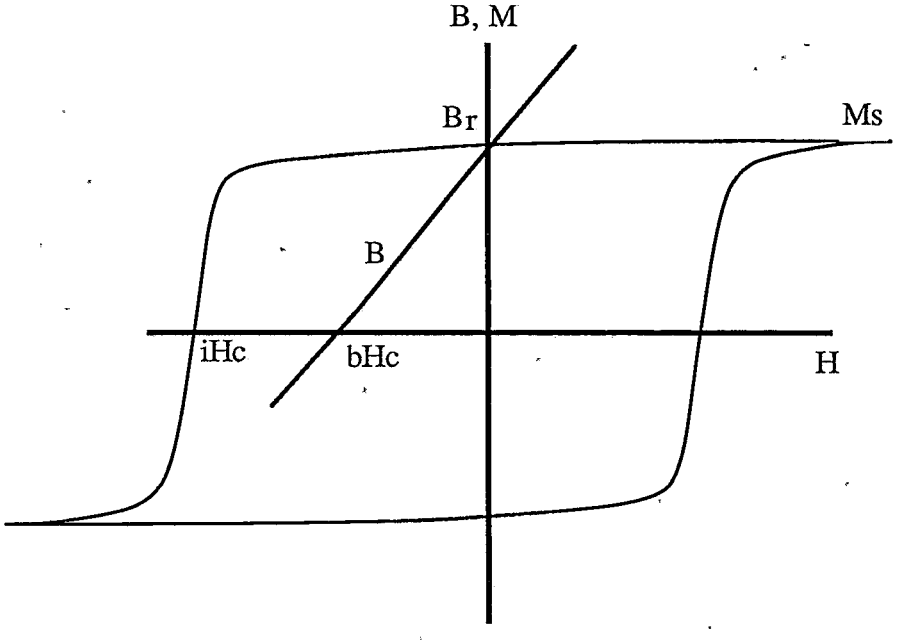

Fig.2.3.1 Typical hysteresis loop for a hard ferromagnetic material.

At sufficiently large values of **H**, the magnetisation in a specimen reaches its maximum value where a further increase in **H** no longer causes any increase in **M**. Magnetically soft materials require only small fields to reach saturation ($\mathbf{M}_s$), whereas magnetically hard materials may require very large fields. The shape of the magnetisation curve can also provide a great deal of information on the intrinsic characteristics of the material.

On removing an applied magnetic field **H** the material may retain some remanent magnetism. Such materials can be made into permanent magnets. Reducing the applied field to zero from saturation causes the flux density to drop to the remanence, $\mathbf{B}_r$. Reversing the field between the same positive and negative limits a symmetrical loop is traced out (see Fig.2.3.1). The negative applied field where the magnetization falls to zero is called the intrinsic coercivity ${}_i\mathbf{H}_c$. If **B** is plotted against **H**, then the field required to reduce the flux density to zero is the inductive coercivity ${}_b\mathbf{H}_c$. In the second quadrant the point where the product of **B** and **H** assumes a maximum value is called the maximum energy product, $(\mathbf{BH})_{max}$.

2.4 Types of Magnetic Order

All substances can be classified magnetically, according to their response to an applied magnetic field, in terms of the strength and direction of the magnetization of the material. Thus materials can be classified into five groups, diamagnetic, paramagnetic, ferromagnetic, ferrimagnetic and antiferromagnetic.

The magnetic moment of any atom is composed of three parts:

the intrinsic spin of the electrons; their orbital angular momentum about the nucleus; and the change in the orbital moment induced by any applied magnetic field. The first two effects are responsible for a paramagnetic contribution while the third gives a diamagnetic contribution. The materials in which the individual magnetic moments of the atoms in a lattice are ordered belong to the other three classes: ferromagnetic, ferrimagnetic and antiferromagnetic. One of the most important criteria by which they can be distinguished from each other is the magnetic susceptibility, χ,

$$\chi = \mathbf{M} / \mathbf{H} \qquad 2.4.1.$$

Diamagnetic materials develop a small magnetisation only in the presence of an applied field and the individual magnetic moments align such as to oppose this field. Thus they have negative susceptibilities in the order of 10^{-6} to 10^{-5}. Almost all materials exhibit some diamagnetism but this can be masked by other, stronger effects.

Paramagnetic materials have positive susceptibilities and several orders of magnitude greater than in diamagnetic materials (10^{-5} to 10^{-3}). The magnetization is due to the energetically favourable orientation of electron spin or orbital moments parallel to the applied field. Thermal energy tends to disrupt this alignment and so the susceptibility decreases with increasing temperature. In general paramagnetic susceptibilities follow a modified form of the Curie law (χ=Curie constant/Temperature) known as the Curie-Weiss law :

$$\chi = C / (T - \theta) \qquad 2.4.2$$

where C is the Curie constant and θ is a constant, dimensionally

equivalent to temperature.

Ferromagnetic materials do not require an external magnetic field in order to possess a magnetic moment. Such materials include Fe, Ni and Co as well as alloys containing some or none of these elements. They have a spontaneous magnetism in the absence of an applied field, arising from a parallel alignment of existing atomic moments. When a magnetic field is applied to these materials the spontaneous magnetisation, $\mathbf{M}_s$, is forced to point in the same direction as the applied field, resulting in a large positive susceptibility. Thermal energy also tends to disrupt the parallel alignment causing a decrease in the magnetisation with increasing temperature. This is shown in Fig. 2.4.1. The temperature at which the spontaneous magnetism is reduced to zero is known as the Curie temperature and above this temperature the material becomes paramagnetic.

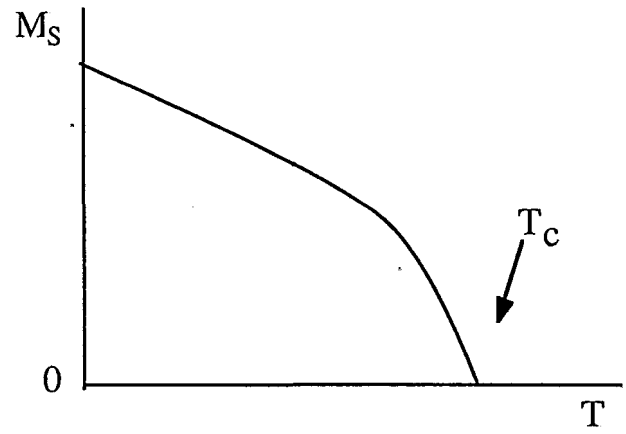

Fig. 2.4.1 Variation of $\mathbf{M}_s$ with T for a ferromagnetic material.

Antiferromagnetism is a magnetic state related to ferromagnetism where antiparallel alignment of atomic moments results in no net spontaneous magnetisation. These materials have a

small positive susceptibility similar in magnitude to paramagnetic materials. Their magnetic behaviour is similar to ferromagnetic materials in that above a critical temperature, the Néel point, the material becomes paramagnetic. In this region the susceptibility varies accordingly to equation 2.4.2, except that θ is negative.

The distance between neighbouring atoms must satisfy the requirements for ferromagnetism or antiferromagnetism. If the distance between atoms produces what is termed a positive exchange energy, the electronic spins of neighbours tend to align and the material is ferromagnetic. This is best shown by the empirically determined Bethe-Slater curve, shown in Fig. 2.4.2, which plots the exchange energy against the ratio of the atomic radius to the radius of the 3d shell. A positive exchange energy favours parallel spin arrangement, leading to ferromagnetism, and the negative exchange energy gives an antiferromagnetic behaviour.

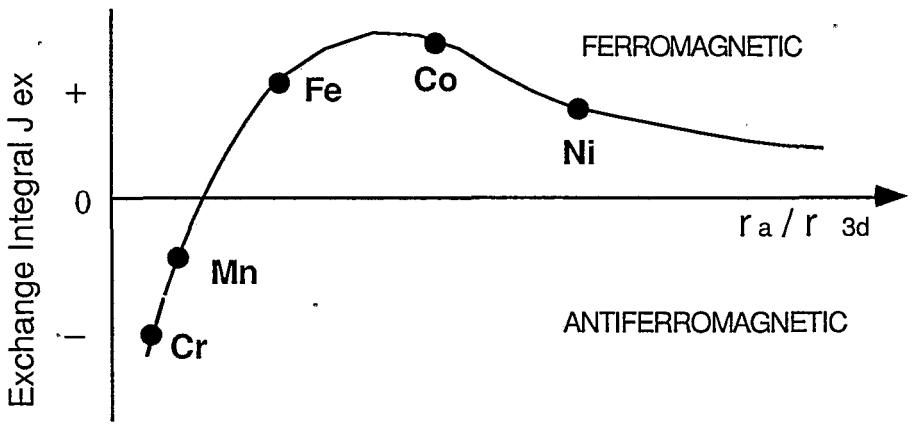

Fig. 2.4.2 Schematic of the Bethe-Slater curve.

When antiferromagnetic ordering exists between two distinct magnetic sublattices which have unequal partial magnetisations, a net magnetisation will result. Materials having these structures are called ferrimagnetic materials, the best known being ferrites.

2.5 Magnetism in the RE-TM-B Alloys

Ferromagnetism in a substance originates from the electrons with unpaired electronic spins interacting favourably with each other within and between atoms. An electron spin contributes a magnetic moment to the atom by a fixed amount of one unit, adding or subtracting according to whether the spin is up or down. A magnetic moment is the strength of the magnetic field associated with the electron. This quantity, called the Bohr magneton and designated by μ_B, is equal to

$$\mu_B = e\,h / 4\,\pi\,m_e = 0.927 \times 10^{-20}\ (\text{erg/Oe}) = 9.27 \times 10^{-24}\ \text{Am}^2 \qquad 2.5.1$$

where e is the charge of the electron , h is Planck's constant, and m_e is the mass of the electron. Electrons which are paired give no net contribution to the magnetic moment.

The transition metals (TM) consist of the elements with incomplete filling of the 3d, 4d and 5d shells in the periodic table but only iron, nickel and cobalt exhibit ferromagnetism in the elemental state. They have large magnetic moments (Fe:2.22, Co:1.72 and Ni:0.6 μ_B) because the 3d shell is rather more than half full, in comparison with its complete complement of 10 electrons. The incomplete shells are almost outermost shells so that the orbital motions are quenched by crystals fields and consequently the magnetic moments are due mainly to electron spins.

The magnetism in the rare earth (RE) metals comes from the partially filled 4f shell, which causes an orbital and also a spin magnetic moment of the unpaired electrons. In this case the 4f

orbitals are effectively shielded from the influence of external forces by the overlying $5s^2$ and $5p^6$ shells and consequently the orbital moment is not quenched. Hence the total magnetic moment has both orbital and spin components.

The transition ferromagnetic elements have a relatively weak preferred direction to the magnetic moments, and a relatively weak applied field can change them from their preferred direction to the direction of the applied field. This directionality is called magnetocrystalline anisotropy, and it is required of a material to be used as a permanent magnet that the magnetic moments have a strong preference to align in only one crystal direction.

A combination of 4f and 3d magnetism exists in the RE-TM compounds. The RE elements with large orbital moments may show a large anisotropy, but they only show magnetic ordering at low temperature because the 4f-4f magnetic interactions are much weaker than the 3d interactions in the transition metals. The TM elements Fe, Co and Ni can stabilize ferromagnetic ordering well above room temperature, but the magnetocrystalline anisotropy is generally very small due to the quenching of the orbital contribution. The large difference in the atomic radii between the RE atoms and the Fe, Co or Ni atoms results in the formation of several types of intermetalic compounds. In these compounds, the 4f anisotropy remains strong and the 3d interactions stabilize the magnetic ordering above room temperature.

In RE-Fe-B alloys, the magnetic moments of Nd and Pr combine ferromagnetically, parallel to the c-axis as opposed to anti-ferromagnetic coupling which occurs with the heavy rare-earths.

Boron atoms play a role in expanding the Fe-Fe interatomic distances and/or decreasing the number of iron nearest neighbours, leading to a high Curie temperature compared with Nd-Fe binary compounds so producing a ferromagnetic material at relatively high temperatures.

2.6 Magnetic Anisotropies

A factor which strongly affects the shape of the hysteresis loop is the magnetic anisotropy. This term simply means that the magnetic properties of a material depend on the direction in which they are measured. There are several kinds of magnetic anisotropy but the three most common are the magnetocrystalline, shape and stress anisotropy.

Magnetocrystalline anisotropy is intrinsic to the material and the magnetic hardness of the material depends greatly on the anisotropy of the crystal structure. In a ferromagnetic single crystal there are certain definite crystallographic axes which can be magnetised to saturation easier than others. An illustration of this is shown in fig. 2.6.1 where a much smaller field is required to saturate an iron single crystal along the easy [100] direction than along one of the other hard directions. In the hexagonal structure of cobalt the easy direction is along the c-axis [0001]. A measure of the magnetic hardness is the anisotropy field, H_A, which is the field necessary to reverse all the spins as one unit in a saturated single crystal. The anisotropy field is given by

$$H_A = 2\,K / M_s \qquad 2.6.1$$

where K is the anisotropy constant and M_s is the saturation magnetisation.

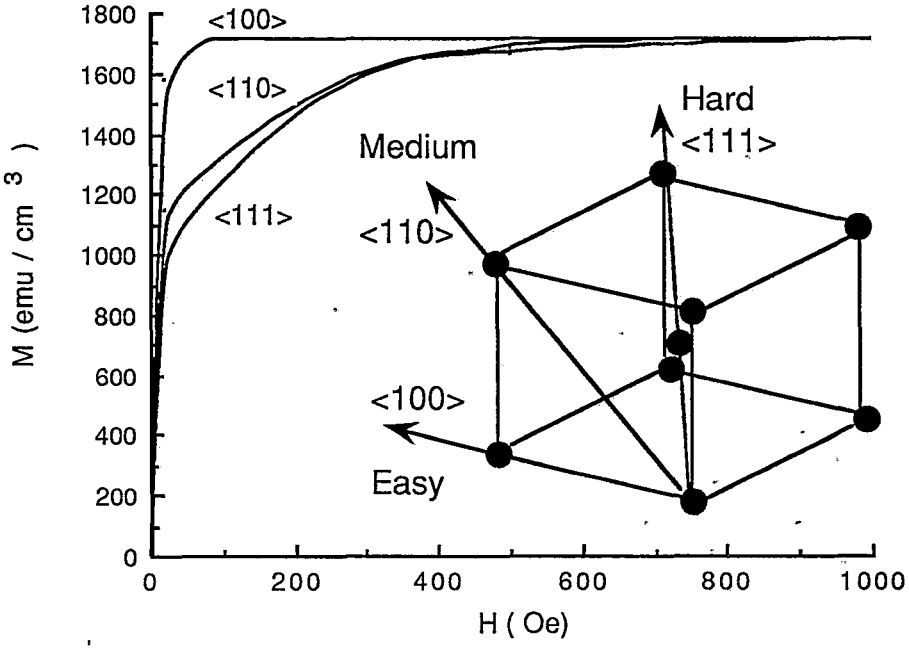

Fig. 2.6.1 Magnetisation curves for a single crystal of iron.

To magnetise a crystal in a hard direction some additional energy is required. This energy, the magnetocrystalline anisotropy energy, E_A, for a material with a single easy axis of magnetisation such as cobalt, is given by

$$E_A = K + K_1 \sin^2 \theta + K_2 \sin^4 \theta + \cdots\cdots \qquad 2.6.2$$

where K_1 and K_2 are materials constants and dependent on the temperature and θ is the angle between the single uniaxial easy direction and the direction of magnetisation. E_A is minimum when the magnetisation is parallel to the easy direction, i.e., θ is equal to 0. The crystal anisotropy is largely due to spin-orbit coupling.

Shape anisotropy, unlike crystal anisotropy, depends mainly on the external characteristics of a material. A spherical, randomly aligned polycrystalline sample will be magnetic to the same extent in any direction. However, for a non-spherical specimen it is easier to magnetise the specimen along its long axis than the short axis. This is due to the demagnetising field along the short axis being stronger than that along a long axis. Hence a larger field is required along a short axis to achieve the same field inside the specimen.

Stress or tension when applied to a material can influence the shape of the magnetisation curves. Properties such as remanence and intrinsic coercivity are also affected and the variations are dependent on the material. This phenomenon can be explained considering magnetostriction and using thermodynamic methods.

2.7 Magnetic Domains

The concept of magnetic domains was first postulated by Weiss in 1906 to explain how a ferromagnetic material with spontaneous magnetisation could exist in a demagnetised state. Almost half a century later domains were first used to explain the shape of a magnetisation curve only after evidence of their existence had been published by Williams, Bozorth and Shockley. Since then domain theory has become central to any discussion of magnetism.

In a single crystal spontaneously magnetised parallel to the easy axis, as illustrated in fig. 2.7.1a, free poles at its ends are the source of a magnetic field. This results in a magnetostatic energy, which can be reduced by splitting into two domains, magnetised in

opposite directions, as shown in fig. 2.7.1b. This process can be repeated until the sum of magnetostatic energy and the energy inherent in the domain walls is minimized, as illustrated in fig. 2.7.1c.

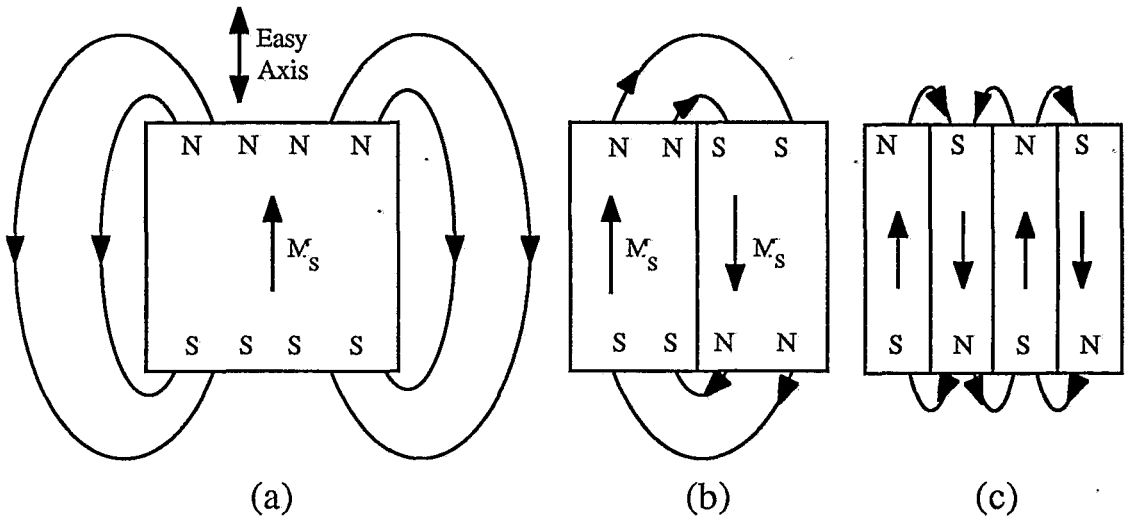

Fig. 2.7.1 Division into magnetic domains.

Magnetic domains can be viewed using a method which highlights the domain walls or a method which shows different domains with differing contrast. The former, developed in 1931, known as the Bitter method is based on a fine suspension of iron oxide (magnetite) in a low viscosity liquid. A small drop of this suspension is placed on the polished surface of the sample to be investigated and the domain patterns observed using an optical microscope. Modern suspensions are called ferrofluid and use chemicals to prevent the clustering of the particles of magnetite. The latter method is based on magneto-optical effects and known as the Kerr methods. It involves illuminating the specimen with polarised light and observing using a polariser on an optical microscope. The

various directions of magnetisation cause different rotations of the plane of polarised light in the reflected beam and consequently give different contrasts when observed through a polarising filter.

Domain walls, often referred to as Bloch walls, are boundaries where the spontaneous magnetisation has different directions on neighbouring atomic sites. The change in direction of magnetisation at the domain boundary is gradual since this reduces the exchange energy between neighbouring spins by avoiding antiparallel spins, as illustrated in fig 2.7.2. The width of the domain wall is the result of two competing effects; the exchange energy trying to minimise the angle between adjacent spins by making the wall as wide as possible and the anisotropy energy trying to reduce the number of non easy axis spins making the wall as thin as possible. The combination of these two competing effects is to make the wall with finite thickness.

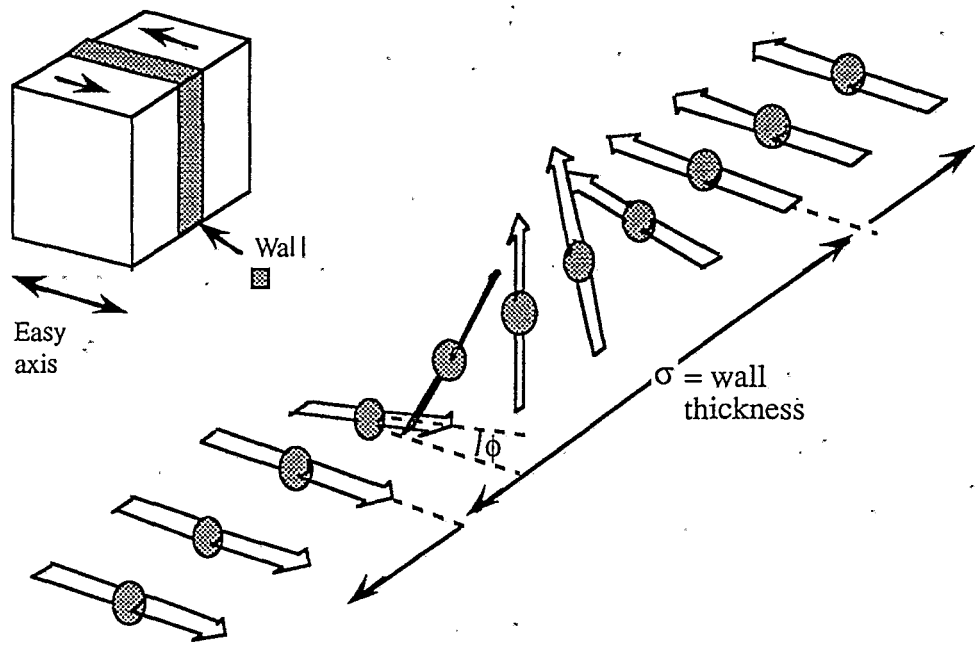

Fig.2.7.2 The structure of a 180° domain wall.

Various types of domain walls are possible (e.g. 71^0, 90^0 , 109^0 and 180^0) depending on the orientation of the easy axis of magnetisation. Their movement has been demonstrated by Barkhausen in 1919 using a magnetizing field, a magnet and a search coil linked to a loud speaker. By increasing the magnetising field in the steep part of the magnetisation curve, small voltage pulses, registered as "clicks" in the loud speaker, are induced in the search coil by the discontinuous changes in the magnetisation.

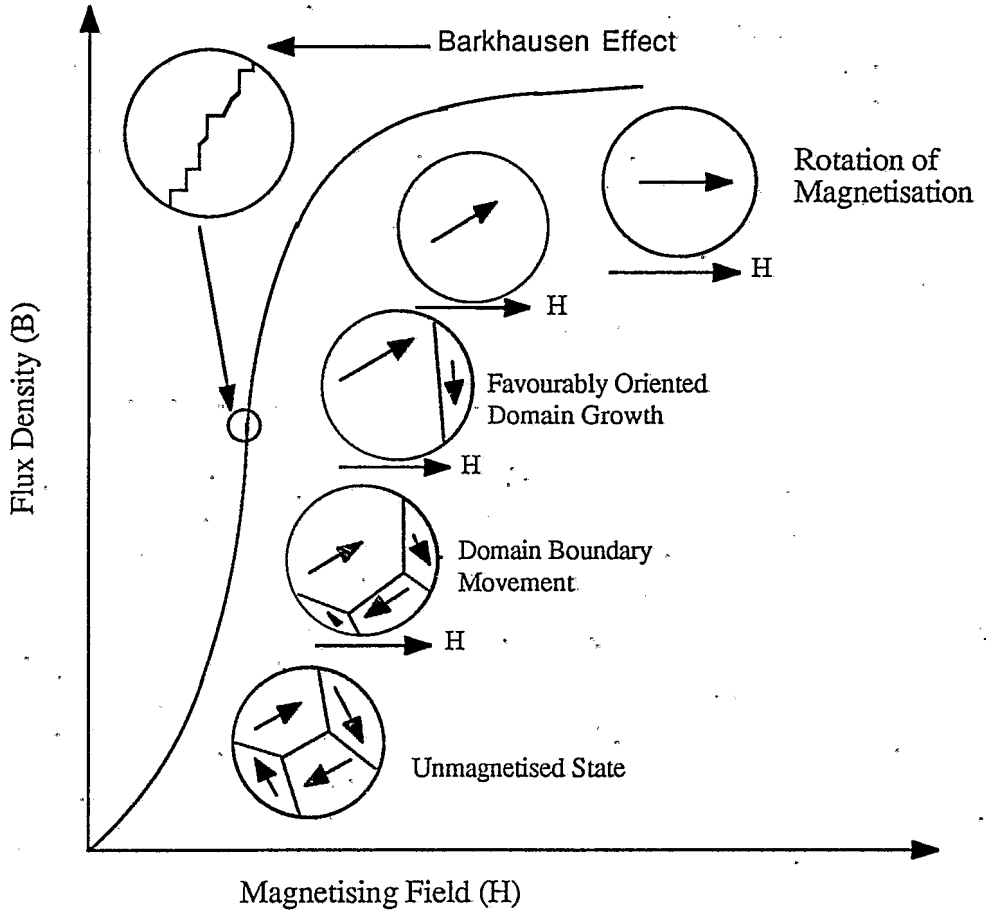

Fig. 2.7.3 Changes in domain structure on magnetisation.

The changes in domain structure of a polycrystalline material during the magnetisation is illustrated in fig. 2.7.3. In the steep part of the curve wall movement occurs causing growth of the domains

in the direction approximately parallel to the field. Then when the material contains only single domains approximately in the direction parallel to the field an increasing field rotates the direction of magnetisation away from the easy axis and aligns it with the field. At this point the material reaches the saturation magnetisation.

In a sufficiently small particle it is energetically unfavourable to contain a domain wall and hence it will be impossible for magnetisation reversal to occur by wall movement which generally requires relatively weak applied fields. In this case the domain must rotate as a whole, a process which may demand large fields. Permanent magnets are generally prepared from multi-domain particles. Consequently a method to avoid domain walls nucleating and moving in applied fields is necessary to maintain a single direction of magnetisation.

2.8 Coercivity Mechanisms

The coercivity is a measure of the capacity of a magnetic material to resist being demagnetised by its own or an external demagnetising field. In a single domain particle the only mechanism for magnetisation reversal is the rotation of the electron spin vectors. In a multidomain particle the demagnetisation may take place through the nucleation of reverse domains and domain wall movement.

To achieve high coercivities in a magnetic material two steps should be taken. Firstly magnetisation rotation must be avoided. This can be achieved by developing a high magnetic

anisotropy in the material. Secondly nucleation or growth of reverse domains must be avoided.

Magnets that reverse their magnetisation via domain-wall processes can achieve high coercivities in either two ways : (1) make the nucleation of a domain wall difficult; (2) make the movement of the wall through the grain difficult. These two methods lead to two classes of permanent magnets. The former corresponds to nucleation controlled magnets and the latter corresponds to pinning controlled magnets. The initial magnetisation curves for the two types are schematically illustrated in fig. 2.8.1.

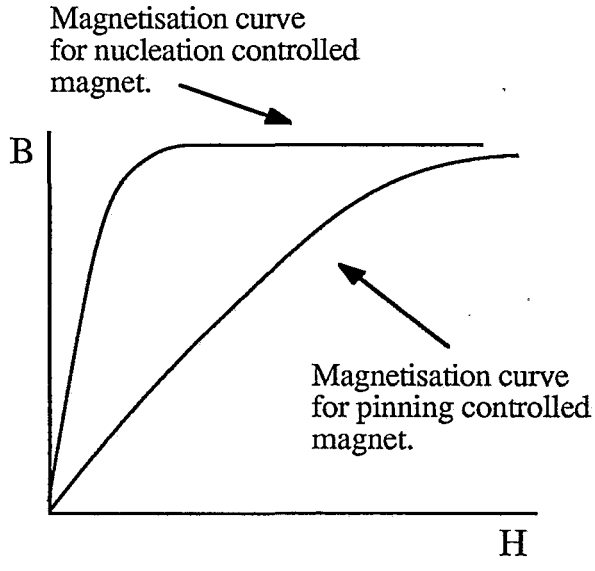

Fig. 2.8.1 Magnetisation curves for nucleation and pinning magnets.

The nucleation of reverse domains usually occurs at surface irregularities or at chemical or physical defects in the lattice, where the crystal anisotropy is locally reduced. These reverse domains move away from these regions and cause demagnetisation. The nucleation of domain walls at defects may occur spontaneously or under the influence of an externally applied reverse field. In this

case the field necessary for domain wall nucleation is usually referred to as the nucleation field strength.

The movement of a domain wall can be impeded by inclusions, second phase precipitates and residual microstresses. Further wall movement can occur only when the applied field exceeds the so-called pinning field strength. Usually inclusions are oxides, carbides, cracks, and holes in a multicomponent alloy. From a magnetic point of view, an inclusion in a domain may be regarded as a region having different spontaneous magnetisation from the surrounding material. Growth of reverse domains may also be hindered by second phase precipitates. As with inclusions, they pin the domain walls by locally reducing the domain wall energy. Residual microstress impedes the movement of a domain wall due to magnetostriction. Microstress in a permanent magnet can be caused by dislocations, impurities in the matrix or interaction between the domains with spontaneous magnetostriction in different directions.

2.9 RE-Fe-B-Hydrides

Hydrogen reacts readily with many RE-Fe-B alloys/compounds to form hydrides. It is the lowering of the system's energy by hydrogen which makes these alloys ready absorbers of hydrogen. These reactions are of great technological importance and consequently have been the subject of many studies. The hydride formation is generally accompanied by a volumetric expansion and its magnitude is dependent on the size of the interstitial site, the hydrogen solute concentration, and also the electronic and strain energy factors. This lattice expansion, in combination with the

extremely brittle nature of the RE-Fe-B alloys, results in flaking and cracking on exposure to hydrogen. The use of this decrepitation effect for the formation of fine powders has been of significant importance to the production of permanent magnets via powder metallurgy (Harris 1987).

The tetragonal crystal structure of $Nd_2Fe_{14}B$ occurs for the whole of the lanthanide series except for Pm, Eu and Yb. The hydride maintains the same structure, with an increase in the lattice parameters (a and c) in accordance with the absorption of hydrogen. The value of the ratio c/a for the hydride remains the same as that for the original structure, indicating an isotropic expansion in both directions (McGuiness 1989).

The anisotropy field and coercivity decreases with the formation of $RE_2Fe_{14}B$ hydrides. Thus a "softening" of the magnetic properties is obtained on hydriding. This is a significant factor during the preparation of a sintered permanent magnet. Firstly, the hydride powder is still capable of c-axis alignment in the presence of a magnetic field which means that fully aligned green compacts can be made from the milled powder. Secondly, the green compacts do not exhibit any significant coercivity, unlike those made from standard powder which do exhibit a small remanence. This absence of permanent magnetism facilitates the handling of the green compacts prior to sintering (Harris and McGuiness 1990).

Hydrogen desorption in these compounds usually is obtained in two temperature ranges: most at RT-260^{0}C and a smaller amount at 550-650^{0}C (RT: room temperature). This behaviour is interpreted in terms of the hydrogen loss from the tetragonal matrix phase and

RE-rich intergranular material during the first step and then from the RE-rich material during the second step. The desorption of hydrogen from the green compacts during heating is also an advantage since it produces a non-oxidising environment during the sintering step (Harris and McGuiness 1990).

An extremely thorough review of RE-Fe-B-hydrides as well as the detailed theory of hydrogen absorption and desorption is given by McGuiness (1989). The Pr-Fe-B-hydrides studies, the powder metallurgy process and other topics relevant to Pr-Fe-B alloys and magnets will be covered separately in chapters 5 and 6.

CHAPTER THREE

SOLIDIFICATION

3.1 Introduction

The theory of solidification can be found in most textbooks on the subject (see Refs. : Pfann 1958, Winegard 1964, Chalmers 1964, Flemings 1974, McLean 1983, Kurz and Fisher 1989), thus only a brief survey on the main topics of solidification will be included here. The presentation of some specialised subjects such as mould and directional solidification, and vertical floating zone will be emphasized.

3.2 Solids and Liquids

Some of the relevant properties of the solid and liquid states in the region of the melting temperature are the density, interatomic distance, electrical resistivity, diffusivity and fluidity. The main differences between the two states are the variations in fluidity and diffusivity. Both properties vary significantly upon melting because they rely on the structure of the condensed (ordered) phase.

Properties that rely intrinsically on the distance between atoms, and not upon the order, are changed very little during melting or freezing. Conductivity and density, for instance, do not vary as much as diffusivity, and might be thought of, at least in principle, as structure-insensitive properties.

3.3 The Freezing Temperature

One of the striking features of the liquid→ s o l i d transformation is that, in a pure metal, it occurs at a unique temperature which is characteristic of the metal and of the pressure, and is a function of both the liquid and the solid. Since the internal energy of the liquid must be higher than that of the solid an evolution or absorption of heat is expected when a transformation occurs. The heat evolved when a liquid transforms to a solid is denoted by the latent heat of fusion, L. The freezing temperature is defined as the temperature at which the free energies of the two phases are equal:

$$G_L = G_S \qquad 3.3.1$$

where G_L is the Gibbs free energy of the liquid and G_S is the free energy of the solid. The free energy G is defined by:

$$G = U + PV - TS \qquad 3.3.2$$

where U is the internal energy of the phase, T is the absolute temperature, P is the pressure, V is the volume and S is the entropy, which is a measure of the disorder of a phase. Since the enthalpy of a phase can be defined as:

$$H \doteq U + PV \qquad 3.3.3$$

the free energy can be defined as:

$$G = H - TS \qquad 3.3.4$$

At the freezing temperature, T_E , G_L equals G_S , therefore:

$$H_L - T_E S_l = H_S - T_E S_S \qquad 3.3.5$$

since: $$H_L - H_S = L \qquad 3.3.6$$

thus: $$\Delta S = L / T_E \qquad 3.3.7$$

Therefore a measure of the change in order during a liquid→solid transformation can be obtained from the ratio of the latent heat to the freezing temperature. Since the structure difference between one solid and another is much less than that between a solid and a liquid, the variation in entropy, ΔS , during the freezing of a metal, should be virtually independent of the structure of the solid metal.

3.4 Undercooling

Liquid metals are often experimentally shown to undercool, and freezing starts at some temperature that is lower than the established freezing temperature. This phenomenon is illustrated in Figure 3.4.1, and the liquid is referred to as "undercooled" when the temperature of the liquid is below T_E . Once freezing starts, the temperature of the remaining liquid increases fast to the standard freezing temperature due to the liberation of latent heat.

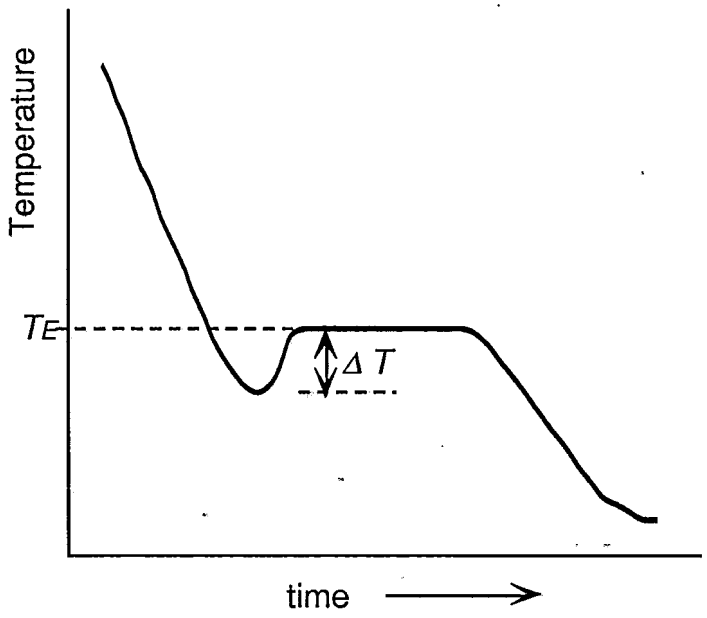

Fig. 3.4.1 Cooling curve showing changes with time for a mass of cooling pure metal.

3.5 Homogeneous Nucleation

Nucleation can be defined as the formation of a new phase in a discrete region, isolated from the surroundings by a specific boundary. In the case of solidification, nucleation concerns the formation of a minute crystal of solid enveloped by liquid. According to thermodynamic principles, only at the melting or freezing temperature, can a pure solid metal exist in equilibrium with the pure liquid metal, since at this temperature the free energies of the two phases are equal (see Fig. 3.5.1). Above this temperature, T_E , the liquid phase is stable, since it has the lowest free energy; below T_E , the solid phase is stable.

A metal should always be solid when it is at a temperature below T_E , because there is a decrease in free energy related with

the liquid→ solid transformation and the larger the degree of undercooling, ΔT , the larger the driving force to transform liquid to solid.

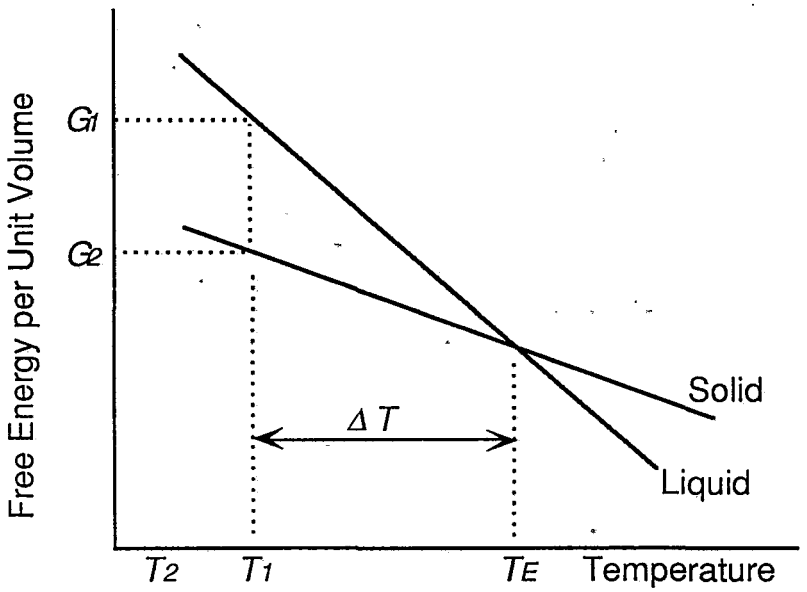

Fig 3.5.1 Diagram of free energy versus temperature for a pure metal.

Although the change in free energy, ΔG , is negative when the liquid turns to a solid, the liquid does not transform to solid immediately below the freezing temperature. The reason for this behaviour is that the free energy in discussion applies only to the volume of the material. If some atoms cluster together to form a potential nucleus, or embryo, a surface is formed. The existence of this surface generates a positive free energy which leads to an increase in the free energy related to the embryo. The embryo can survive only if the total free energy decreases.

When a solid embryo is formed, at the liquid metal undercooled temperature T_1 , there will be a decrease in the

volume free energy per unit volume from G_1 to G_2 (illustrated in fig. 3.5.1). This part of the change in free energy, ΔG_v , for a sphere, is given by:

$$\Delta G_v = - (L/ T_E) \Delta T \ (3/4)/\pi \ r^3 \qquad 3.5.1$$

The change of ΔG_v with r , the radius of the spherical particle formed, is shown in Fig. 3.5.2.

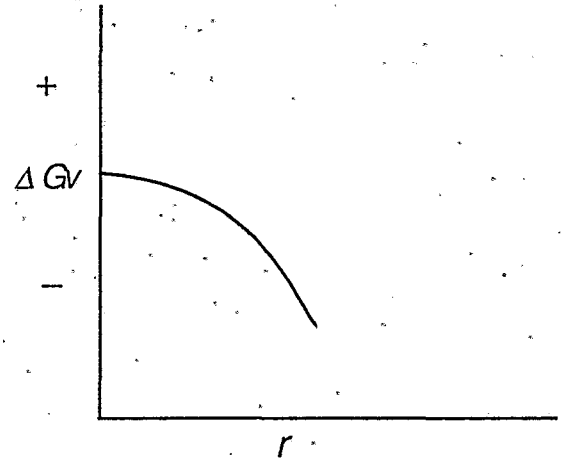

Fig 3.5.2 Variation of ΔG_v with the radius of a particle.

Once a particle is formed a solid-liquid interface is established with energy associated with it, and the variation in free energy of the system due to the interface is denoted by ΔG_S. The total variation in free energy due to the formation of this particle can be written as:

$$\Delta G = \Delta G_v + \Delta G_S = -(L/ T_E) \Delta T \ (3/4) /\pi \ r^3 + 4 \pi \ r^2 \gamma \qquad 3.5.2$$

where γ is the specific interfacial free energy per unit area. The change of these two terms and also the total free energy are

illustrated in fig. 3.5.3.

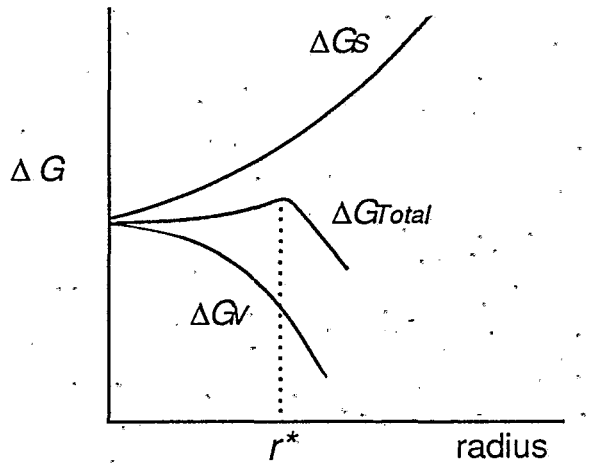

Fig.3.5.3 Change of ΔG with the radius of the particle.

It can be seen that at some critical radius, r^*, ΔG , is a maximum and can be expressed by the equation:

$$\Delta G_{max} = -L\ (\Delta T/T_E)\ (3/4)\ /\pi\ r^{*\,3} + 4\ \pi\ r^{*\,2}\ \gamma \qquad 3.5.3$$

where $r^* = 2\ \gamma\ T_E\ /\ L.\ \Delta T$

When a particle is formed so that its radius r is larger than r^*, there will be a decrease in ΔG with a further increase in r. Therefore, any nucleus greater than r* will tend to grow and any nucleus smaller than r* will tend to disappear in order to decrease ΔG.

3.6 Heterogeneous Nucleation

When solidification of a metal is to occur on a foreign substance, which can be the container or insoluble impurities, it is crucial that the surface of the substrate is wetted by the liquid metal and the liquid solidifies easily on the substrate. This is accomplished when the angle of contact , θ , between the substrate and the solid metal being deposited is very small (see fig. 3.6.1). If this is the case, the interface between the solid and the substrate has a low surface energy, compared to a larger θ , and the atoms in the liquid easily form the nucleus on the surface of the substrate.

The contact angle is a function of such factors as the lattice spacings of the two structures and the chemical nature of the surface of the substrate. Nucleation occurs with a small amount of undercooling if the angle of contact is small.

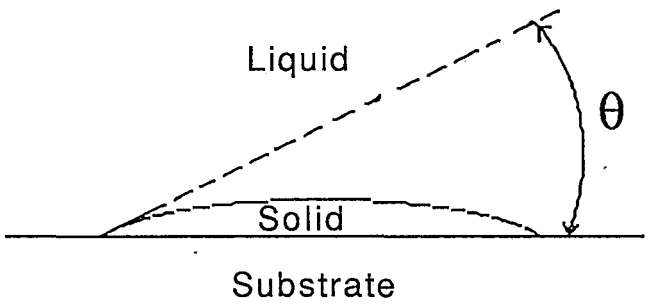

Fig.3.6.1 Angle of contact between the substrate and the solid metal.

A substance, soluble or insoluble, which is intentionally added to the liquid to act as a nucleation catalyst is called a nucleating agent.

3.7 Constitutional Supercooling

In pure metals, and also in alloys, the microstructure can be directly related to undercooling. In pure metals undercooling can be produced only by thermal means. In alloys, however, undercooling may be produced indirectly by changes in temperature and composition. If it is produced by changes in composition combined with temperature changes it is referred to as constitutional undercooling (or constitutional supercooling), and it is this type of undercooling that determines the growth structures usually found in alloys.

Under non-equilibrium conditions, concentration gradients develop in the liquid ahead of the solid/liquid interface because the composition of the forming solid is different from the composition of the liquid from which it is freezing. When the concentration of solute in the solid is less than that of the liquid from which it is forming there must be a rejection of solute into the liquid at the solid/liquid interface. If sufficient time is not allowed for this solute to distribute itself throughout the remainder of the liquid a concentration gradient will develop and persist in the liquid ahead of the interface. This concentration gradient promotes the constitutional undercooling that is responsible for the microstructures found in ingots of alloys.

In a freezing simple binary alloy, with a phase diagram such as that illustrated schematically in figure 3.7.1, the distribution coefficient, k_o, is defined as the ratio of the concentration of solute in the solid to the concentration of solute in the liquid with which the solid is in equilibrium, and K_o is < 1.

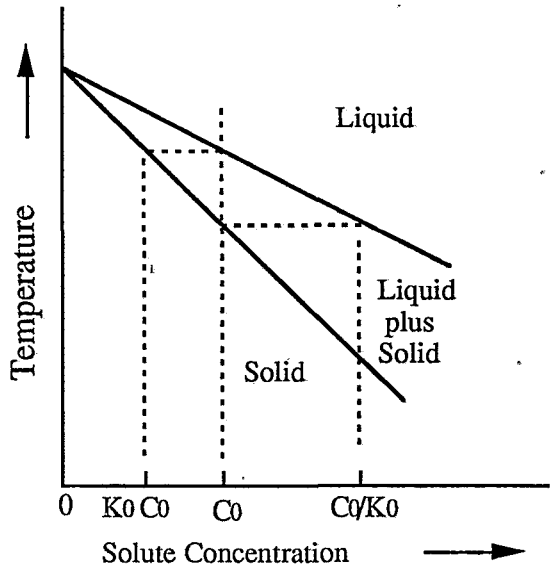

Fig. 3.7.1 Portion of binary constitutional diagram for a solute which lowers the freezing point of the solvent ($K_o < 1$).

For the mathematical treatment of constitutional supercooling it is necessary to define the conditions which apply during solidification. For this, it is assumed that : K_o is a constant, diffusion in the solid is negligible, diffusion is the only mechanism involved for mixing the liquid and also the equilibrium is maintained at the solid/liquid interface.

When an alloy of composition C_o is solidified unidirectionally the first solid to freeze will be of composition K_oC_o ; the liquid adjacent to the solid must then become richer in solute concentration than C_o. The next solid to freeze will have a higher solute concentration, since it is freezing from a liquid of higher solute concentration. Both the solid and liquid increase in solute concentration until, at a constant rate of growth, a steady state is reached, when the solute rejected per unit time by the solid at the interface equals the amount of solute diffusing away from the interface into the bulk liquid per unit time. Under this steady state

a definite distribution of solute ahead of the solid/liquid interface will exist for any given rate of solidification. The solute concentration at the interface reaches a maximum or limiting value of C_o/K_o (such that a solid of composition C_o freezes from it), and decreases exponentially into the liquid until the bulk composition C_o is reached. The solute profile which exists ahead of an advancing interface is illustrated in fig. 3.7.2.

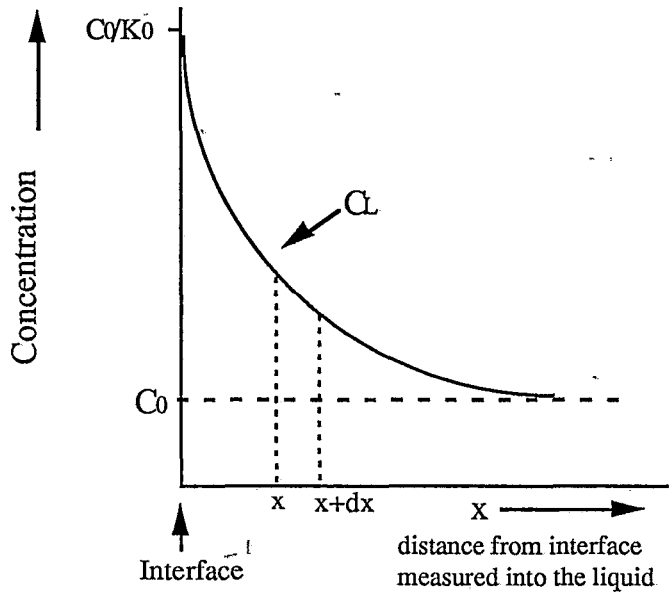

Fig. 3.7.2 Steady-state solute distribution in the liquid ahead of the advancing solid/liquid interface.

As the interface advances, the profile moves into a liquid of composition C_o and freezes a solid of composition C_o. The distribution of solute in the region of the interface is controlled by: (1) diffusion of solute away from the interface into the bulk liquid, and (2) the freezing process that supplies solute to the interface region. The diffusion of solute away from the interface is controlled by D , the diffusion coefficient of solute in the liquid, while the

supply of solute to the region is controlled by R, the rate of interface advance.

Considering fig. 3.7.2, the amount of solute diffusing into a unit area of face x is $-D(\partial c/\partial x)_x$. The amount diffusing out per unit area of face x+dx is $-D(\partial c/\partial x)_{x+dx}$. The net diffusion flow per unit volume is $D(\partial^2 c/\partial x^2)$. The net flow out of the same volume element due to freezing is $R(\partial c/\partial x)$. The equation describing the steady-state distribution with respect to this system is

$$D\left(\frac{\partial^2 c}{\partial x^2}\right) + R\left(\frac{\partial c}{\partial x}\right) = 0 \qquad 3.7.1$$

which gives a solution

$$C_L = C_0\left[1 + \frac{1 - K_0}{K_0}\exp\left(-\frac{R}{D}x\right)\right] \qquad 3.7.2$$

Where C_L = solute concentration in the liquid at any point x;

C_o = original solute concentration in the melt;

K_o = the distribution coefficient for the system;

R = the rate of solidification;

D = the diffusion coefficient of the solute in the liquid;

x = the distance ahead of the solid/liquid interface measured into the liquid.

At large values of x, C_L equals C_o, and when x is zero, C_L equals C_o/K_o; this is shown schematically in fig. 3.7.2. When this steady state has been reached the composition of the solid that is freezing at the interface is C_o.

The effect of this solute-rich layer at the interface in terms of producing undercooling is not made clear until the temperature distribution is considered. The liquid at every point x (fig. 3.7.2), has an equilibrium freezing or liquidus temperature which may be obtained directly from the phase diagram, or can be calculated from the phase diagram if it is assumed that K_0 is a constant and the slope of the liquidus line, m, is a constant. Using this assumption, the liquidus temperature for liquid of any composition may be obtained from the freezing temperature of the pure solvent by the equation

$$T_L = T_0 - (m C_L) \qquad 3.7.3$$

where T_L is the liquidus temperature for liquid of composition C_L,and T_0 is the freezing temperature of the pure solvent metal.

It is possible, therefore, to obtain an equilibrium freezing temperature for every concentration of solute in the liquid by combining equations 3.7.2 and 3.7.3.:

$$T_L = T_0 - m C_0 \left[1 + \frac{1 - K_0}{K_0} \exp \left(-\frac{R}{D} x\right) \right] \qquad 3.7.4$$

The solute distribution in the liquid, equation 3.7.2, and the equilibrium freezing-temperature distribution, equation 3.7.4, are illustrated schematically in fig 3.7.3a and b, respectively.

While fig. 3.7.3b represents the freezing temperatures for the liquid ahead of the interface, it does not give the real temperature that exists at every point ahead of the interface, i.e. the actual

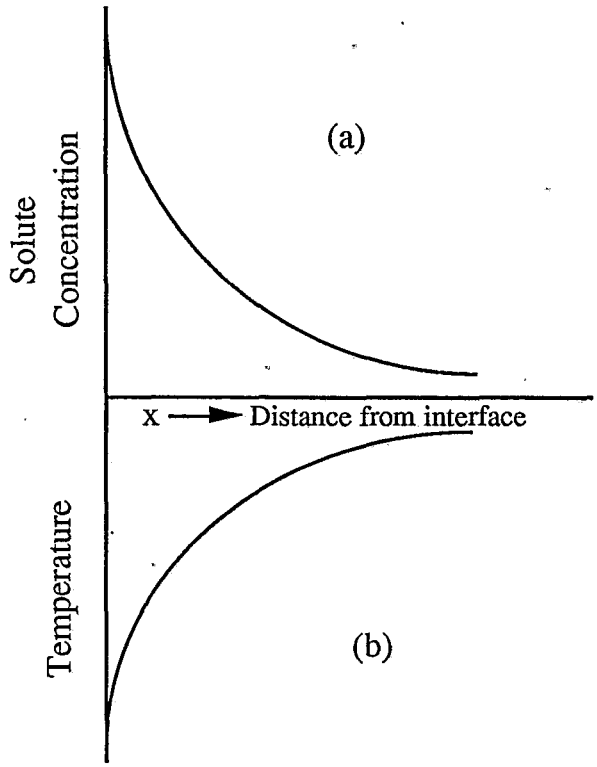

Fig. 3.7.3.(a) Concentration of solute in the liquid ahead of the interface , (b) equilibrium freezing-temperature distribution ahead of the interface.

temperature T_A. Since it was assumed that the freezing occurs only at an advancing solid/liquid interface, the temperature there, T_I, must correspond to the equilibrium liquidus temperature for that liquid existing under steady state at the interface. In other words,

$$T_I = T_o - m C_o / K_o \qquad 3.7.5$$

The temperature at any point x in the liquid is then given by

$$T_A = T_I + G_L x \qquad 3.7.6$$

where G_L is the temperature gradient in the liquid and T_A is the real temperature (actual temperature) at any point x. Thus

$$T_A = T_o - m C_o / K_o + G_L x \qquad 3.7.7$$

When this temperature (T_A) is superimposed upon the curve for equilibrium freezing temperature, as illustrated in fig 3.7.4, it may be seen that part of the liquid ahead of the interface is below its normal freezing temperature. This undercooling, termed constitutional undercooling (or constitutional supercooling), is a direct result of the concentration gradient that exists in the liquid.

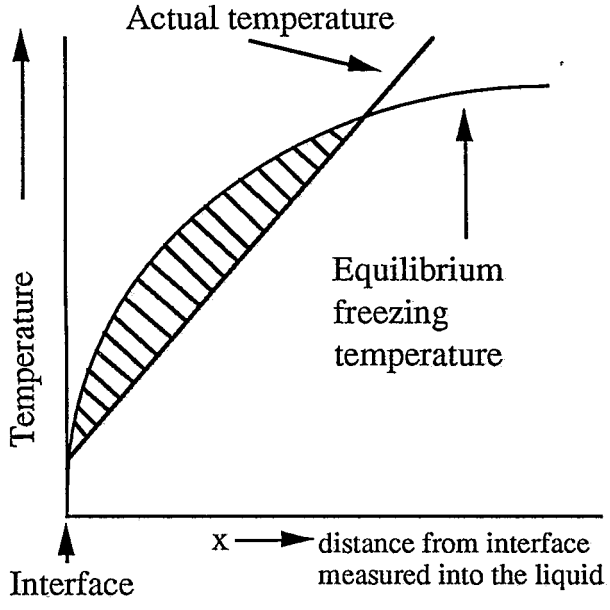

Fig. 3.7.4 Illustrating constitutional undercooling.

The zone of undercooling can be eliminated if the slope of the actual temperature is made equal to or greater than the slope of the liquidus temperature curve at the interface, as illustrated in fig.3.7.5.

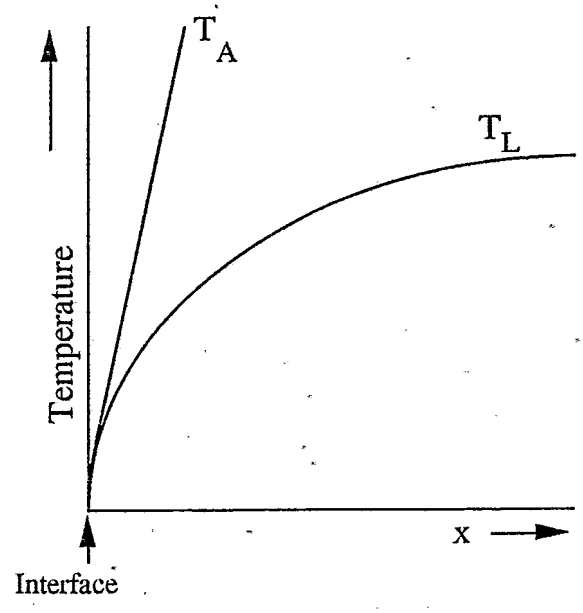

Fig. 3.7.5 Undercooled zone eliminated by increasing G_L.

The undercooled zone is eliminated when the following relationship is satisfied:

$$\frac{G_L}{R} \geq \frac{m C_0}{D} \left(\frac{1 - K_0}{K_0} \right) \qquad 3.7.8$$

The argument just presented is also valid when k_o is > 1, and undercooling also develops by combined solute and temperature distributions in the liquid ahead of an advancing solid/liquid interface, regardless of whether k_o is > or <1 . The constitutional undercooling is responsible for the growth structures found in alloy ingots and castings, and is one of the most important concepts in solidification of alloys.

3.8 Cellular and Dendritic Solidification

The conditions given by Chalmers (1969) for the stability of a planar solidifying interface are given by equation 3.7.8. As the experimental value of G_L/R increasingly deviates from the critical value (by decreasing G_L, increasing R or increasing C_o, for a constant actual temperature), a progression of microstructural forms, shown schematically in fig.3.8.1, have been observed in many materials.

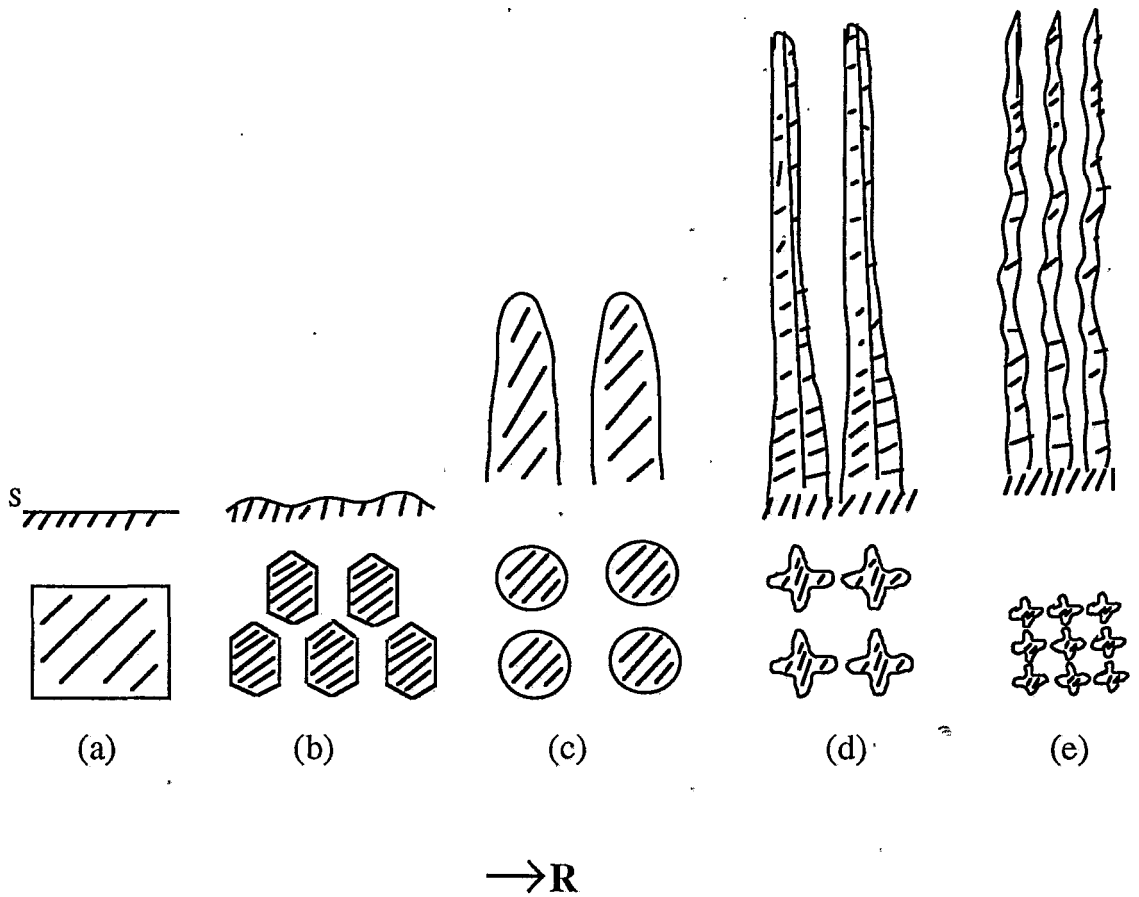

Fig.3.8.1 Schematic illustration of the changing shape of the solidifying front with increasing R, for a constant G, as the range of constitutional supercooling extends to the equilibrium melting range of the alloy.

The categorisation of these morphologies can be described according to Flemings (1974) and McLean (1983) (see also fig.3.8.1):

a)**Plane front** .

b)**Cellular** with cylindrical cells parallel to the direction of heat flow.

c)**Cellular** with near cylindrical cells parallel to the crystallographic direction of easy growth(<100> for cubic materials). Normally the heat flow and the easy growth directions are only slightly misoriented.

d)**Cellular / Dendritic** with flanged cells, having sections shaped like maltese crosses, parallel to the crystallographic direction.

e)**Dendritic** where the flanges of the cellular /dendritic structure have broken down further to form secondary, and higher order, arms.

f)**Equiaxed** with no obvious directionality (see fig. 3.9.1).

Although as yet there are no rigourous theories describing the evolution of these solidification morphologies some qualitative observations can be made. There is clearly a progressive increase in the ratio of surface area to volume for the cells with increasing R and G. This is necessary to generate, by radial diffusion, the greater latent heat of solidification required to balance the greater heat losses at high R and G. The factors leading to the transitions between the various solidification morphologies are quite similar and it is probably possible to identify a different critical value of G/R for each transition, although a theoretical expression is only available for the plane front to cellular transition.

The form of a solidification microstructure depends not only upon the cooling conditions, but also upon the alloy composition, as shown by equation 3.7.8. The effects of composition can be illustrated using the schematic phase diagram shown in fig. 3.8.2. There are essentially two basic growth morphologies which can exist during an alloy solidification. These are the dendritic and eutectic morphologies (peritectic alloys grow in a dendritic manner). Generally, a mixture of both morphologies will be present. Therefore, using fig. 3.8.2, the following morphologies can be distinguished :

1)Pure substances, which solidify in a planar or dendritic manner.
2)Solid-solution dendrites (with or without interdendritic precipitates).
3)Dendrites plus interdendritic eutectic.
4)Eutectic.

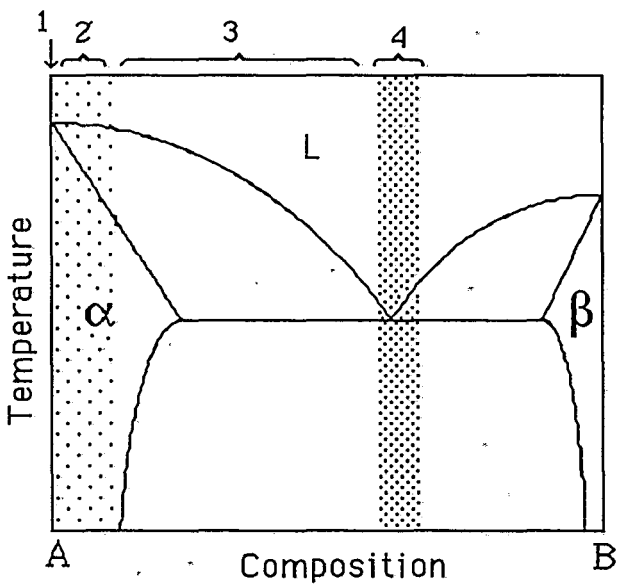

Fig. 3.8.2 Schematic binary phase diagram.

3.9 Solidification in a Mould

The process of solidification of an alloy is governed by three main parameters (Chalmers1969):

1) The rate R of advance of the interface
2) The temperature gradient G in the liquid
3) The alloy composition C or alloy impurity level

They can be related by the principles of constitutional supercooling by the following simplified relation (equation 3.7.8) :

$$G / R\,C \geq \text{Constant} \qquad 3.9.1$$

The equation indicates that if one wishes to avoid constitutional supercooling in any given alloy, one has to (a) increase G, (b) decrease R, (c) decrease C (increase the purity), or some combination of these three factors, such that the quotient G/RC exceeds some particular value for the alloy system under investigation. As is well known, unidirectional solidification at an appropriately high value of G/RC permits the alloy to solidify with a planar, or substantially planar, freezing interface. If G/RC is less than the critical value, the alloy is likely to solidify with a nonplanar (cellular or dendritic) freezing mode. In this case, the equation is no longer applicable because another assumption made in its derivation was that solidification proceeds with a flat solid-liquid interface.

When an alloy is poured into a mould and allowed to solidify, it may do so in various ways, depending mainly on the rate of heat extraction (R and G are variable, decreasing in value with time), the amount of metal and its composition (C, also variable during the

process of freezing), the potency of the nucleants that are present (if any), the degree to which the molten alloy is superheated when it is introduced into the mould and the fluid motion. The alloy is characterized by its composition, its nucleation characteristics, its temperature when it is poured, and its motion as it enters the mould. The mould is characterized by its thermal properties, temperature and geometry.

The solidification in a mould occuring under a constitutional supercooling regime (G/CR $<$ critical value) normally results in the formation of three characteristic zones (see fig.3.9.1) :

1) The outer chill zone
2) The intermediate columnar zone
3) The central equiaxed zone

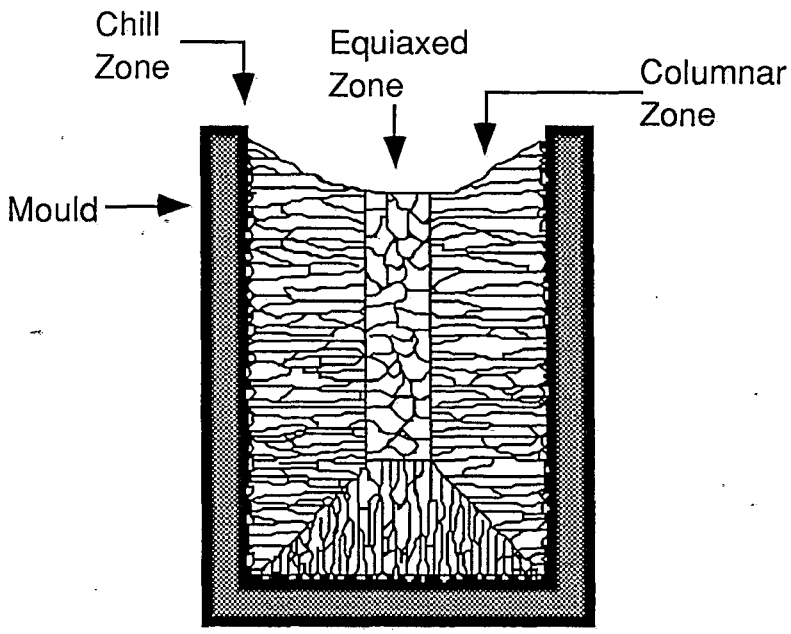

Fig.3.9.1 Ingot microstructures.

Although depending on the variables mentioned above just one or two of the zones can exist alone according to the following explanation.

1) Chill and Columnar

If a molten alloy is poured into a cold mould, the liquid that comes into contact with the mould is chilled, which causes nucleation to take place. A layer of crystals forms in contact with and close to the mould wall. These crystals grow as a result of the continued extraction of heat by the mould. These crystals constitute the "chill" zone; they are, usually, of random orientations. Their growth away from the mould wall is competitive, in the sense that, while a very large number of crystals are nucleated, rather few of them grow inward to any important extent. It is observed that, under these conditions, the crystals that survive have a strongly preferred orientation; in fcc and bcc structures, for example, the crystals all have a <100> axis perpendicular to the mould wall. It is significant that this is the growth direction of dendrites, and that a dendritic structure can always be found in the region in which these crystals establish their dominance. The crystals with other orientations are suppressed because they do not grow away from the mould as fast as those that are more favourably orientated. The crystals that survive continue to grow inward; under some conditions, this persists until they encounter those that are growing from the opposite side of the mould. These crystals then form the columnar zone of the casting. Their length is many times their lateral dimensions, and their structure is cellular dendritic. Figure

3.9.2 illustrates the influence of the pouring temperature on the length of columnar zone. The two main characteristics by which a structure can be described are the extent or length of the columnar zone, and the grain size of the equiaxed region.

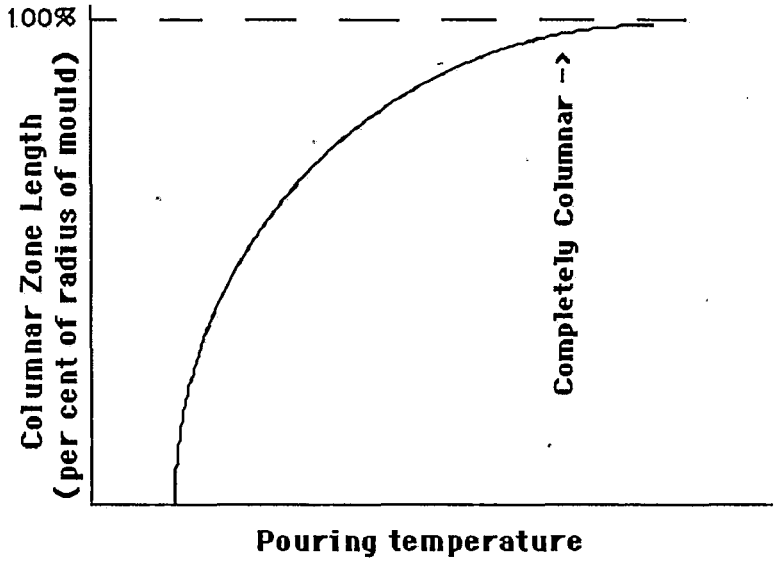

Fig. 3.9.2. Percentage variation of length of columnar zone with pouring temperature.

2) Columnar/ Equiaxed (usually referred to as an "ingot structure")

One of the major variables that can be controlled, in a process in which a molten alloy is poured into a mould, is the superheat, that is, the extent to which the melt is above its liquidus temperature. The sequence of events that leads to the fully columnar structure, described above, takes place when the superheat has an intermediate value. If the superheat is increased sufficiently, the crystals that are nucleated initially are remelted

by the heat remaining in the liquid after its surface has been chilled. The part of the mould near the region of contact with the liquid is heated to a temperature above the liquidus. As cooling continues, nucleation occurs when the liquid near the mould wall again falls to its nucleation temperature. Because cooling is slow (compared with the drastic chill which produces primary nucleation), few nuclei are formed. These grow dendritically, both parallel to the wall and inward; their dendritic structure is coarse because cooling is relatively slow. The result is a coarsely dendritic structure consisting of large crystals of random orientation. The interdendritic liquid at and near the surface remains liquid for a long time, and some of this liquid is sucked inward as solidification shrinkage occurs. Thus the dendritic structure is seen in relief on the surface of the casting. If the superheat is decreased, an equiaxed zone appears in the interior of the casting. It has not been shown that the crystals that form this zone do not originate by nucleation while the columnar crystals are growing. It has been shown that they can be reduced in extent, or in some cases suppressed entirely if fluid motion is prevented by the application of a magnetic field.

It is reasonably certain that, when the equiaxed zone is relatively small, the crystals in it originate as fragments that are detached from the tips of columnar dendrites. It is most likely that this occurs after the temperature of the interior liquid has become uniform, so that free, as distinct from cellular, dendritic growth can occur, and after the slowing down of the heat-extraction rate has allowed the temperature of the interior liquid to rise. It is also possible that the tips are detached by the mechanical action of

moving liquid or that dendrites are so bent that different parts of them grow as separate crystals. As the superheat is decreased, the volume occupied by the equiaxed zone increases (that is, the columnar zone becomes shorter) and the grain size of the equiaxed zone decreases. Figure 3.9.3 illustrates the influence of the pouring temperature on the equiaxed grain size and columnar length.

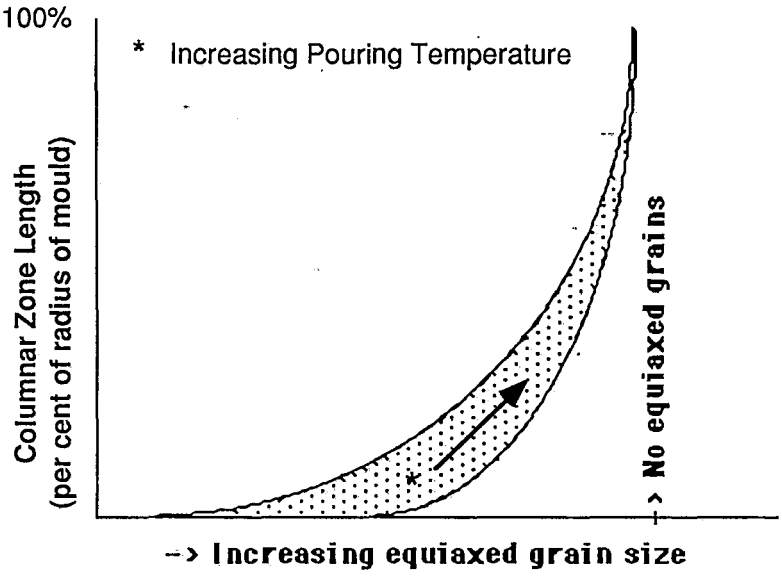

Fig.3.9.3. Percentage variation of equiaxed grain size with columnar length.

3) Equiaxed (usually regarded as being characteristic of "castings")

There is evidence that, for low superheat, the equiaxed crystals arise from nuclei that form during the initial chill as the metal enters the mould. In this situation, the whole of the melt cools soon enough for floating nuclei to survive and to grow. Some small equiaxed crystals are "trapped" in the columnar zone; columnar growth stops when the equiaxed crystals have begun to impinge on each other, forming a skeletal network. The transition

between "fragmentation" is probably gradual. If the effective superheat is decreased still further, the columnar zone disappears, and the surface chill zone and the interior equiaxed zone become continuous with each other. The chilling effect of the mould is then sufficient to cool the whole of the metal to its nucleation temperature, in spite of the fact that the crystals that nucleate first immediately start to grow and therefore to give out latent heat. The grain size that is produced is decreased by the use of a nucleant, by more rapid heat extraction, by reduced superheat, and by reduced section of the mould. In addition, motion, and particularly turbulent motion, of the liquid while it is being rapidly cooled will tend to decrease the grain size by exposing more nucleant particles to the rapid cooling that occurs close to the mould wall. Figure 3.9.4 illustrates the influence of the pouring temperature on the equiaxed grain size.

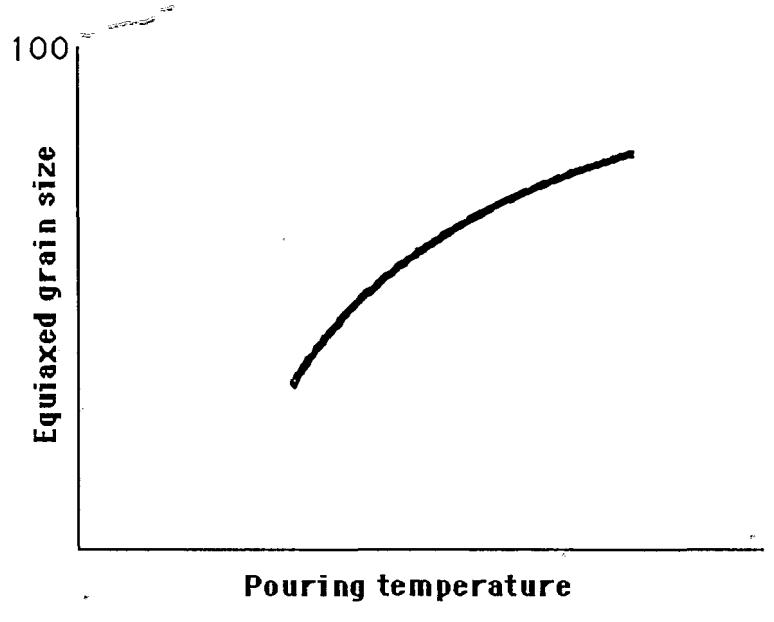

Fig.3.9.4. Percentage variation of equiaxed grain size with pouring temperature.

3.10 Vertical floating zone

In a zone melting techique only a portion of the material is melted and this molten zone is slowly moved throught the material. Zone melting is carried out either with or without a crucible. The crucibleless zone melting, or vertical floating zone, is widely used for reactive and high-melting-point materials, and is illustrated in figure 3.10.1. The molten zone is held in place by surface tension forces sometimes aided by a magnetic field.

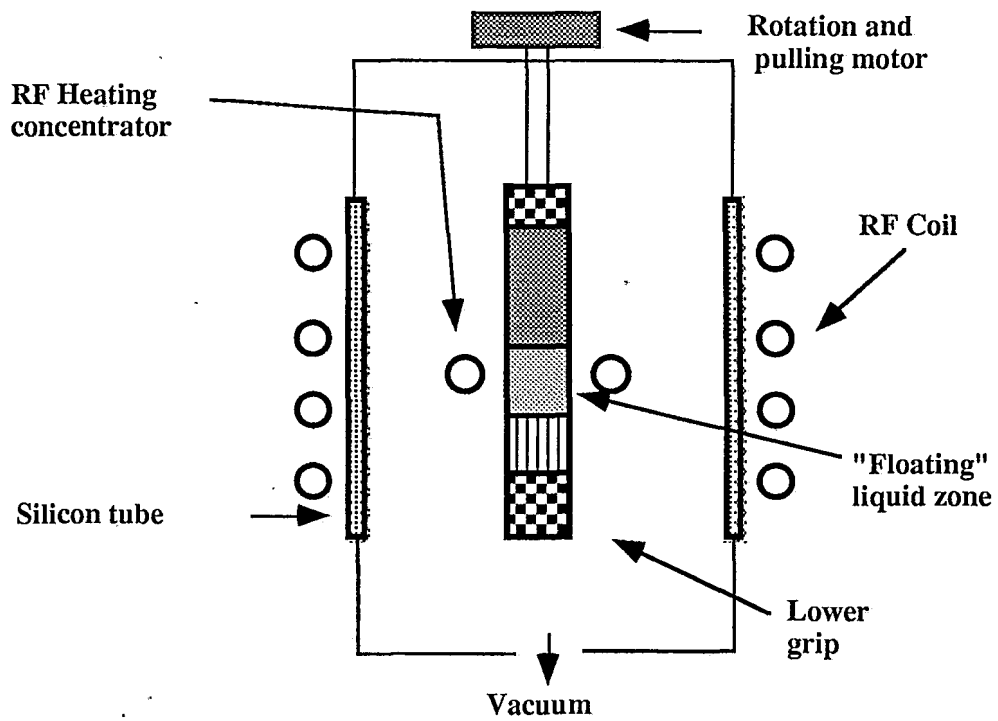

Fig. 3.10.1 Vertical floating zone method.

The general influence of the growth rate on the shape of a growing interface of silicon has been given by Keller and Muhlbauer (1981), and will be summarized here with the variable nomenclature changed to the ones adopted for this thesis. Although

the analysis is specifically for silicon and only qualitative, it can be seen as a guide for other materials.

The thermal power necessary to generate a stable floating zone in a crystal is brought about by the electromagnetic field of the induction coil, which heats predominantly the neighbouring shallow ring of the zone. This thermal power is dissipated by irradiation, conduction, and convection (if a gaseous ambient is present). Moreover, in a floating zone the growth rate also plays an important role in any thermal considerations, as it defines the amount of heat per unit time that must be introduced into the system to melt adequate amounts of feed rod per unit time. The growth rate also influences the cooling rate of the frozen crystal (i.e., its temperature gradients), but this effect is neglected here. Furthermore, the simplified heat-transfer analysis considered here neglects all supercooling effects at the growing interface.

For a crystal growing under steady-state conditions (plane front), the same amount of heat spent melting the feed rod is liberated at the growing interface. For a stationary melt, the heat balance at the growing interface is

$$K_s G_{sg} A_g = K_l G_{lg} A_g + L_f R A_g \qquad 3.10.1$$

where K_s and K_l are the thermal conductivities in the solid (s) and in the liquid (l), G_{sg} and G_{lg} are average temperature gradients near the growing interface in the crystal (s) and in the melt (l), A_g is the area of the growing interface, L_f is the latent heat of fusion, and R is the growth rate. Equation (3.10.1) states that the heat carried away into the solid equals the heat transferred from the adjacent melt

plus the heat of fusion liberated at the interface. Figure 3.10.2 illustrates the rate of liberation of latent heat as a function of crystal diameter for several growth rates.

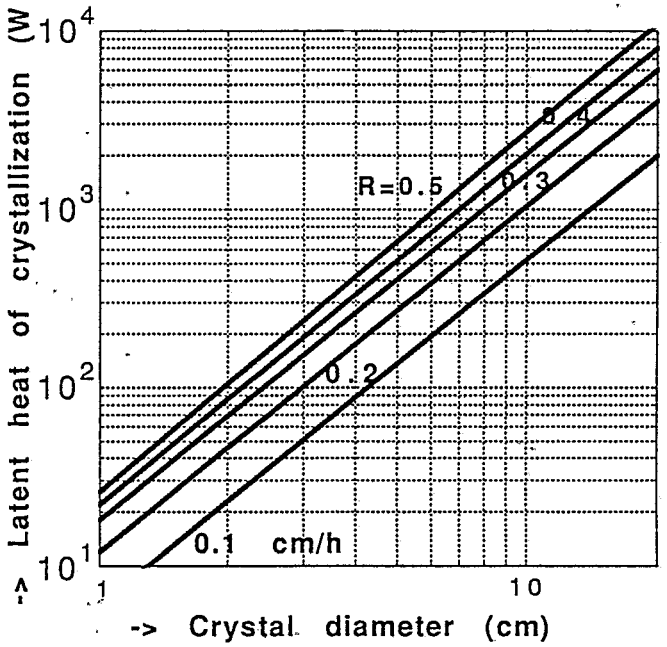

Fig 3.10.2 Rate of liberation of latent heat generated at the freezing interface in relation to crystal diameter and growth rate.

Whereas for Czochralski growth only the heat flux across the growing interface must be considered (according to Eq.3.10.1), the floating-zone method requires us to take into account the heat flux across two interfaces. For the melting interface the heat flux into the feed rod is equal to the heat coming from the adjacent melt minus the heat of fusion necessary for melting the feed rod:

$$-K_s G_{sm} A_m = -K_l G_{lm} A_m + L_f R_m A_m \qquad 3.10.2$$

where K_s and K_l are again the thermal conductivities in the solid (s) and liquid (l), G_{sm} and G_{lm} are the average gradients near the melting interface in the feed rod (s) and in the melt (l), A_m is the area of the melting interface and R is the melting rate.

For steady-state crystal growth, the heat of crystallization ($L_f R A_g$) must equal the heat required for melting ($L_f R_m A_m$). Therefore, the addition of Eqs. (3.10.1) and (3.10.2) gives

$$(k_l G_{lm} A_m - K_s G_{sm} A_m) = -(K_l G_{lg} A_g - K_s G_{sg} A_g) \quad 3.10.3$$

since the difference between the fluxes in the liquid and solid at both interfaces must be of opposite sign. Equations (3.10.1) to (3.10.3) demonstrate that a large number of variables are involved. It is difficult to obtain quantitative results because some of these variables are not known. Qualitatively though, it is obvious from equation (3.10.1) that a maximum growth rate R is obtained for a zero gradient G_{lg} in the liquid near the growing interface. To properly melt the feed rod, G_{lm} should be high (equation. 3.10.2) unless the feed rod is preheated. So, in practice G_{lg} cannot be made very small. Experience shows that, for Si, even for 7.5 cm-diameter crystals, growth rates of 30 cm/h are feasible. For crystals with diameters of $\sim$1.0 cm the growth rate can be increased to about 90 cm/h. Above 120 cm/h the mode of growth begins to become dendritic, with oval cross sections due to the thermal supercooling of the melt. The oval cross section enlarges the radiating surface, so that the liberated latent heat of fusion can be transferred away more efficiently.

Because of the finite thermal conductivity of the system, the

heat of fusion consumed at the melting interface above and liberated at the growing interface below leads to higher temperature variations in the inner regions of the melt than at the periphery, where the heat can readily be dissipated. Thus the shape of the inner region of the floating zone is particularly influenced by the growth rate. This relationship is shown schematically in Fig.3.10.3 and 4 (Braun and Pellin1961).

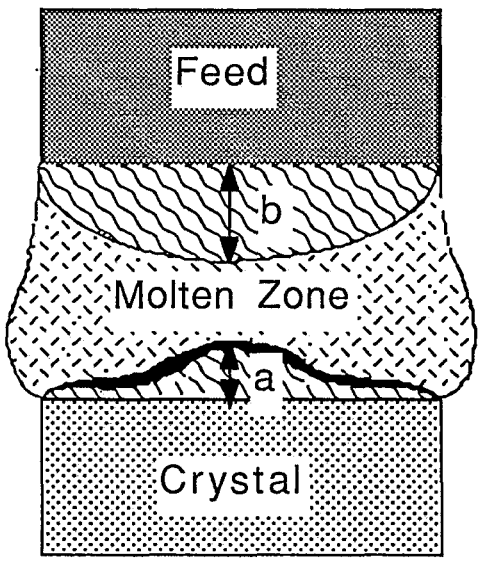

Fig. 3.10.3 Model of the influence of R on the shape of the floating zone.

Whereas for a zero growth rate both interfaces look similar (under zero-gravity conditions they must look identical), a complementary change of their shapes occurs with increasing growth rate. The melting interface becomes more and more convex, approaching the shape of an icicle at high growth rates, whereas the growing interface becomes increasingly concave. Moreover, the position of the coil relative to the zone moves upwards because of the inertia of the latent heat removal.

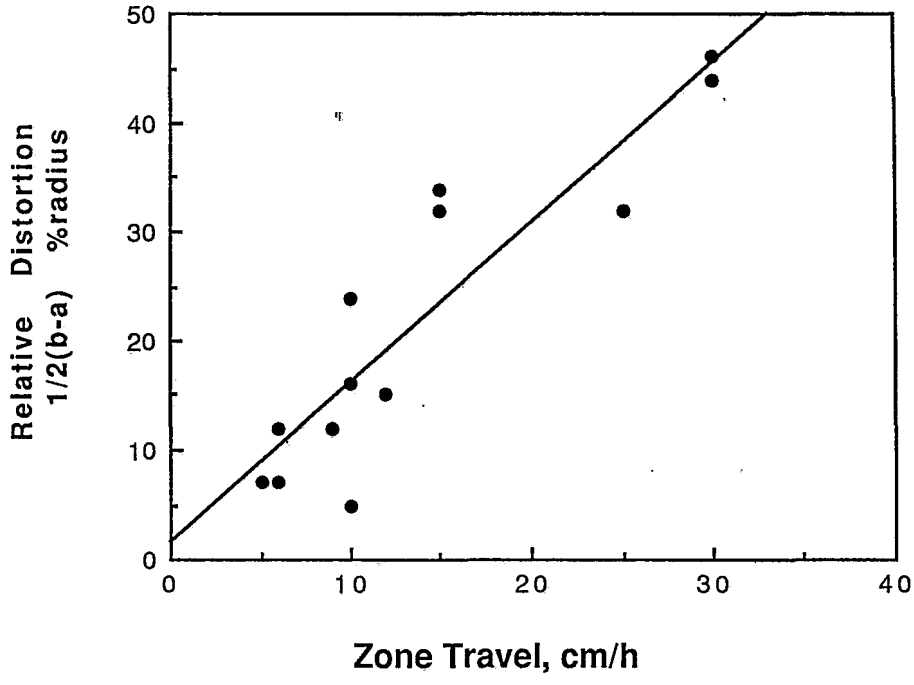

Fig.3.10.4 Distortion caused by increase in the growth rate (The quantities **a** and **b** are illustrated in fig 3.10.3).

The gradient (G_S) in the solid for the case of a vertical floating zone has been calculated by Flemings (1974), with the following assumptions:

(1) the crystal is of circular cross section,

(2) heat transfer from the crystal to surroundings is by convection,

(3) growth is at steady state, and

(4) temperature gradients within the crystal transverse to the growth direction are low.

The thermal gradient in the solid at the liquid-solid interface is given by

$$G_S = -(T_M - T_0)\left[\frac{R}{2\alpha s} - \sqrt{\left(\frac{R}{2\alpha s}\right)^2 + \frac{2h}{aK_S}}\right] \qquad 3.10.4$$

where T_M is the melting point of the metal, T_0 is the temperature far from the hot zone, α_S is the thermal diffusivity of the solid, a is the radius of the crystal and h is the heat coefficient for heat loss to surrounding.

For crystals of high melting point, where $(T_M - T_0)$ is large and the coefficient of heat transfer h is increased by radiation heat transfer, thermal gradients attainable are quite high, 100°C/cm or more. For lower-melting-point materials, other cooling is necessary to attain steep gradients.

CHAPTER FOUR

GENERAL REVIEW OF SOLIDIFICATION OF MAGNETIC MATERIALS

4.1 Introduction

In this chapter a brief review of relevant works directly or indirectly related to solidification or techniques of solidification of magnetic materials is carried out. Although not used in the present work, attention is given to work on directional solidification in a magnetic field since this can be used in future work based on this thesis. Work on cast and sintered Pr-Fe-B magnets were not included and will be dealt with separately in chapters 5 and 6.

Directional solidification (DS) of materials has been applied to many ferromagnetic compounds. The main purpose was to produce cheaper magnets, although some studies were directed towards other objectives, as shown in table 4.1.1.

Table 4.1.1 Controlled solidification studies.

MATERIALS	APPLICATIONS	REFERENCES
ALNICO	Hard Magnetic Properties.	Makino and Kimura (1965)
Sm2Co17-Co	Hard Magnetic Properties.	Sahm and Hofer (1970)
SmCo5-SmCu5	Hard Magnetic Properties.	Kimura and Kamino (1970)
Sm-Fe-Co-Cu-Zr	Hard Magnetic Properties.	Heng-zhy Fu et al. (1989)
Nd15Fe77B8	Hard Magnetic Properties.	Ward and Taylor (1989)
Co-Nb-Fe	Soft Magnetic Properties	Colling and Kossowsky (71)
Fe-Si	Soft Magnetic Properties	Fisher and Walter (1962)
SmCo3Cu2	Mechanical Properties	Glardon and Kurz (1978)
Nd15Fe77B8	Hydrogen Absorption	Abell and Harris (1988)
TERFENOL-D	MagnetostrictiveProperties	Verhoeven et al. (1990)
Nd-Fe-B (Co,Al,Dy)	Microstructural studies	Thorsen and Jorgensen (90)
Sm2Co17-Co	Degree of Macrosegregation	Pirich (1986)
Pr-Fe-B-Cu	Hot Pressed Magnets	Shimoda et al (1990)

4.2 Alnico

Magnetic materials like alnico which derive their magnetic hardness from shape anisotropy consist of a fine dispersion of magnetic needles in a matrix of non-magnetic or weakly magnetic material. The ferromagnetic Fe-Co or Fe rich particles (α_1 phase) and the non-ferromagnetic or weakly ferromagnetic Ni-Al rich matrix (α_2 phase) have bcc structures and are formed by spinodal decomposition (Cahn and Hilliard 1958-59) rather than by a nucleation and growth process.

Hoselitz and McCaig (1949) showed that a further improvement in the magnetic properties of field cooled polycrystalline alnico 5 could be obtained if the grains have a preferred crystal orientation so that the α_1 (Fe-Co) particle's [100] axes, in the whole alloy, are as well aligned as possible. Fortunately, if iron-base alloys such as the alnicos are allowed to solidify on a cold surface, the [100] axes tend to grow preferentially perpendicular to the surface so that the desired grain orientation or columnar grain structure can be produced relatively easily. Thus when alnico alloys are cast with a columnar microstructure, or preferred grain orientation, thermomagnetic treatment with the applied field parallel to the preferred, or columnar, axis results in a significant improvement in the magnetic properties compared with the alnico 5 alloys, which have randomly oriented grains.

In order to obtain well oriented columnar magnets it is necessary to use pre-heated or exothermic moulds and to cast the magnets on water cooled copper slabs. Several techniques were used in the investigations and production of alnico 5-7 via

directional solidification. The earliest investigation into this material using unidirectional casting in a controlled manner was carried out by Ebeling and Burr (1953). More than a decade later Gould (1964) employed an exothermic mould with chill on the lower face. A year later Makino and Kimura (1965) applied zone melting with directional water cooling for the production of columnar crystals of alnico and soon after Hoffmann and Stablein (1966) used horizontal zone melting. In the early 70's, Higuchi and Miyamoto (1970) used zone melting on this material, and Sergeyev and Larichkina (1970) applied the Bridgemann technique with an oriented seed. Finally Durand-Charre, Bronner and Lagarde (1978) employed vertical zone melting to alnicos. All these investigations led to significant improvements in the magnetic properties of the alnicos, but the interest in these materials progressively diminished as they were gradually replaced by oriented $BaFe_{12}O_{19}$ and $SrFe_{12}O_{19}$ magnets, which were much cheaper.

4.3 Elongated Single Domain Magnets (ESD)

Independent of alnico magnets, intensive efforts were made to develop ESD magnets composed of very fine needles of a Fe or Fe-Co alloy consolidated by soft metals, such as lead (Luborsky1961). The coercivity of both alnico and ESD magnets originate from the shape anisotropy of elongated fine particles. The theory (Stoner and Wohlfarth1948) predicted that a sufficiently long fine particle of Fe containing no domain walls would have a coercivity as large as 800 KAm^{-1} (10 kOe) if all of the magnetic moments in the particle rotated simultaneously while maintaining

each direction parallel (in the coherent mode). In order to increase the coercivity of such elongated fine particles or rod-like particles extensive work was carried out using unidirectional solidification, which can be summarized as follows.

Albright, Conard and Kraft (1967) applied controlled solidification to Fe-FeS eutectic passing a molten zone through the specimen and producing an aligned parallel array of Fe rods of approximatelly 2 μm in diameter (continuous length) embedded in and separated by a matrix of FeS. The magnetic properties were improved when compared to the as-cast material.

In the InSb-NiSb (Muller and Wilhelm1967) system for instance, the diameter of the needles decreases from 5 to 0.5 μm if the growth rate was increased from 0.6 cm/h to 6 cm/h (continuous length). The diameter of the rod-like inclusions is proportional to the square root of the growth rate. A similar result was obtained by Livingston (1970) in the Au-Co eutectic: the diameter of the cobalt needles decreased with increasing growth rate and the coercivity also increased substantially. Those experiments demonstrated that the intrinsic coercivity increases with increasing growth rate, however the usefulness of the method of increasing the growth rate was limited, since at higher rates the microstructure was more lamellar than rod-like, which again reduces the coercivity.

Sahm (1969-71) modified the microstructure of eutectic Au-Co alloys by use of a magnetic field during directional solidification using a vertical growth method. The advantage of applying a magnetic field is due to the Curie temperature in this material being higher than the eutectic temperature ($T_{curie} > T_{eutectic}$), thus the magnetic field was used to orientate the ferromagnetic

component.

Basic studies on ESD magnets revealed that, upon increasing the packing density of fine particles, the coercivity decreases as a result of interactions between particles (Néel 1947), and that the coercivity of elongated single domain particles is not so large as that expected for the coherent rotation. This is because the magnetic moments in an elongated single domain particle do not necessarily keep each direction parallel in its magnetization reversal; that is, there exist several modes of easier rotation of magnetic moments such as fanning, curling and buckling modes (Jacobs and Bean 1956). Thus, about 160 KAm^{-1} (2 KOe) was the limit of coercivity obtained from shape anisotropy in Alnico as well as ESD magnets.

4.4 Mn-Bi

Extensive work has been done in the controlled solidification of Bi-Mn alloys by Noothoven van Goor and Zijlstra (1968), Notis et al. (1978), Pirich and Larson (1979) and Notis et al (1979) to obtain microstructures consisting of aligned particles of Mn-Bi dispersed in a Bi-matrix. Sahm (1969-71) and later Savitsky et al. (1981) studied the effect of Bi-Mn crystallization in a magnetic field.

Bi-Mn is an intermetallic compound, which is somewhat difficult to produce in a pure state. It has a high coercivity based on crystal anisotropy but both fall to zero at low temperatures. The Curie point is low and the material is subject to corrosion.

4.5 Sm-Co

Since the appearance of rare earth based magnets wide attention has been paid to the development of RE-TM permanent magnets via directional solidification. Alloys with compositions close to $RECo_5$ are magnetic, but have low coercivities in the as cast state. Permanent magnets can be made by casting and subsequent heat treatment, if copper is also present. Nesbitt and Wernick (1973), who discovered this process in 1968, describe it in more detail than is possible here. Fundamentally they consider that $RECo_5$ and $RECu_5$ form a solid solution at high temperatures, but that this solid solution dissociates at lower temperatures, possibly by a spinodal process. In this way a fine structure conducive to permanent magnetism is produced.

Increasing the amount of Co that is replaced by Cu tends to reduce Ms and consequently Br, but increases iHc. As with powders and sintered material, Sm appears to be the best rare-earth metal, but with these cast alloys the difference between the results obtained with Sm and with the cheaper Ce or even misch-metal are comparatively small. Attempts to produce magnets by this method, using Pr, have so far failed. Replacement of part of the Co by Fe, which is disastrous in sintered $RECo_5$ magnets, is actually beneficial in these cast alloys. As mixtures of Sm and Ce or misch-metal may be used, many composition variations are possible in this five component system. The optimum heat treatment for these magnets involve typically a quench from 1000°C, followed by a few hours at about 400°C. (BH)max values up to about 100 kJ/m^3 (just over 12 MGOe) have been obtained.

Kimura and Kamino (1970) also showed that the intrinsic coercivity of the intermetallic compound $SmCo_5$ was not sufficient for its application as a permanent magnet in the cast state. They also observed directional magnetic properties in the $SmCo_5$-$SmCu_5$ system alloy, as a result of freezing, in a direction normal to the cold surface of a copper hearth (arc melt furnace). The maximum energy product of a 65 W% Sm Co_5 - 35W% Sm Cu_5 alloy was 5.78 MGOe, in the cast state. By annealing their specimens at 300°C for 1 hour, the $(BH)_{max}$ value increased to 7.73 MGOe with a Br of 6.45 kG and a bHc of 3.4 kOe.

Sahm and Hofer (1970) in pioneering work studied the directional solidification of eutectic Sm_2Co_{17}-Co alloys using an induction heated crystal grower. According to these workers the diameter, D_f, of the rounded cobalt fibers may be described as a function of the growth rate, R, where $D_f=10^{-5}\,R^{-1/2}$. Metallographic characterization and magnetic measurements suggested that the observed magnetic anisotropy could be related to both shape anisotropy of Co-fibers and the crystal anisotropy of the Sm_2Co_{17}-matrix. The most recent report on this alloy was carried out by Pirich (1986), who studied the effects of directional solidification processing on the microstructural, compositional, and magnetic properties of near eutectic Sm_2Co_{17} alloys. The magnetic properties obtained from the magnets were very poor.

Cullen (1971) succeeded in casting small buttons of RE-Cu-Co alloy in an arc melting apparatus with a water cooled copper hearth equipped for vacuum work. A cerium alloy, Permaflux C, with an energy product of 7.0 MGOe was produced in larger quantities.

Gilbert et al. (1972) working with Ce-Co-Fe-Cu alloys and

using a modified Bridgman technique prepared permanent magnets with columnar grain structure and preferred crystallographic orientation. Samples melted at low superheat temperatures ($\Delta T \approx 20°C$ above the melting point of about 1100°C) and solidified at moderate rates (~2.3 cm/h) resulted in a reasonably homogeneous columnar grain structure with a preferred crystallographic orientation. The c-axis was generally aligned within 15° of the growth axis. Increasing the speed of solidification led to a fine-grained structure with no texture, while decreasing the speed led to coarse columnar grains with erratic orientation. A large superheat temperature (Δ T 300-400°C) resulted in a reaction of the liquid with the alumina crucible wall and led to the formation of face-centered cubic Co-rich dendrites. With the modified Bridgman technique, oriented samples 8 cm long and 2.54 cm in diameter have been prepared with good magnetic properties. After annealing at 1000°C followed by aging at 400°C the alloy exhibited values of iHc= 6 kOe, Br = 6.25 kG, and (BH)max= 9. 5 MG Oe.

A DS technique was applied by Colin and Racek (1974) to $SmCo_{5-x}Cu_x$ and $CeCo_{5-x}Cu_x$ alloys in order to obtain single-phase, homogeneous alloys. The single-crystal orientation was found to be dependant on the alloy composition and only in the case of low rare-earth dendritic alloys was the 0001 direction of growth clearly established.

Glardon and Kurz (1978 and 1981) and Draper (1979) used controlled solidification to improve the mechanical properties of Sm-Co alloys. The problems due to inherent brittleness of sintered RE-Co magnets could be alleviated with the use of the controlled solidified alloy.

The most recent report on Sm-Co-type magnets via directional solidification was carried out on Sm-Ce-Fe-Cu-Zr-Co alloy by Heng-zhi Fu et al. (1989). They have succeeded in preparing good magnets from this alloy using directional solidification technology with liquid metal cooling (DSTLMC). The advantage of this technique is that much higher thermal gradients can be obtained when compared with conventional techniques. They used thermal gradients of 200-300 °C/cm in the solid-liquid interface and growth rates of 0.3-240 cm/h. The best obtained values of remanence, intrinsic coercivity and energy product (after heat treatment) are 9.5 kG, 5.0 kOe and 18 MGOe respectively. They showed that the magnets prepared using DSTLMC are much less brittle than the sintered magnets, although no ductile phase was introduced. This was attributed to the very long fibers (2/17 and 1/5 phases) of the magnets, having a length/diameter ratio of 100.

4.6 Nd-Fe-B

A thorough investigation of solidification has been carried out by Ogilvy, Gregan and Davies (1984), who studied the influence of the cooling rate during solidification and of the boron concentration on the constitution and microstructure of Nd-Fe-B alloys. Their results from studies on 5 mm thick buttons of $Nd_{13.5}Fe_{81.7}B_{4.75}$ alloy cast in an argon arc furnace (studied as a function of the distance from the chill face) revealed that : up to ~ 100 μm from the chill face (i.e. at cooling rates approximately > 773 °C/s) no free iron was present, the primary phase being ø ($Nd_2Fe_{14}B$). Clearly, at the high cooling rate, the formation of free Fe

was being suppressed. However, beyond ~100 μm, partly consumed free iron was present and thus also more of the $Nd_{1+\varepsilon}Fe_4B_4$ and Nd-rich phases.

Shimoda et al. (1988) carried out a brief study in cast NdFeB magnets with and without Cu additions. In their work on the $Nd_{17}Fe_{79}B_4$ alloy, the cast ingots showed very poor magnetic properties after annealing at 1000 °C for 24 hours (for eliminating free iron), with a remanence of 3.4 kG, an intrinsic coercivity of 0.7 kOe and an energy product of 0.6 MGOe. Their results with the alloy with copper substitution ($Nd_{17}Fe_{76.5}B_5Cu_{1.5}$) were also rather disappointing, after the same annealing the magnetic results were: Br=2.9 kG, iHc=0.6 kOe and $(BH)_{max}$=0.4 MGOe. Their results in the PrFeB cast magnets were more promising and will be presented in the next chapter.

An extremely thorough investigation of the modification of the microstructure of $Nd_{15}Fe_{77}B_8$ alloy by controlled solidification has been carried out by Abell and Harris (1988). They studied the influence of the solidification behaviour on the microstructure, hydrogen absorption characteristics and magnetic domains of this alloy. Their microstructural observations on the $Nd_{15}Fe_{77}B_8$ alloy solidified by horizontal and vertical float zoning techniques (growth rates of 2-5 cm/h) allowed the phase distribution, grain size distribution and the nature of the solid-liquid growth interface to be studied and compared with the as-cast microstructure. Their investigations on the hydrogen absorption behaviour of controlled solidified $Nd_{15}Fe_{77}B_8$ alloy showed that the absorption of hydrogen in such alloys depends upon the phase distribution. They showed that samples taken from the clean, large grained region of the

horizontally solidified bar absorbed no detectable hydrogen when subjected to a pressure of 1 bar at room temperature (DTA equipment). However, a sample from the quenched multi-phase structure, showed a large exothermic reaction associated with the Nd-rich material. A summary of the DS best results is shown in table 4.6.2.

TABLE 4.6.2 Best hard magnetic properties obtained using DS.

ALLOY TYPE TECHNIQUE	Br [kG]	iHc [kOe]	BHmax [MGOe]	Ref.
SmFeCoCuZn DSTLMC	9.5	5.0	18.0	Heng-zhy Fu et al.(1989)
SmCoCu FLOATING ZONE	8.0	5.5	14.0	Draper (1979)
RECoCu BRIDGMAN	7.0	5.5	10.0	Glardon Kurz (1978)
CeFeCoCu MODIFIED BRIDGMAN	6.1	7.0	9.5	Gilbert et al. (1972)
SmCo-SmCu ARC-MELTING	6.4	3.4	7.7	Kimura and Kamino (1970)

4.7 Solidification in a Magnetic Field

The effects of a magnetic field on natural-convection heat transfer in a conducting fluid have been described by Cole (1969). A magnetic field decreases the heat transfer rate by a viscous-drag effect; that is, the fluid is constrained by Lorentz forces to move in a plane normal to the directions of field and flow. If the magnetic flux lines cross, say a downward moving flow, the flow will be "dragged" and inhibited. The result is that the convective heat transfer rate is decreased; and at sufficiently high fields, the Nusselt number (relative amount of heat transferred by convection) approaches unity and the fluid transfers heat by conduction only.

Studies done by Wojciechowski and Chalmers (1968) showed that the application of mechanical stirring during the unidirectional solidification of Al-Cu samples resulted in a significant change in the structure as compared with samples solidified without stirring. A significant acceleration of the columnar to equiaxed transition (i.e., a decrease of the length of the columnar zone) was caused not only by an increase of the solute content and a lowering of the temperature at which the cooling was initiated but also by an increase in the intensity of stirring.

Morando et al. (1970) showed that certain relationships such as the length of the columnar region as function of superheat described by Chalmers (1964) are valid only for small ingots. Their conclusions can be summarized as follows (for Al-Cu alloys).

In the absence of a magnetic field the length of the columnar zone, proceeding from the base of the ingot, provided a good indication of structure change. For small ingots the columnar zone did lengthen with increased superheat, as expected and reported by Chalmers (1964). In the medium ingots the extent of the columnar zone also varied somewhat from the base of the ingots; but for large ingots the extent was really invariable for all superheats. The complete suppression of the equiaxed zone for intermediate and large superheats was possible for Al-Cu alloys by an applied magnetic field (2.2 kG), which dampened convection during the whole process of casting to the end of freezing (small ingots).

For small ingots there was a critical superheat : below 40°C the ingot structure was practically 100 pct equiaxed; for the superheats between 60 and 150°C the equiaxed grains were eliminated and a completely columnar structure was developed.

Medium ingots revealed distinct differences. Below 40°C practically 100% equiaxed structure was again noted. At 60°C superheat only a perimeter effect remained, i.e., a peripheral zone of fine grains outlining the ingot. Then in the superheat range between 80 and 150°C this fine-grain peripheral zone disappeared and only the typical gross columnar and gross equiaxed grain structures were seen. It was notable that the extent of the columnar zone was practically independent of the superheat. For large ingots, the results were essentially equivalent to medium ones, except for a shift in the temperature at which peripheral grains disappeared.

The values of the temperature gradient for the columnar to equiaxed transition are much higher for stirred samples. This means that transition may occur in stirred samples even when the temperature gradient ahead of the solidification front is much steeper than in unstirred samples. The probability of nucleation of the equiaxed crystals is therefore reduced.

Their observations include the configuration of the columnar to equiaxed transition and the copper distribution at this transition. It was found that the first equiaxed crystals may form something like a network and the solute build-up is very similar to that of the terminal transient of a normally frozen sample. They concluded that the columnar crystal growth can be stopped by the already existing network of equiaxed crystals. Their explanation of the stirring effect consists of two important mechanisms. The first one is the generating of a 'cloud" of crystals in the liquid, which results from the melting off of dendrite fragments. The other mechanism is the lowering of the actual temperature at some distance ahead of

the solidification front which enables the survival and, subsequently, the growth of these dendrite fragments. The lowering of the temperature in the melt results from the better heat extraction out of stirred liquid as well as from the latent heat consumption by the partly remelting dendrite fragments.

Directional solidification has been applied to binary eutectics (see Table 4.7.1) in which the Curie temperature is higher than the eutectic temperature ($T_{Curie} > T_{Eutectic}$) and where a magnetic field has been used to crystallographically orient the ferromagnetic component (Sahm1969). Controlled solidification is used to produce a fibrous composite and the magnetic field is expected to keep the alignment in one preferred orientation.

Table 4.7.1 Eutectic and Curie temperatures of binary systems.

Composition* (at.-fraction)	Te(°C)	Tc(°C)
Co - Co_5As_2	918	925
$Co_{0.04}$ - $Bi_{0.96}$	271	1121
Co - Co_2P	1023	1115
Bi - Bi Mn	262	360

Directional solidification in a magnetic field has also recently been applied by Mikelson and Karkin (1981) to paramagnetic and diamagnetic materials with the same purpose. They studied the following alloys Al-Ni, Cd-Zn, Bi-Cd and Al-Cu. According to them the orienting action of the magnetic field must always affect the oblong crystal of any alloy depositing from the melt, because there always is a difference in the magnetic properties of the crystal and the melt. Although this effect is not so strong as in the case of ferromagnetic eutectic alloys it can be used to align the forming crystals.

CHAPTER FIVE

PrFeBCu CAST MAGNETS

5.1 Introduction

Praseodymium and neodymium are very similar in the elemental state and in $RE_2Fe_{14}B$ compounds. However, in $Nd_2Fe_{14}B$ a spin reorientation occurs at lower temperatures (150 K) whereas, $Pr_2Fe_{14}B$ exhibits no spin reorientation down to liquid helium temperatures and has a higher anisotropy field compared with that of $Nd_2Fe_{14}B$ ($H_{A\ (at\ 300\ K)}$: 87 and 67 kOe respectively). Thus at low temperatures, $Pr_2Fe_{14}B$ exhibits smaller variations in the magnetic properties than $Nd_2Fe_{14}B$, indicating more stability for low temperature applications. The hard magnetic properties of $Nd_2Fe_{14}B$ alloys are generally very poor in the cast state. Recently, however, it has been found that the PrFeB-based alloys can exhibit appreciable magnetic properties even in the bulk ingot state by employing a proper heat treatment and the addition of a minor element such as Cu or Al. In this chapter, a detailed discussion of such magnets will be carried out.

5.2 Development of Cast PrFeB Magnets

In 1988 Shimoda et al. (1988) announced a new development in the field of cast magnets based on Pr-Fe-B alloys. They showed that, after annealing, some of these cast alloys achieved good hard magnetic properties. As a preliminary investigation a thorough examination of the dependence of the intrinsic coercivity and the energy product on a wide range of compositions of cast Pr-Fe-B

alloys after a heat treatment at 1000°C for one day was carried out. As an illustration their results are reproduced in Figs. 5.2.1 and 2.

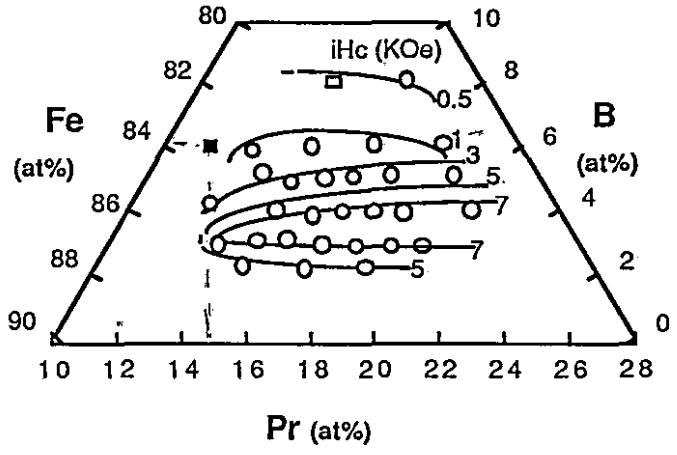

Fig.5.2.1 Dependence of iHc on the composition of Pr-Fe-B cast magnets. (Solid black square represents the stoichometric composition $Pr_2Fe_{14}B$, and the white square the composition $Pr_{15}Fe_{77}B_8$)

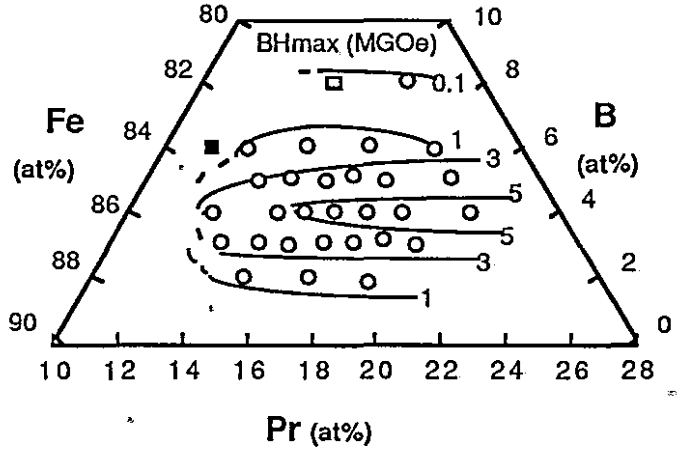

Fig.5.2.2 Dependence of (BH)max on the composition of the Pr-Fe-B cast magnets (after Shimoda et al. 1989a).

Examining the composition upon this wide range of cast alloys they detected magnetic hardening on the Pr-rich side as well as in the B-less side of $Pr_2Fe_{14}B$. The largest coercivity was obtained when the boron content was lower than the stoichiometric composition ($Pr_2Fe_{14}B$). Plotting the relationship between the amount of boron, iHc and (BH)max they showed that both properties reach their peaks when the boron concentration is 4 at% (see fig. 5.2.3). In the same way these magnetic properties were plotted against the Pr content when boron was fixed in 4 at% (see fig. 5.2.4) and it was shown that the intrinsic coercivity and energy product increase with increasing Pr content. In this work it was also noticed that the boron content in the best composition of cast magnets ($Pr_{17}Fe_{79}B_4$) is lower than the optimum composition reported by Sagawa et al. (1984) for sintered magnets ($RE_{15}Fe_{77}B_8$), and the Pr content is higher.

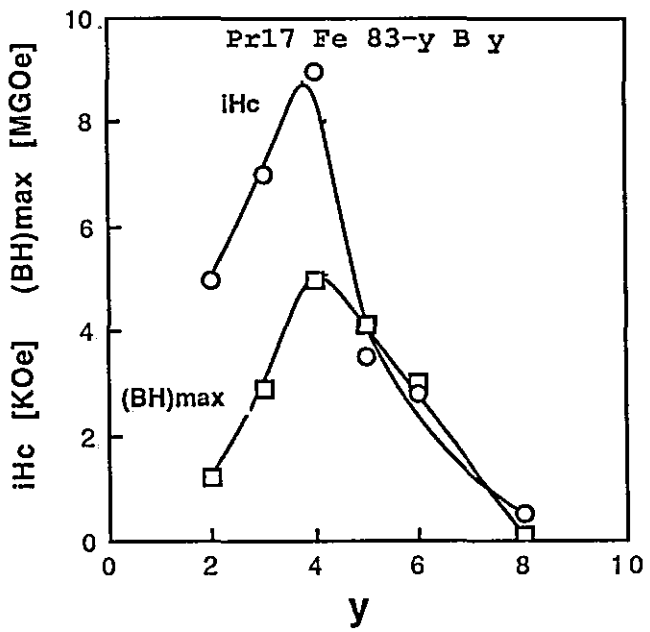

Fig 5.2.3 Dependence of magnetic properties of Pr-Fe-B magnets on boron content ($Pr_{17}Fe_{83-y}B_y$).

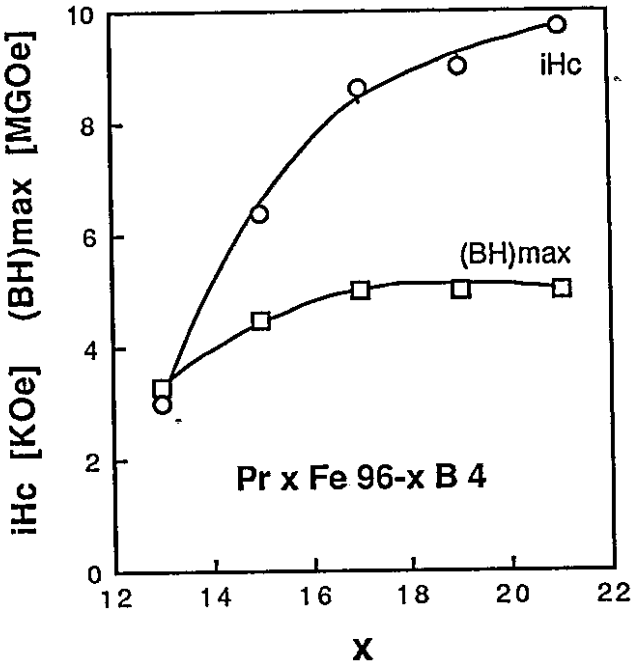

Fig 5.2.4 Dependence of magnetic properties of Pr-Fe-B magnets on Pr content ($Pr_xFe_{96-x}B_4$).

The dependence of the intrinsic coercivity on the annealing time at various temperatures has also been investigated in this work (Shimoda et al. 1989a) for the $Pr_{17}Fe_{79}B_4$ alloy (see fig 5.2.5). The increasing pattern of the iHc with annealing time was very similar for the various temperatures, i.e., the iHc increased sharply up to 1 hour, gently up to 10 hours and then it saturated after that. The highest iHc was 9.6 KOe, obtained from the composition of $Pr_{17}Fe_{79}B_4$ and after annealing at 1000°C for 24 hours. The remanence and energy product of this magnet was 5.8 kG and 6.2MGOe, respectively. The steep rise in the initial magnetization curve indicated a type of nucleation controlled coercivity mechanism. The best magnetic properties in these cast magnets were also obtained by measurements perpendicular to the crystals growth direction , i.e.,

parallel to the mould walls. The easy magnetization direction was found to be in the plane perpendicular to the grain growth direction.

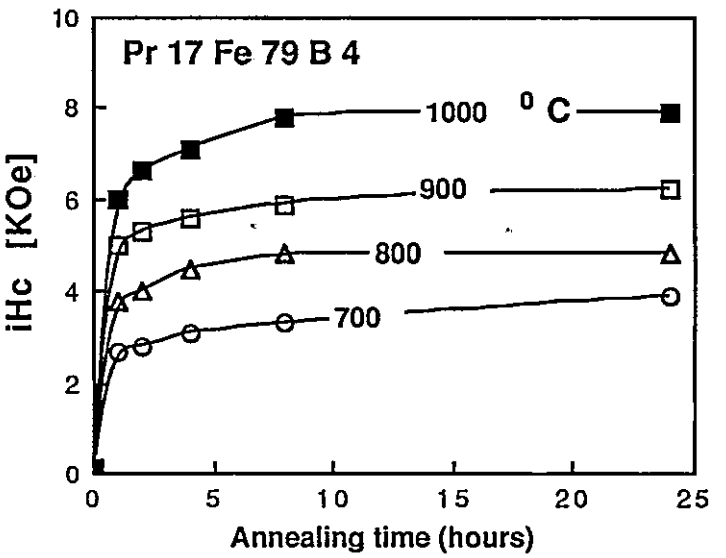

Fig 5.2.5 Dependence of the magnetic properties of Pr-Fe-B magnets on annealing time ($Pr_{17}Fe_{79}B_4$).

5.3 The Effect of Substitutions on PrFeB Alloys

Shimoda et al. (1988-1989a,b,c) also investigated cast magnets based on the Pr-Fe-B alloys with the substitution of a fourth element. As a result of assessing numerous elements (Cu, Ag, Au, Pd) they found that copper was the most applicable. Using the optimum composition for the ternary cast alloy ($Pr_{17}Fe_{79}B_4$) they substituted Fe by Cu and found that the magnetic properties reached a maximum when the Cu substitution was between 1.5 and 2.0 at%. Thus, by fixing the amount of copper at 1.5 at% the

relationship between boron and magnetic properties was again established (see fig 5.3.1).

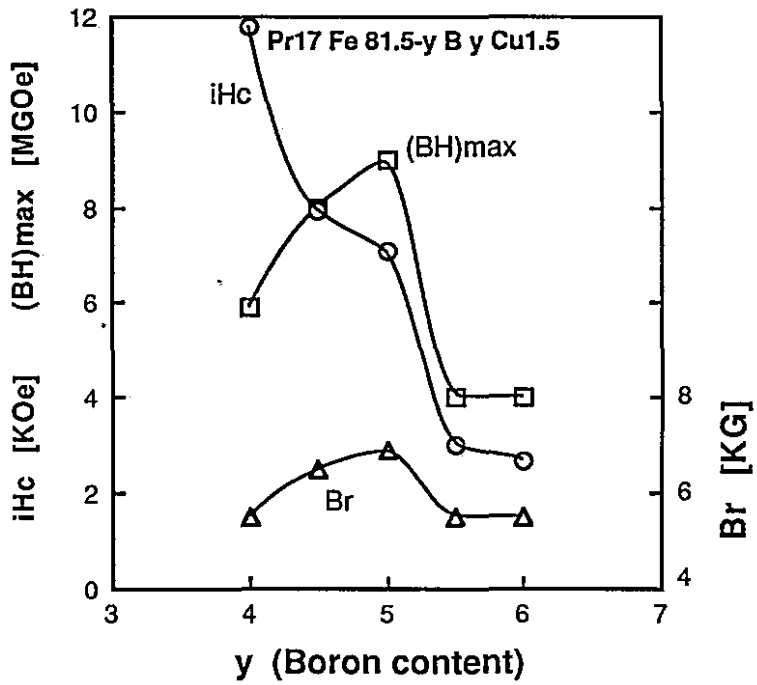

Fig 5.3.1. Dependence of magnetic properties of Pr-Fe-B-Cu magnets on boron content ($Pr_{17}Fe_{81.5-y}B_yCu_{1.5}$).

Two compositions emerged from this investigation: $Pr_{17}Fe_{76.5}B_5Cu_{1.5}$ and $Pr_{17}Fe_{77.5}B_4Cu_{1.5}$. The magnets from the first alloy showed the best remánence and energy product. The magnets prepared from the second alloy were found to have higher intrinsic coercivity than the former but at the expense of a reduction in Br and (BH)max. The best magnetic properties in these cast magnets were also obtained by measurements perpendicular to the crystals growth direction.

Recent studies carried out by Kwon, Bowen and Harris (1991) investigated the Pr-Fe-B-Cu alloys with higher Pr content than 17 at%. A detailed microstructural study of the $Pr_{20.5}Fe_{73.8}B_{3.7}Cu_2$ alloy was carried out. This study will be discussed in a later section of this chapter. A comparison of the magnetic properties of the $Pr_{20.5}Fe_{73.8}B_{3.7}Cu_2$ magnet with the previous ones is given in table 5.3.1. In this study the standard $Pr_{17}Fe_{76.5}B_5Cu_{1.5}$ alloy was also investigated. The magnetic properties obtained were inferior (Br=5.8 kG, iHc = 3.9 kOe, BHmax = 4.8 MGOe) than that reported by Shimoda et al. (1988) for this alloy. The casting conditions could be the cause of such differences.

Table 5.3.1 Magnetic properties of Pr-Fe-B(Cu) cast magnets after annealing at 1000°C for 24 hours.

Alloy type	Br [KG]	iHc [KOe]	BHmax [MGOe]
$Pr_{17}Fe_{76.5}B_5Cu_{1.5}$	6.6	7.4	8.8
$Pr_{20.5}Fe_{73.8}B_{3.7}Cu_2$	6.1	10.7	7.6
$Pr_{17}Fe_{79}B_4$	5.8	9.6	6.2
$Pr_{17}Fe_{77.5}B_4Cu_{1.5}$	5.6	11.8	5.8
$Pr_{15}Fe_{77}B_8$	0.8	0.5	0.1

The addition of other elements by Shimoda et al. (1989a) were also effective in raising the coercivity in the cast magnets, although not as much as copper. For a comparison and reference, the magnetic properties of cast $Pr_{17}Fe_{76.5}B_5M_{1.5}$ (M=Cu, Ag, Au or Pd) are given in table 5.3.2. They also showed that the magnetic properties of Pr-Fe-B-Cu magnets, versus the annealing temperature, saturated at a lower temperature than in the case of Pr-Fe-B magnets. It was concluded that for Pr-Fe-B-Cu alloys the

heat treatment can be carried out at a fairly low temperature (see figure 5.3.2). The values of the intrinsic coercivity in these experiments are rather low for the $Pr_{17}Fe_{76.5}B_5Cu_{1.5}$ magnets, indicating that even using alloys with the same composition different results can be expected. Finally, Faria, Abell and Harris (1991), in a work on controlled solidification of a $Pr_{20.5}Fe_{73.8}B_{3.7}Cu_2$ alloy, obtained cast magnets with an energy product of 12.3 MGOe.

Table 5.3.2 Magnetic properties of Pr-Fe-B-M cast magnets after annealing at 1000°C for 24 hours.

$Pr_{17}Fe_{76.5}B_5M_{1.5}$	Br [KG]	iHc [KOe]	BHmax [MGOe]
M = Cu	6.9	7.3	9.2
Ag	6.4	6.5	7.9
Au	6.3	5.8	7.7
Pd	6.2	6.7	7.5

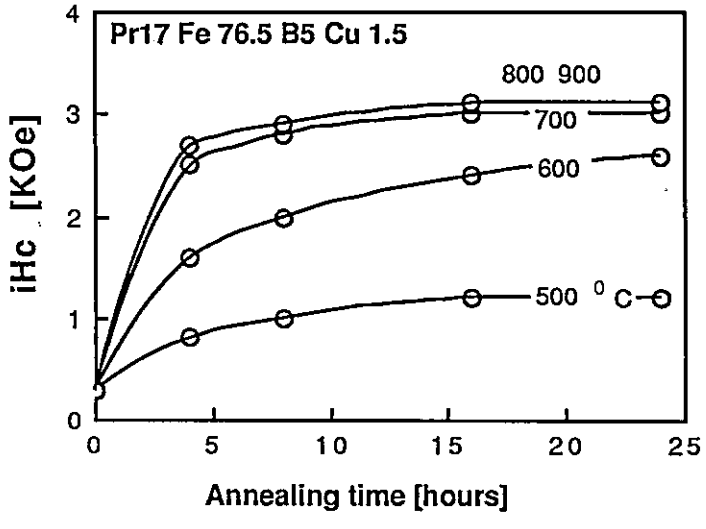

Fig. 5.3.2 Dependence of the intrinsic coercivity of $Pr_{17}Fe_{76.5}B_5Cu_{1.5}$ magnets on the annealing time and temperature.

5.4 Phase Relationships in the PrFeB and PrCu Systems

A study of the Pr-Fe-B ternary system has been carried out by Jinghua, Yiying and Jingkui (1987). The vertical section diagram of Fe-$Pr_2Fe_{14}B$-Pr is reproduced here in fig. 5.4.1. The phase diagram was established from thermal analysis data and can be described as follows.

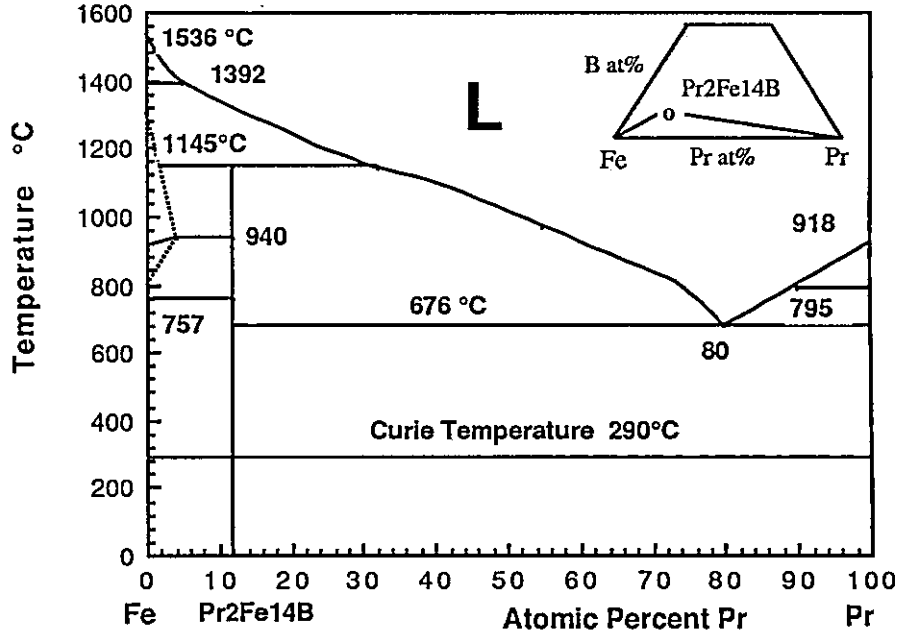

Fig. 5.4.1 The vertical section diagram of Fe-$Pr_2Fe_{14}B$-Pr.

The vertical section diagram of Fe-$Pr_2Fe_{14}B$-Pr is quite similar to the binary phase diagram of the Pr-Fe system. The ternary compound $Pr_2Fe_{14}B$ is formed peritectically at 1145°C and the corresponding liquid temperature of $Pr_2Fe_{14}B$ is about 1298 °C. A eutectic isotherm exists between $Pr_2Fe_{14}B$ and Pr, the eutectic point is situated at the position of $Pr_{80}Fe_{18.6}B_{1.4}$ and the eutectic temperature is 676°C. The Curie temperature of $Pr_2Fe_{14}B$ is 290°C

measured by DTA. The phase diagram indicates that the $Pr_2Fe_{14}B$ phase does not melt congruently, which means that solidified melts of the stoichiometric composition are not single phase, the primary crystallites consisting of Fe. The amount of Fe depends to some extent on the cooling rate, with single phase materials being obtained by a long annealing treatment of the as-cast material. An excess of boron and Pr is required to suppress the formation of α-Fe as primary crystals.

Subramanias and Laughlin (1988) investigated the binary phase diagram of the Pr-Cu system, which is reproduced in fig. 5.4.2.

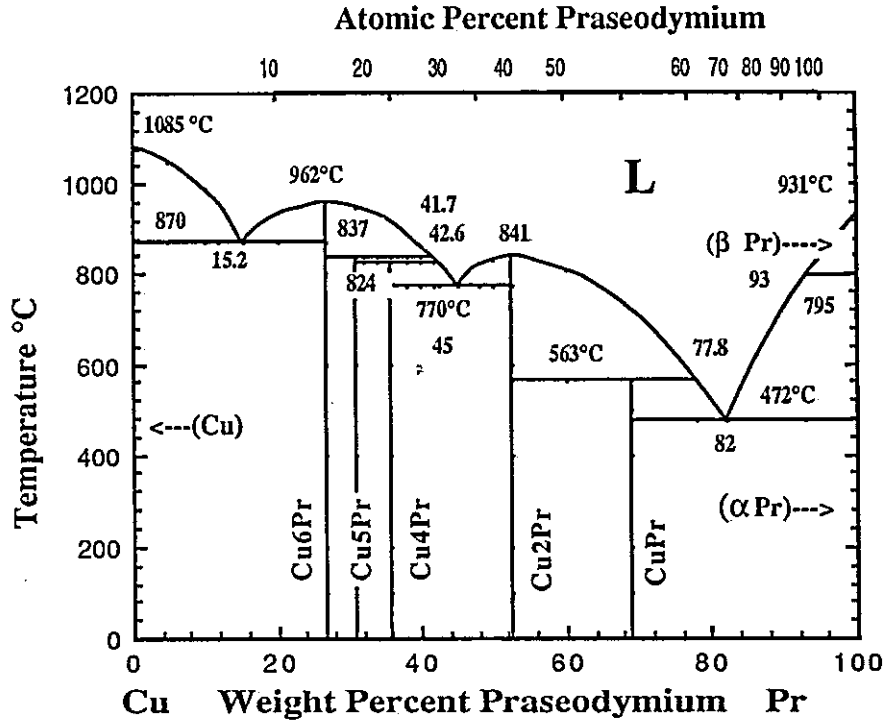

Fig. 5.4.2 The Pr-Cu binary phase diagram.

On the Pr side of the binary diagram, which is of interest in the present work, or more precisely, between CuPr and αPr, there

exists a eutectic isotherm, at which the eutectic point is about 68 at% of Pr and the eutectic temperature is 472°C. It has been suggested that this eutectic reaction plays an important role in the coercivity of Pr-Fe-B-Cu cast magnets. A detailed discussion of this eutectic reaction will be presented in the next sections.

5.5 Crystal Structure of $Pr_2Fe_{14}B$

Jinghua, Yiying and Jingkui (1987) also carried out some determinations of the $Pr_2Fe_{14}B$ crystal structure. The structure of the $Pr_2Fe_{14}B$ is the same as that of $Nd_2Fe_{14}B$, and the Pr atoms occupy the positions of the Nd atoms (see fig. 5.5.1).

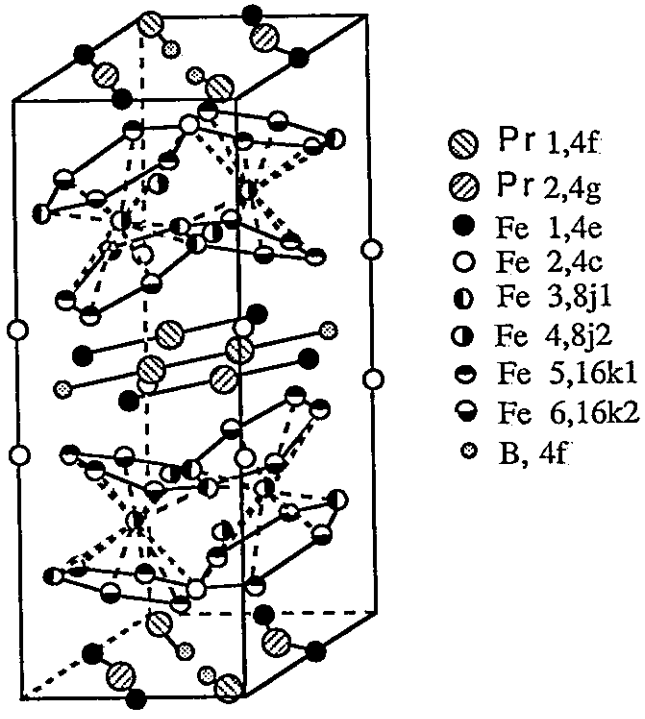

Fig.5.5.1 Crystal structure of $Pr_2Fe_{14}B$.

The $Pr_2Fe_{14}B$ cell is tetragonal with space group $P4_2/mnm$,

the lattice constants are a=0.8808nm, and c= 1.2244 nm. The calculated density is 7.513 g/cm^3 and the observed is 7.51 g/cm^3 . In a unit cell there are four formula units, i.e., 8 atoms of Pr, 56 atoms of Fe and 4 atoms of B.

5.6 Typical Microstructures of PrFeB(Cu) Alloys

A brief study on the composition and solidification behaviour of Pr-Fe-B alloys has also been carried out by Shimoda et al. (1989b). Using a fixed casting condition the investigation was based on two alloys: $Pr_{17}Fe_{79}B_4$ and $Pr_{15}Fe_{77}B_8$. It was shown that a columnar growth perpendicular to the iron mould wall occurred in each alloy, however, the average diameter of the columnar $Pr_2Fe_{14}B$ grains was quite different. The $Pr_{17}Fe_{79}B_4$ alloy solidified with a columnar structure with grain diameters of 10 to 20 μm whereas the alloy richer in boron ($Pr_{15}Fe_{77}B_8$) solidified with a greater grain diameter of 30 to 50 μm (see Table 5.5.1).

Table 5.5.1 Details of the macrostructure of Pr-Fe-B alloys.

Description	Alloys	
	$Pr_{17}Fe_{79}B_4$	$Pr_{15}Fe_{77}B_8$
Macrostructure	Short columnar grains perpendicular to mould walls	Long columnar grains perpendicular to mould walls
Grains diameter	10 - 20 μm	30 - 50 μm
Grains orientation	Fair	Good
Free Iron	Present	Not present

It was concluded therefore, that the macrostructure of cast ingots coarsened with increasing amount of boron. In the former ($Pr_{17}Fe_{79}B_4$) free iron is found inside the dendrites whereas in

the latter ($Pr_{15}Fe_{77}B_8$) this phase is hardly observed. In this work no details of the casting conditions were given. In a second work, using a fixed composition and changing the casting conditions (not given) Shimoda et al. (1990) showed the differences in the distribution of the grain size ($Pr_2Fe_{14}B$) of the $Pr_{17}Fe_{76.5}B_5Cu_{1.5}$ alloy (see fig.5.5.1). The columnar grains of this alloy were similar to the $Pr_{17}Fe_{79}B_4$ alloy.

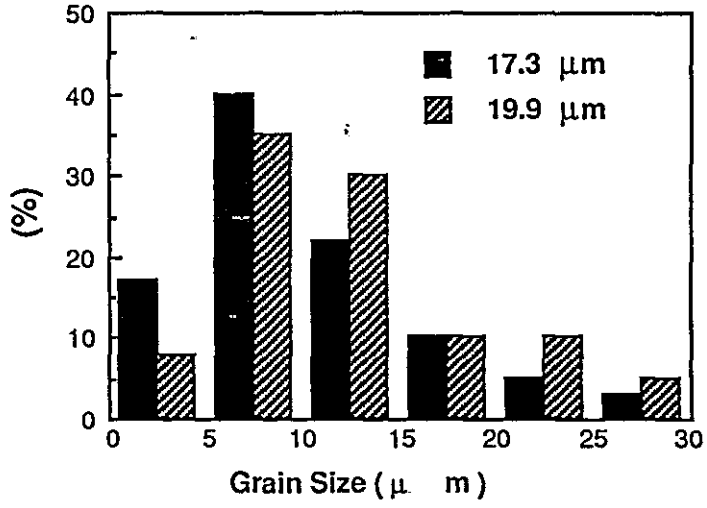

Fig.5.5.1 Histogram of grain size distribution for as-cast $Pr_{17}Fe_{76.5}B_5Cu_{1.5}$ alloy cast in two particular conditions. The average of grain size are 17.3 and 19.9 μm.

Although Shimoda et al. (1988-89) reported that copper has a refining effect on the microstructure of the Pr-Fe-B alloys, no significant differences can be seen from these results (fig.5.5.1) and the previous one for the $Pr_{17}Fe_{77.5}B_4$ alloy (Table 5.5.1). The higher boron content in this alloy ($Pr_{17}Fe_{76.5}B_5Cu_{1.5}$) must also be a predominant factor. A comparison between two alloys with the same amount of Pr and B (e.g. $Pr_{17}Fe_{77.5}B_4Cu_{1.5}$ and $Pr_{17}Fe_{79}B_4$) has not been reported.

5.7 Phases in PrFeB(Cu) Alloys

Microstructural studies (Shimoda et al. 1989b,d) on annealed $Pr_{17}Fe_{79}B_4$ alloys (cast magnets) showed that the free Fe phase, which existed in the as-cast ingots, disappeared with annealing. Thermomagnetic measurements in the $Pr_{17}Fe_{83-y}B_y$ alloys (y=2, 4 and 6) showed that the $Pr_2Fe_{14}B$ matrix phase has a Tc=294°C and the Pr_2Fe_{17} (Tc=10°C) phase was present only for y=2 and 4. Takahashi et al. (1991) also carried out DTA measurements on $Pr_{17}Fe_{79}B_4$ and $Pr_{17}Fe_{77.5}B_4M_{1.5}$ alloys (M=Cu, Ga, Ag, Al, In and Pb), determining Tc and Te (see Table 5.7.1).

Table 5.7.1 Curie and eutectic temperatures (DTA measurements) for $Pr_{17}Fe_{77.5}B_4M_{1.5}$ alloys (M=Cu, Ga, Ag, Al, In and Pb).

M	Tc (°C)	Te (°C)
$Pr_{17}Fe_{79}B_4$	284	681
Cu	285	461
Ga	289	543
Ag	285	534
Al	281	670
In	285	656
Pb	285	669

They showed that the microstructure of annealed $Pr_{17}Fe_{79}B_4$ alloys consist of the $Pr_2Fe_{14}B$ matrix phase, the Pr_2Fe_{17} phase and a Pr-rich phase which exists as a grain boundary phase. The Pr-rich phase contains a small amount of iron and is a liquid phase at the annealing temperature of 1000°C. The DTA curves for the $Pr_{17}Fe_{79}B_4$ alloy showed a peak for Tc at 284°C and a second peak for Te at 681°C. Their study of the annealed $Pr_{17}Fe_{77.5}B_4Cu_{1.5}$ alloys

showed that the alloy microstructure consisted of $Pr_2Fe_{14}B$, Pr_2Fe_{17}, Pr-rich and a eutectic structure with Pr and the PrCu compound. It was also found that most of the added Cu to the alloys existed in the eutectic structure. Similar results were obtained for this alloy in a work by Chang et al. 1990.

Recently, a detailed study on the microstructure of alloys $Pr_{20.5}Fe_{73.8}B_{3.7}Cu_2$ and $Pr_{17}Fe_{77.5}B_4Cu_{1.5}$ has been carried out by Kwon, Bowen and Harris (1991). They showed that in the cast condition the former ($Pr_{20.5}Fe_{73.8}B_{3.7}Cu_2$) consisted of three phases: $Pr_2Fe_{14}B$ matrix phase, Pr-rich grain boundary phase, and free iron inside the matrix phase. The microstructure of the latter ($Pr_{17}Fe_{77.5}B_4Cu_{1.5}$) in the cast state consisted of four phases: the same three phases as those observed in the $Pr_{20.5}Fe_{73.8}B_{3.7}Cu_2$ alloy together with a $Pr_{1+\varepsilon}Fe_4B_4$ phase.

Their observations also showed that on annealing the $Pr_{20.5}Fe_{73.8}B_{3.7}Cu_2$ alloy, an extra phase with needle-like or irregular form was present in the grain boundary regions. EDX/WDX analysis indicated that this phase was of composition $Pr(Fe_{0.94}Cu_{0.06})_2$. In the $Pr_{17}Fe_{77.5}B_4Cu_{1.5}$ alloy, the microstructures were not altered radically by the annealing at 1000°C for 25 hours except for the disappearance of the free iron. The Cu content in the primary Pr-rich phase was found to be around 0.3 at% (see Table 5.7.2).

Table 5.7.2 Chemical composition of the phases (at%) for the $Pr_{20.5}Fe_{73.8}B_{3.7}Cu_2$ and $Pr_{17}Fe_{77.5}B_4Cu_{1.5}$ alloys.

Phase	Pr	Fe	B	Cu
Primary Pr-rich	96.3	1.1	2.3	0.3
Needle-like/Grey	32.3	62.5	1.1	4.1

The microstructural studies also showed that the effects of annealing at 1000°C and then quenching or furnace cooling was to remove the free iron from the matrix phase and to change the nature of the grain boundary phases. In the quenched state the grain boundary region in the $Pr_{20.5}Fe_{73.8}B_{3.7}Cu_2$ alloy consisted of primary Pr-rich dendrites and a very fine eutectic, and the effect of annealing and slow cooling was to produce a much coarser and more clearly defined eutectic mixture (dark and light) and to sharpen the morphology of the Pr-rich phase. In the $Pr_{17}Fe_{77.5}B_4Cu_{1.5}$ alloy the eutectic coexisted with the Pr-rich and $Pr_{1+\varepsilon}Fe_4B_4$ phases in both furnace cooled and quenched conditions with the latter (quenched $Pr_{17}Fe_{77.5}B_4Cu_{1.5}$) exhibiting a more finely defined eutectic mixture. It was visible from their microstructural studies that the $Pr_{20.5}Fe_{73.8}B_{3.7}Cu_2$ alloy contained a larger amount of the Pr-rich grain boundary phase and had a smaller grain size compared with the $Pr_{17}Fe_{77.5}B_4Cu_{1.5}$ alloy. Their microanalysis results showed that the eutectic phase region in both alloys was enriched in Cu atoms (see Table 5.7.3).

Table 5.7.3 Chemical composition (EDX) of the eutectic mixture for the $Pr_{20.5}Fe_{73.8}B_{3.7}Cu_2$ and $Pr_{17}Fe_{77.5}B_4Cu_{1.5}$ alloys (at%).

Eutectic	Pr	Fe	Cu
Dark	93.1	2.9	4.0
Light	63.1	2.9	34.0

The Cu content in the light and dark phases in the eutectic region was found to be around 34.0 at% and 4.0 at%, respectively. The composition of the phases common to both alloys appeared to be essentially the same.

Their examination of the microstructure of the $Pr_{20.5}Fe_{73.8}B_{3.7}Cu_2$ alloy showed the presence of a grey phase (needle-like) in the grain boundary regions and the chemical composition indicated a Pr to Fe ratio of about 1:2. This phase was identified as the $Pr(Fe_{0.94}Cu_{0.06})_2$ phase. The presence of this phase was more evident in the sample which was subjected to a post-annealing treatment at the lower temperature of 500°C. Since the magnetic properties of this sample were inferior, this phase was attributed to the decrease in the magnetic properties of the $Pr_{20.5}Fe_{73.8}B_{3.7}Cu_2$ alloy. In this work there was no evidence that the eutectic reaction is responsible for the increase in the coercivity as alleged by Chang et al. (1990) and Takahashi et al (1991).

The much better magnetic properties of the $Pr_{20.5}Fe_{73.8}B_{3.7}Cu_2$ alloy was attributed to a smaller grain size and better magnetic isolation between the magnetic phase grains due to the presence of a greater amount of grain boundary phase in this alloy. Finally, they also concluded that, furnace cooling following annealing at high temperature led to higher intrinsic coercivity than on quenching due to the improvement of the surface character (smoothness) of the magnetic phase grain boundary during the furnace cooling and/or to constitutional changes in the grain boundary material.

A summary of the phases in all the annealed alloys described above is given in Table 5.7.4. In the cast state all the alloys showed

free iron inside the matrix phase.

Table 5.7.4 Reported phases in annealed Pr-Fe-B(Cu) alloys.

Alloys	Phases
$Pr_{20.5}Fe_{73.8}B_{3.7}Cu_2$	$Pr_2Fe_{14}B$, Pr-rich, $Pr(Fe_{0.94}Cu_{0.06})_2$ phase and a eutectic structure with Pr and the PrCu phases.
$Pr_{17}Fe_{76.5}B_5Cu_{1.5}$	$Pr_2Fe_{14}B$, Pr-rich, $Pr_{1+\varepsilon}Fe_4B_4$ phase and a eutectic structure with Pr and the PrCu phases.
$Pr_{17}Fe_{77.5}B_4Cu_{1.5}$	$Pr_2Fe_{14}B$, Pr-rich, Pr_2Fe_{17} phase and a eutectic structure with Pr and the PrCu phases.
$Pr_{17}Fe_{79}B_4$	$Pr_2Fe_{14}B$, Pr_2Fe_{17} , Pr-rich

CHAPTER SIX

PrFeBCu SINTERED MAGNETS

6.1 Introduction

The announcement by Sagawa et al. (1984) in Japan of a new magnetic alloy based on neodymium, iron and boron generated intensive research on sintered permanent magnets based on this alloy. These investigations led to Nd-based magnets with outstanding magnetic properties. Recently more attention has been paid to the other rare-earth elements.

Praseodymium, the nearest neighbour of neodymium in the periodic table, behaves analogous to neodymium in certain aspects of the $RE_2Fe_{14}B$ compounds. For instance, both $Nd_2Fe_{14}B$ and $Pr_2Fe_{14}B$ have a tetragonal structure with a space group of $P4_2/mnm$ and similar Curie temperatures. However, $Pr_2Fe_{14}B$, unlike its neodymium counterpart, does not exhibit a conical spin reorientation at lower temperatures and could be used in conjunction with YBCO superconductors. Furthermore, $Pr_2Fe_{14}B$ possesses a higher magnetocrystalline anisotropy field than that of $Nd_2Fe_{14}B$ ($H_{A\ (at\ 300\ K)}$: 87 and 67 kOe respectively), indicating the possibility of achieving a higher intrinsic coercivity than in the Nd-based magnets.

All these factors made Pr-Fe-B-based magnets attractive for applications over a wide temperature range, particulaly at low temperatures. Thus, several investigations have been carried out on sintered Pr-Fe-B permanent magnets, and some of them are discussed in this chapter.

6.2 Magnetocrystalline anisotropy field of $Pr_2Fe_{14}B$

Hirosawa et al. (1986) measured the magnetocrystalline anisotropy field (H_A) of $RE_2Fe_{14}B$ single crystals (see fig 6.2.1). $Pr_2Fe_{14}B$ has the largest H_A at low temperatures, followed by $Tb_2Fe_{14}B$ and $Dy_2Fe_{14}B$. However, the magnetocrystalline anisotropy field (H_A) of $Pr_2Fe_{14}B$ falls rapidly as the temperature increases while H_A of $Tb_2Fe_{14}B$ persists even at high temperatures. At room temperature, the magnetocrystalline anisotropy field of $Pr_2Fe_{14}B$ is still higher than that of $Nd_2Fe_{14}B$, but at higher temperatures they converge to similar values as does $Ho_2Fe_{14}B$.

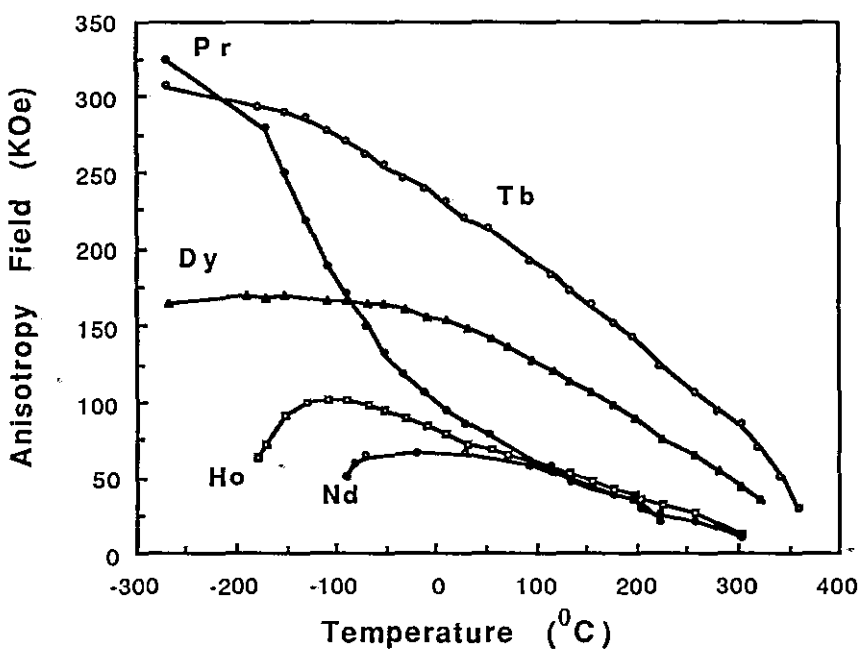

Fig.6.2.1 Temperature dependence of the magnetocrystalline anisotropy field (H_A) of $RE_2Fe_{14}B$ for RE= Pr, Tb, Dy, Ho and Nd.

6.3 The effect of boron content on PrFeB sintered magnets

Paik et al. (1989) investigated the dependence of the magnetic properties of Pr-Fe-B sintered magnets on B content ($Pr_{17}Fe_{83-x}B_x$, see fig. 6.3.1). The magnetic properties were measured after sintering at 1040°C for 4 hours. The magnetization curve for the sample with x=6 showed a rectangular loop, but the ones of x=1 and 3 showed Knee-shape loop.

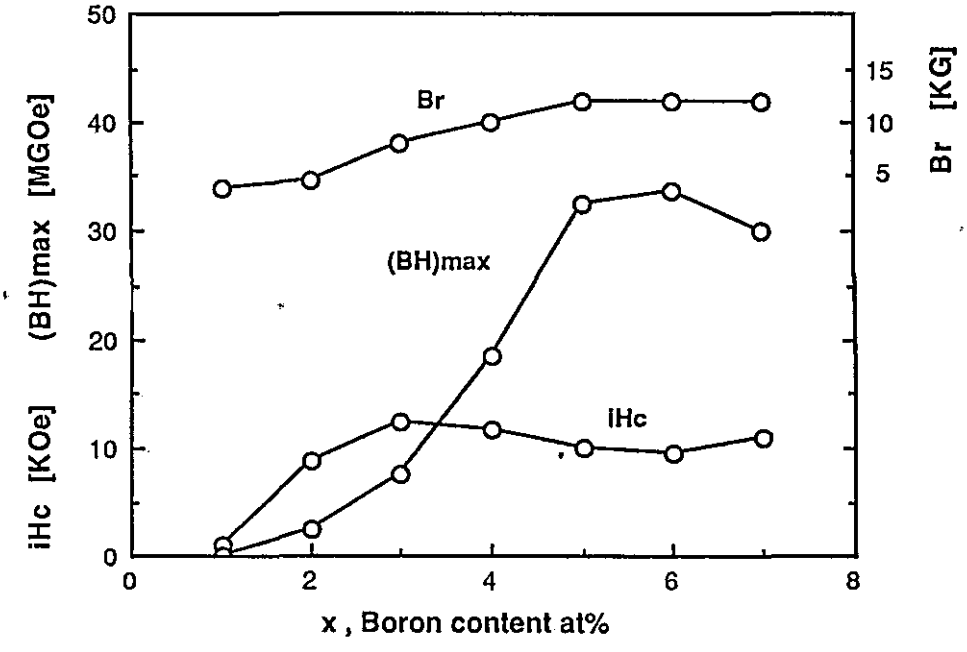

Fig 6.3.1 Dependence of magnetic properties of Pr-Fe-B sintered magnets on boron content ($Pr_{17}Fe_{83-x}B_x$).

This was attributed to the existence of a magnetic phase in these magnets (x=1 and 3) besides the $Pr_2Fe_{14}B$ phase. X-ray diffraction of the sample with 1 at% of B indicated that Pr_2Fe_{17} was the main phase with minor $Pr_2Fe_{14}B$ phase. The volume fraction of Pr_2Fe_{17} phase decreased and that of $Pr_2Fe_{14}B$ phase increased with

increasing boron content. Only the $Pr_2Fe_{14}B$ phase was observed in the sample of 6 at%B. The SEM micrographs of the sample with 1 at% of B showed a small amount of $Pr_2Fe_{14}B$ phase surrounded by large quantities of Pr_2Fe_{17} phase (see table 6.3.1). In this work it was considered that the Pr_2Fe_{17} phase retarded the grain growth of the $Pr_2Fe_{14}B$ phase, and the measured Curie temperature of the Pr_2Fe_{17} phase was 15°C. The magnets were prepared using conventional powder metallurgy processing and no post sintering heat treatment was applied to the magnets.

Table 6.3.1 Phases found in Pr-Fe-B sintered magnets and grain size of the matrix phase ($Pr_2Fe_{14}B$).

$Pr_{17}Fe_{83-x}B_x$	Grain Size	Phases
$Pr_{17}Fe_{82}B_1$	4 μm	Pr_2Fe_{17} ($Pr_2Fe_{14}B$)
$Pr_{17}Fe_{80}B_3$	6 μm	$Pr_2Fe_{14}B$ + Pr_2Fe_{17}
$Pr_{17}Fe_{77}B_6$	8 μm	$Pr_2Fe_{14}B$

6.4 The effect of heat treatment on PrFeB magnets

Jiang et al. (1988) investigated sintered permanent magnets based on the $Pr_{15}Fe_{79}B_6$ alloy. The magnets were isostatically pressed and sintered at 1050-1100°C for 1 hour and then quenched. A post sintering heat treatment at temperatures of about 1000°C for 30 minutes and slow (1.2°C/min) cooling to 600°C prior quenching was found to increase the magnetic properties of the $Pr_{15}Fe_{79}B_6$ magnets. A typical magnet showed the following magnetic properties after heat treatment : Br=12.9 kG, iHc=12.4kOe, (BH)max=39.4 MGOe, Tc=303°C and a density of 7.5 g/cm^3.

6.5 The effect of substitutions on PrFeB magnets

Jiang et al. (1988-89) investigated sintered permanent magnets based on the Pr-Fe-B alloys with substitution of iron with Co, Al and praseodymium with Dy and Tb (see Table 6.5.1). The increase in the intrinsic coercivity led to a decrease in the remanence and consequently energy product. A proper heat treatment for each case was found to improve the magnetic properties of the substituted magnets.

Table 6.5.1 Magnetic properties of substituted Pr-Fe-B magnets.

Alloy type	Br [KG]	iHc [KOe]	BHmax [MGOe
$Pr_{15}Fe_{62.5}Co_{16}B_{5.5}Al_1$	12.7	9.6	38.0
$Pr_{14}TbFe_{79}B_6$	12.3	16.6	33.5
$Pr_{13}Tb_2Fe_{62.5}Co_{16}B_{5.5}Al_1$	11.3	15.2	31.1
$Pr_{11}Dy_4Fe_{62.5}Co_{16}B_{5.5}Al_1$	10.4	22.0	26.2

6.6 PrFeB Hydrides

Pourarian, Huang and Wallace (1986) studied the effect of absorbed hydrogen on the magnetic behaviour of $Pr_2Fe_{14}B$. The hydride samples were obtained by exposing the host material at room temperature to about 60 atm of pure hydrogen. Table 6.6.1 summarizes their findings.

Table 6.6.1 Lattice parameter data, anisotropy field (H_A) and direction of magnetization of $Pr_2Fe_{14}B$ and its hydride (300K).

Compound	a (A)	c (A)	V(A^3)	H_AKOe	Direc.
$Pr_2Fe_{14}B$	8.814	12.253	951.90	79.3	Axis
$Pr_2Fe_{14}BH_5$	9.006	12.464	1010.9	----	Plane

6.7 PrFeB Sintered Magnets via Hydrogen Decrepitation

The main processing steps for preparing magnets using powder metallurgy are: pre-milling, milling, alignment-pressing, sintering and heat treatment. The hydrogen decrepitation (HD) process has been successfully applied to NdFeB alloys (Harris 1987). It replaces the pre-milling step with the following advantages:

(1)The difficulties found with breaking up the ingot by conventional means, associated with the presence of free iron, are removed by the use of hydrogen.
(2)Intergranular failure should ensure the production of single crystal particles.
(3)Significant reduction in the pick up of oxygen during the process.
(4)Almost zero remanent magnetism of aligned green compacts makes for easier handling.
(5)The desorption of hydrogen from the green compact during heating produces a non-oxidising enviroment.

Not many works have been carried out on PrFeB sintered magnets using the HD process. Jiang et al. (1989) studied HD magnets of $Pr_{14}TbFe_{79}B_6$ alloy sintered under flowing argon. They observed the appearance of pores in the magnets and also decreased values of remanence and density. The magnetic properties of the best magnet using the HD process was: Br=11.3 kG, iHc=10.4 kOe, (BH)max=28.6 MGOe (without HD, see table 4.3.1). The average of densities with HD processing were 6.93 g/cm^3 and without about 7.34 g/cm^3 .

Lin et al. (1990) annouced a new radially anisotropic $Pr_{15}Fe_{77.5}B_6Cu_{1.5}$ permanent magnet prepared from the HD process. The best magnetic properties obtained along the radial direction are as follows: (BH)max=10.5 MGOe, Br= 7.5 kG, and iHc= 8.5 kOe. They reported that $Pr_2(FeCu)_{14}BH_x$ exhibits planar anisotropy and the tetragonal c-axis of the HD powders lies in the plane perpendicular to the field direction during alignment compaction. This radial alignment is not changed in the subsequent dehydrogenation and sintering. They have based their experiments on the reports of Pourarian, Huang and Wallace (1986) which showed that the easy axis of magnetization of hydride samples of Pr-Fe-B alloys hydrided at 60 atm lies in the basal plane.

Recently, Faria, Abell and Harris (1991a) studied the magnetic properties of Pr-Fe-B-(Cu) HD sintered magnets. They showed that using a pressure of 10 bar during decrepitation the final sintered magnet does not exhibit radial anisotropy. In a second work, Faria, Abell and Harris (1992) studied the influence of the cast ingot on the final magnetic properties of Pr-Fe-B-Cu HD sintered magnets.

6.8 X-Ray Determination of Alignment in PrFeB Magnets

The preferred orientation or crystallographic alignment of NdFeB magnets has been studied by Zhou, Zhou and Graham (1988) using X-ray diffraction. It was shown that the magnets with isotropic alignment exhibit a large number of diffraction lines, whereas the well aligned samples showed only three strong peaks. These lines were identified as the (004), (105) and (006). The (004) and (006) are perpendicular to the easy direction [001] in the

tetragonal crystal structure of the $Nd_2Fe_{14}B$ phase, and the (105) is tilted by about 15° from the (00*l*) planes. The (006) reflection is the strongest one. X-ray diffraction patterns of $Pr_{17}Fe_{76.5}B_4Cu_{1.5}$ hot pressed magnets (well aligned) carried out by Shimoda et al. (1989a,b) showed similar results.

6.9 Coercivity of PrFe

Many studies have been carried out in PrFeB and NdFeB magnets with the aim of understanding their coercivity behaviour so that it may be possible to predict a method of improving the magnetic properties. Several reasons led to these studies being more applicable to PrFeB magnets . Firstly, the spin reorientation that occurs in NdFeB at low temperature was a limiting factor for the temperature range studies. Secondly, a practical reason : H_A is equal to $2K_1/Ms$ in PrFeB magnets (K_1= anisotropy constant) and for NdFeB a second anisotropy constant (K_2) must be considered. The way that K_2 in the case of NdFeB should be treated theoretically could be a matter of controversy (Sagawa and Hirosawa 1988). It is well established that the coercivity in RE-Fe-B permanent magnets is governed by the nucleation of reversed domains (Durst and Kronmuller 1987, Sagawa and Hirosawa 1988 and Givord, Tenaud and Viadieu 1988) and this led to a theoretical relation for the coercive force in the form of the following equation (Hirosawa et al. 1986):

$$iHc = c\ Hn - N\ Ms \qquad (6.9.1)$$

where Hn is the nucleation field, and if the second order anisotropy constant is negligible Hn can be replaced by the anisotropy field (H_A 80~90KOe in PrFeB, at room temperatures). Ms is the spontaneous magnetization (Ms ~ 16 kOe in PrFeB). The second term (N Ms) in the equation represents the local stray fields inside the magnet (due to the surrounding grains). The factors c and N are parameters that depend on the magnet microstructure. The parameter c is associated with the decoupling of the individual grains (c = 0 for perfectly coupled and c = 1 for perfectly isolated grains). The magnitude of the N parameter is determined by the shape and the size of the reversed grains and reaches values of about two (N = 2), that means stray fields of (-N Ms) = 32kOe. Using sintered magnets based on PrFeB, the following results were reported by Sagawa and Hirosawa (1988) and Hirosawa and Tsubokawa (1990):

1) Isolation of the $Pr_2Fe_{14}B$ magnetic grains by non-magnetic grains always results in an increase in both c and N. Table 6.9.1 shows reported values of c and N parameters and the intrinsic coercivity values calculated (in the present work) using equation 6.9.1. The isolation of the $Pr_2Fe_{14}B$ magnetic grains by non-magnetic grains was carried out by increasing the amount of B (increasing the amount of the $Pr_{1+\varepsilon}Fe_4B_4$ grains). According to Sagawa and Hirosawa (1988) the RE was too aggressive chemically and inappropriate for these studies. The remanence is reduced as the isolation of the grains is increased (due to dilution of the magnetic phase).

Table 6.9.1 Reported values of c and N parameters for various boron content.

Alloy type	c	N	iHc [kOe]	Br [kG]
$Pr_{17}Fe_{75}B_8$	0.34	0.91	16.0	11.0
$Pr_{17}Fe_{66}B_{17}$	0.41	1.16	18.3	8.0
$Pr_{17}Fe_{53}B_{30}$	0.45	1.21	21.1	5.0
$Pr_{17}Fe_{48}B_{35}$	0.58	1.63	26.1	<1.0

2) Post sintering heat treatment for enhancement of iHc makes the N parameter smaller than in the as-sintered state. The c parameter does not change dramatically upon this heat treatment (see Table 6.9.2). The post sintering heat treatment makes the grain surface very smooth and well defined so that the N parameter becomes smaller than in the as-sintered state.

Table 6.9.2 Reported values of c and N parameters (sintering temperature = 1080 and 1020°C for 1.5 h, post sintering = 627°C for 1 h) .

Alloy type	Sinter Temp.	Post-S Temp.	c	N	iHc [kOe]
$Pr_{17}Fe_{75}B_8$	1080°C	As-Sint	0.30	1.10	9.4
$Pr_{17}Fe_{75}B_8$	1080°C	627°C	0.34	0.91	16.0
$Pr_{20}Fe_{73.3}B_{6.7}$	1020°C	As-Sint	0.39	1.20	15.9
$Pr_{20}Fe_{73.3}B_{6.7}$	1020°C	627°C	0.38	1.00	18.2

From these results it can be observed increasing the Pr content also leads to an increase in the coercivity (although the sintering temperatures are different in each case) confirming that isolation of

the magnetic grains by non magnetic phases results in an increase of the intrinsic coercivity.

3) The grain size affects dramatically the c parameter. A small mean grain size in the sintered body makes the c parameter larger and yields a large iHc (see Table 6.9.3). Small grain size with a shape more round and more smooth increases the intrinsic coercivity.

Table 6.9.3 Reported values of c and N parameters for different grain sizes.

Alloy type	*Grain Size*	c	N	iHc [kOe]
$Pr_{17}Fe_{75}B_8$	14μm	0.34	0.91	16.0
$Pr_{17}Fe_{75}B_8$	16μm	0.33	0.99	13.8
$Pr_{17}Fe_{75}B_8$	20μm	0.17	0.61	5.5

4) The degree of alignment of the c-axis affects both c and N parameters. A better alignment yields a smaller iHc through a decrease in c , which overwhelms the effect of a reduction in N (see Table 6.9.4). An improvement in the grain alignment leads to a reduction of the intrinsic coercivity due to an increase of internal demagnetizing fields (Martinek, Kohler and Kronmuller 1991). The coercive field depends on the arrangement of the surrounding grains, i. e. the interaction between the grains cannot be neglected. This coupling is reduced in isotropic magnets, where adjacent grains are in general not oriented in the same direction and the stray fields created by grains with reversed magnetization do not act on the neighbours as effectively as in oriented magnets.

Table 6.9.4 Reported values of c and N parameters for different degrees of alignment (Br/Ms : greater being more aligned).

Alloy type	*Br/Ms*	*c*	*N*	iHc [kOe]
$Pr_{15}Fe_{77}B_8$	0.56	0.43	1.20	19.5
$Pr_{15}Fe_{77}B_8$	0.64	0.44	1.25	19.6
$Pr_{15}Fe_{77}B_8$	0.86	0.39	1.11	17.3
$Pr_{15}Fe_{77}B_8$	0.92	0.38	1.09	16.7

5) There exists a correlation between c and N except for the cases of exaggerated large grain systems. This correlation is expressed by the following equation: $N = 1.865\ c + 0.38$. Implicit parameters involved in this relation are the degree of magnetic isolation and alignment of the c-axis of the magnetic grains.

6.10 Oxidation of Powders during the Preparation of Magnets

The preparation of sintered magnets from RE-Fe-B powders becomes difficult when powders with fine particle sizes are to be sintered. Christodoulou and Schlup (1987) reported a dramatic decrease in remanence and intrinsic coercivity (after a steady increase) of the sintered magnet when the particle size passes below a critical value (see fig 6.10.1). The remanence behaviour was quite similar to the intrinsic coercivity. This behaviour was attributed to the oxidation of the fine powders. Similar results have been reported by McGuiness (1989), which attributed the low values of density and intrinsic coercivity to the increased oxygen

pickup during the prolonged milling times and the increased susceptibility to oxidation of the finer powders resulting from the prolonged milling times. It has also been reported that overmilling reduces the intrinsic coercivity by causing damage to the particle surface and crystal structure (Ormerod 1989).

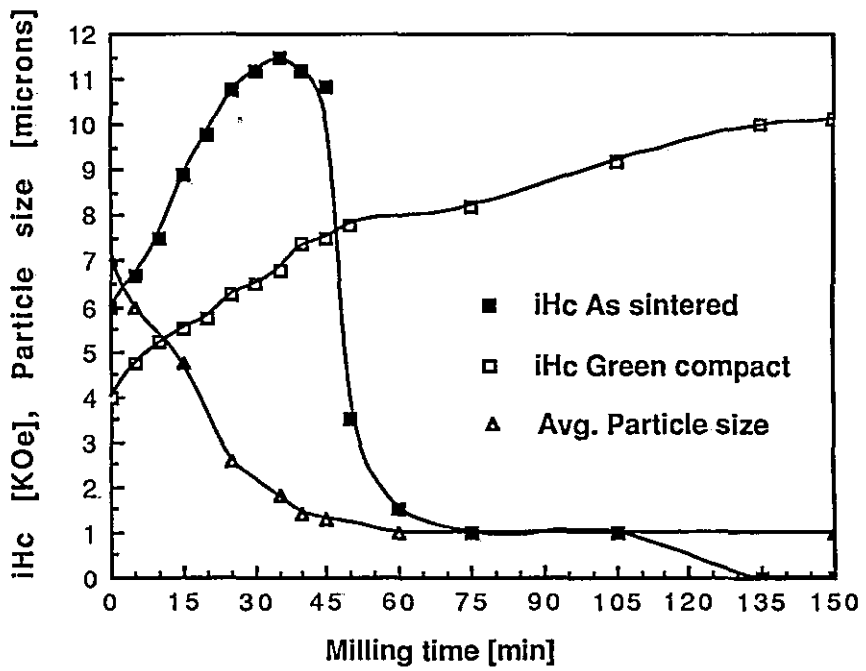

Fig 6.10.1 Coercivity of aligned green compacts and sintered magnets as a function of milling time (attritor milling) and hence particle size (after Christodoulou and Schlup 1987).

CHAPTER SEVEN

EXPERIMENTAL

7.1 Introduction

The experimental work was concerned firstly with the solidification and heat treatment of cast alloys and secondly with processing and heat treatment of HD sintered magnets made from this material and the study of their magnetic properties. The work concentrated basically on four alloys, $Pr_{20.5}Fe_{73.8}B_{3.7}Cu_2$ (alloyI), $Pr_{17}Fe_{76.5}B_5Cu_{1.5}$ (alloyII), $Pr_{16.9}Fe_{79.1}B_4$ (alloyIII) and $Pr_{16}Fe_{76}B_8$ (alloyIV) kindly supplied by REP. Alloys II and III were chosen because they exhibited good magnetic properties in the cast and hot pressed states and the $Pr_{20.5}Fe_{73.8}B_{3.7}Cu_2$ alloy was chosen for comparison in this investigation. Only alloys I and II were used for cast magnets and controlled solidification studies whereas HD sintered magnets were prepared from alloys I, II, III and IV. HD sintered magnets were studied as a function of annealing and milling time. The corresponding Nd-based sintered magnets have also been prepared for a comparison.

7.2 Production of Cast Ingots

Cast ingots were produced by induction melting component metals; ferro-boron, iron and praseodymium (or neodymium and copper), in a Balzers induction furnace. The alloy was melted under a pressure of argon and heated to 1450 °C; the melt was then

allowed to cool to 1400 °C before being poured into rectangular water cooled copper moulds (dimensions: 20x10x3 and 10x10x0.7 cm, referred in the text as 3 and 0.7 cm moulds respectively), where it was allowed to cool. The cooling rate was estimated to be in the order of 500-600 °C per minute.

7.3 The VFZ Procedure

Rod shape material (ø=5mm,L=150mm) was prepared from broken pieces of the Pr-Fe-B-Cu ingot by remelting them in a water cooled copper boat heated by a 350 KHz radio frequency (RF) generator. Directional solidification was carried out on the rods using a conventional VFZ apparatus with RF concentrator (see sequence in fig. 7.3.1, the VFZ apparatus constructional details were given by Fort 1981 and 1989). Growth rates R from 2 to 38 cm/h and an estimated thermal gradient G of approximately 100 °C/cm were used in the VFZ experiments. Suitable cubic samples were cut from the zoned rods for the magnetic measurements.

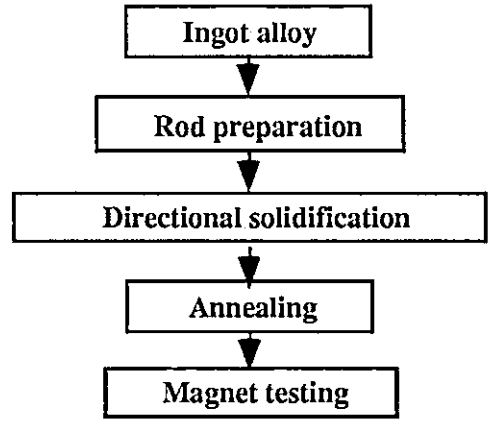

Fig.7.3.1 VFZ magnets processing route.

7.4 HD Sintered Magnets via Powder Metallurgy

In order to prepare the HD sintered magnets the folowing procedure was adopted. Small pieces of the bulk ingot were placed in a stainless steel hydrogenation vessel which was evacuated to backing-pump pressure and hydrogen was then introduced to a pressure of 10 bars. The hydrogen absorption process occurred after a short incubation period of around 3-5 minutes.

The decrepitated material was then transferred to a "roller" ball-mill under a protective atmosphere (glove box under N_2) and milled for several hours using cyclohexane as the milling medium. The resultant fine powder was then dried and encapsulated in a small cylindrical rubber bag, pulsed in a magnetic field of 60 KOe and isostatically pressed at 1400 $Kgcm^{-2}$. The resulting green compacts were then vacuum (10^{-5} Torr) sintered at 1060°C for 1 hour and furnace cooled (see fig.7.4.1).

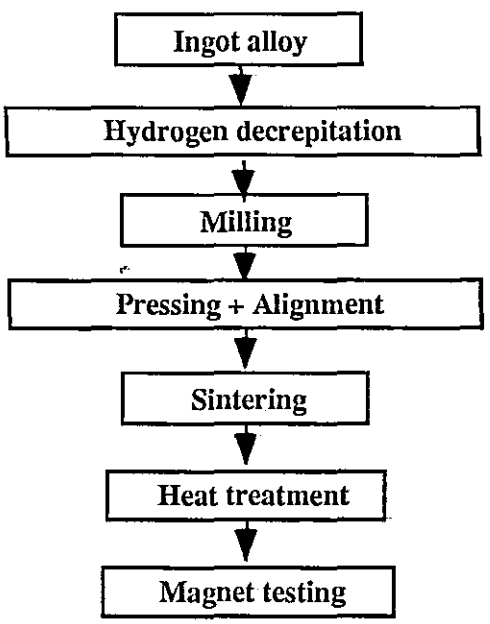

Fig.7.4.1 HD sintered magnets processing route.

7.5 Heat Treatment

The cast alloy, VFZ material and sintered magnets were annealed under vacuum (10^{-5} Torr) at 1000 °C for 24 hours and furnace cooled. A more detailed post sintering annealing treatment was also carried out for the HD magnets. This study consisted of fast heating to 1000 °C and then quenching at 5 hours intervals up to 40 hours (see Fig. 7.5.1).

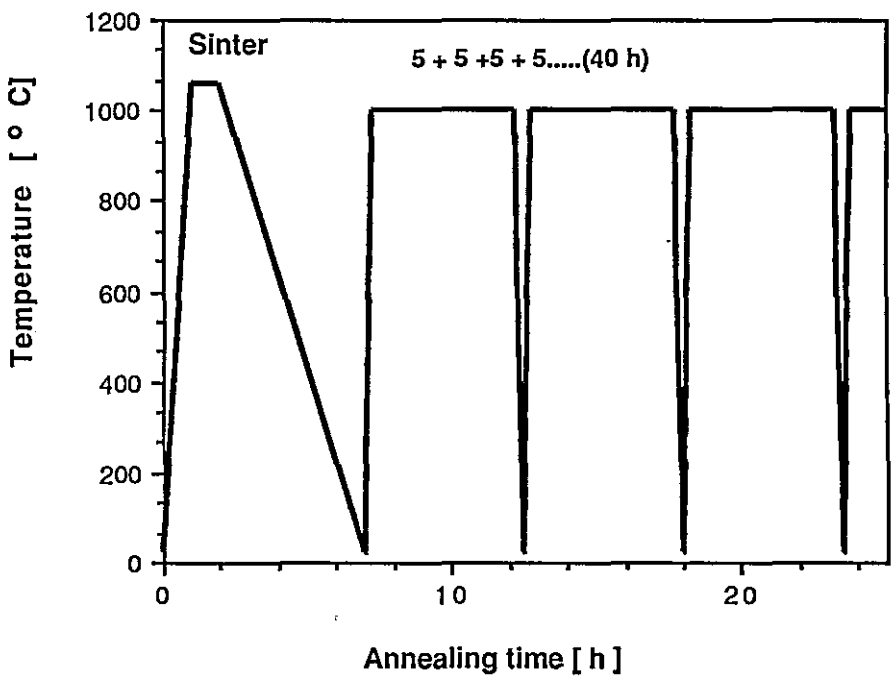

Fig.7.5.1 Heat sequence for HD sintered magnets of alloys I and II.

7.6 Magnetic Measurements

The magnetic measurements were carried out using a permeameter consisting of a "Newport" eletromagnet powered by a "Farnell" power supply, a set of flux coils from which the signals are integrated electronically and a "BBC" microcomputer (see fig.7.6.1).

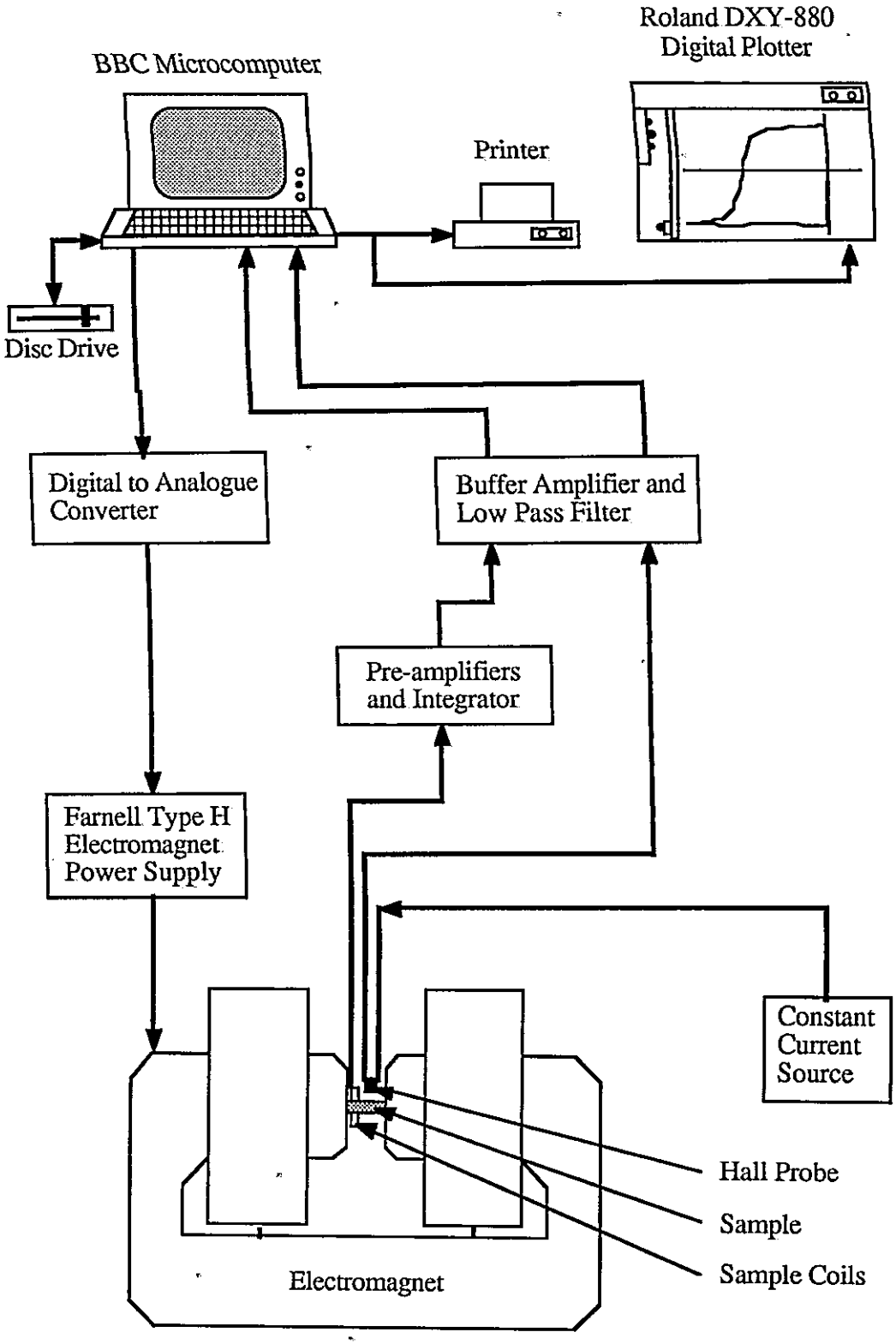

Fig.7.6.1 Schematic diagram of the permeameter.

Prior to the permeameter measurements the samples were magnetized in a "LDJ" pulse magnetiser which delivers a field of up to 60 KOe. The computer calculates the values of remanence (Br), inductive coercivity (bHc), intrinsic coercivity (iHc) and energy product (BHmax) which can then be plotted/printed.

The arrangement used in the thermomagnetic measurements is a variation of the magnetic balance designed by Sucksmith and with the use of a small tube furnace it is possible to determine the temperature dependence of the magnetic properties. The main components are a "Newport type A" electromagnet a "Boulton Paul" inductive displacement transducer and a non-inductively wound furnace. The specimen holder is rigidly attached to two circular restoring springs and actuates the transducer. The pole pieces of the electromagnet are shaped to provide a uniform field gradient. The whole system is interfaced to a BBC microcomputer.

The application of a field causes a ferromagnetic specimen to move against the restoring force of the springs. As the temperature is increased the displacement of the specimen in the magnetic field is recorded. Liquid nitrogen was used as the coolant for the low temperature studies. Samples were cut from the magnets with a "Leco' diamond saw to a size of approximately 4 x 1 x 1 mm.

7.7 Metallographic Examinations

The cast alloys were cut into 1 cm^3 pieces for mounting in Metaserv Resin blocks. The resin was allowed to harden for 24 hours before the samples were ground, first on a succession of SiC 'wet and dry' strips and subsequently polished on 6 , 1 and 1/4 μm

polishing wheels. The samples were washed with alcohol, rather than water, between each of the polishing steps to avoid any corrosion of the Pr-rich grain boundary phase taking place. The samples were viewed using a " Zeiss Jenavert " optical microscope. This also provided a facility for viewing the specimens with polarised light (Kerr effect) and to take photographs using an "Olympus OM4 " camera.

7.8 Density Measurements

Density measurements were carried out by a displacement method using a sensitive balance and diethylphthalate. The apparatus consists of an "OHAUS" digital microbalance able to weigh accurately to $\pm$O.OOOOlg with a sample bucket suspended from below the balance partially submerged in diethylphthalate. This liquid with a nominal density of 1118 kgm^{-3} was contained in a water cooled cylinder so that the temperature of the liquid remains constant.

7.9 SEM/TEM and EDX / WDX Analysis

Cast alloys and magnets were investigated using a "JEOL 5200" scanning electron microscope and a "JEOL JXA-840A" electron probe microanalyser (EDX). Spot analysis was carried out using an Energy/Wavelength Dispersive X-ray Analysis System linked to a microcomputer. A JEOL 4000FX transmission electron microscope (+EDX) has also been used. In order to prepare the TEM specimens thin slices were cut from the magnets. The discs for TEM

were then mechanically ground, dimpled to a thickness of approximately 80 μm and finally thinned by argon ion beam milling at 5 - 6 KV.

7.10 X-Ray Diffraction Measurements

X-ray diffraction measurements were performed using a Philips vertical diffractometer. The diffractometer angles was controlled by a "BBC Master" microcomputer, which also monitored the count rate from the detector. This enabled the d-spacings, line widths and integrated intensities to be easily calculated. CrKα radiation was used throughout the investigation. The Debye-Scherrer film method was also used for lattice parameter measurements.

7.11 Differential Thermal Analysis (DTA)

The DTA unit used consists basically of two platinum/platinum-13% rhodium thermocouples coupled to two tantalum crucibles. One contains the specimen, ground to a powder, and the other containing the reference material, both with good thermal contact with the thermocouple junctions. The output of the temperature difference between the two thermocouples and also the actual temperature are amplified and monitored on a "BBC" microcomputer.

A high vacuum can be obtained in the system. Before heating the samples, the unit was flushed with purified Argon and evacuated twice. The analysis was then carried out in an Ar

atmosphere heating the furnace with a linear controlled programmer.

7.12 Experimental Errors

The standard experimental errors for the various measurements in this thesis are given in table 7.12.1.

Table 7.12.1. Standard experimental errors.

Measurement	Symbol	Error	Units
Energy Product	$(BH)_{max}$	±0.9	MGOe
Remanence	Br	±0.1	kG
Intrinsic Coercivity	iHc	±0.5	kOe
Density	d	±0.05	g/cm^3
Alloy Composition	EDX/WDX	±1.0	at%
Thermomagnetic Analysis	TMA	±5.0	℃
Differential Thermal Analysis	DTA	±7.0	℃
Temperature Readings	Temp.	±1.0	℃

CHAPTER EIGHT

THE PRODUCTION OF CAST AND VFZ PrFeBCu MAGNETS

8.1 Introduction

This chapter describes the annealing effects on two alloys based on the compositions $Pr_{20.5}Fe_{73.8}B_{3.7}Cu_2$ and $Pr_{17}Fe_{76.5}B_5Cu_{1.5}$ (alloy I and II) and also the alloy solidification behaviour when cast in two different moulds. It also describes the directional solidification of the alloys under controlled conditions, for diverse values of the temperature gradient/growth rate ratio G/R, using a Vertical Floating Zone technique (VFZ). The effects of directional solidification (DS) processing on the magnetic properties of the alloys have been investigated as a possible direct means of producing grain aligned rods with enhanced hard magnetic properties. The magnetic behaviour of the VFZ material was compared with that of the as-cast ingots.

DS would have the advantage of being a low cost process of preparing RE/TM magnets. Three steps are needed in the processing: casting, DS and annealing. DS using the container-less VFZ technique is of particular interest since the alloy is almost free of contamination from the melting operation. The Pr-Fe-B-Cu alloy selected for this work ($Pr_{20.5}Fe_{73.8}B_{3.7}Cu_2$) contained more Pr than previously studied alloys (Alloy II, Shimoda1988), in order to facilitate the examination of the grain boundary regions and to assure good magnetic isolation of the individual grains. Alloy II was kept as a comparison.

8.2 Cast Ingot

The chemical analyses of the cast alloys designated I and II, are given in Table 8.2.1. The as-cast microstructures of the bulk alloys with the familiar columnar grain structure are shown in Figs. 8.2.1 and 2. Phase analysis reveals that the alloys are composed of the matrix phase $Pr_2Fe_{14}B$, Pr-rich phase in the grain boundaries, free-iron inside the matrix phase and the $Pr_{1+\varepsilon}Fe_4B_4$ boride phase in II but not in I. A delailed discussion of the phase analysis is given in the next section.

Table 8.2.1 Chemical analyses of the as-cast alloys.

Alloy Description	Wt %				Atomic %
	Pr	Fe	B	Cu	
Alloy (I)	40.0	Bal.	0.60	1.60	$Pr_{20.5}Fe_{73.8}B_{3.7}Cu_2$
Alloy (II)	35.0	Bal.	0.80	1.30	$Pr_{17}Fe_{76.5}B_5Cu_{1.5}$

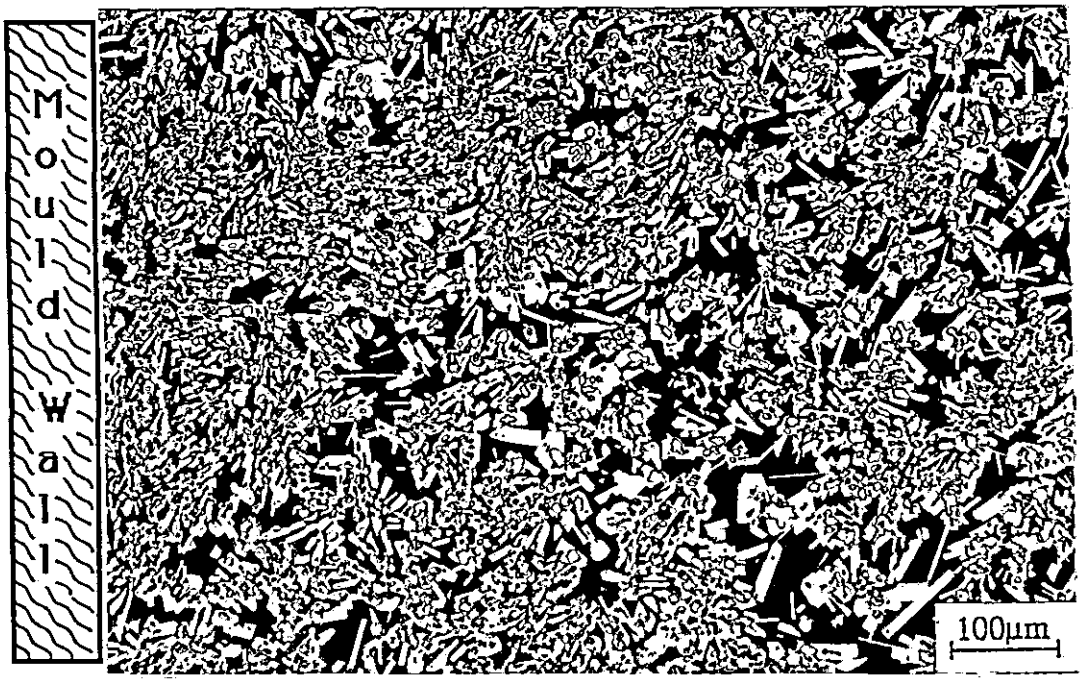

Fig 8.2.1 Microstructure of $Pr_{20.5}Fe_{73.8}B_{3.7}Cu_2$ alloy (3 cm mould, optical, etched with nital, left side = mould wall).

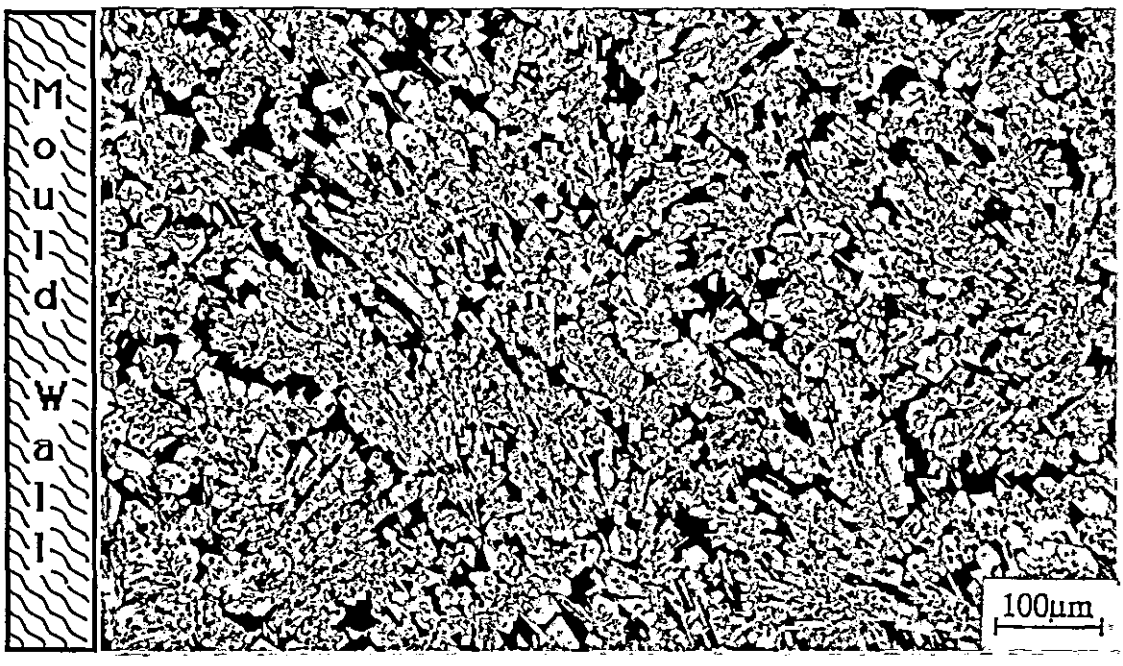

Fig 8.2.2 Microstructure of $Pr_{17}Fe_{76.5}B_5Cu_{1.5}$ alloy (3 cm mould, optical, etched with nital, left side = mould wall).

It is apparent that the $Pr_{17}Fe_{76.5}B_5Cu_{1.5}$ alloy contains a smaller amount of the Pr-rich grain boundary material and has a larger grain size compared with the $Pr_{20.5}Fe_{73.8}B_{3.7}Cu_2$ alloy. It is also evident that better grain isolation by the Pr-rich phase has been obtained in the $Pr_{20.5}Fe_{73.8}B_{3.7}Cu_2$ alloy.

As can also be seen, the as-cast condition of both alloys is very inhomogeneous and the central regions of each grain consists of free iron. This is consistent with the peritectic nature of this phase.

A detailed view of the free iron inside of the $Pr_2Fe_{14}B$ crystals is shown in fig. 8.2.3. The high praseodymium content alloy ($Pr_{20.5}Fe_{73.8}B_{3.7}Cu_2$) showed no $Pr_{1+\varepsilon}Fe_4B_4$ boride phase. Magnets produced with high amounts of rare-earth are often referred to as RE-Fe-B " 2 phase" magnets because of this fact.

The microstructure of the bulk alloys cast in the 0.7 cm mould is essentially the same as the 3 cm mould as far as phases are concerned but a smaller grain size and a higher degree of grain orientation is obtained by casting in the smaller mould (comparasion shown in section.8.5).

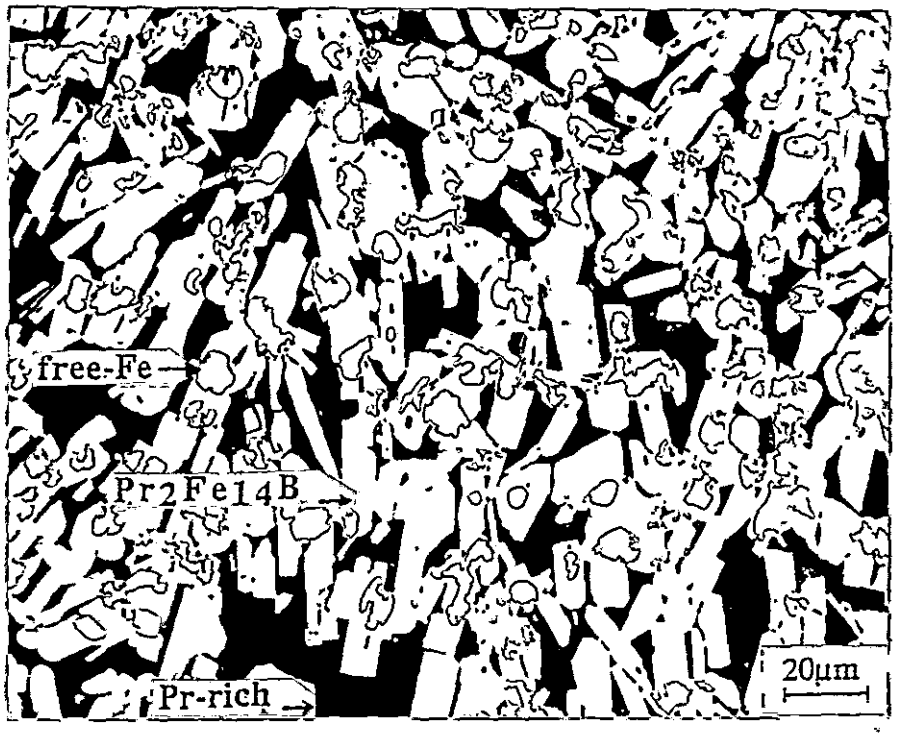

Fig 8.2.3 Details of the central regions of the matrix phase ($Pr_2Fe_{14}B$ crystals) of the $Pr_{20.5}Fe_{73.8}B_{3.7}Cu_2$ alloy (3 cm mould, etched with nital).

8.3 Quantitative EDX/WDX Analysis of Cast Alloys

Quantitative EDX (Pr, Fe and Cu) and WDX (Boron) analysis was carried out on a sample of alloys I and II. The analysis of the matrix phase, grain boundaries, Pr-rich and free iron were carried out by spot analysis on two distinct areas each. A general area, using a 200 μ m spot, has also been analysed.

Table 8.3.1 shows the results of the microprobe analysis and Fig.8.3.1 shows a detailed view of the analysed microstructure of the as-cast $Pr_{20.5}Fe_{73.8}B_{3.7}Cu_2$ alloy. In the cast state this alloy consists of the matrix phase (grey) and free iron inside it (darker grey regions inside the grains, better seen in fig 8.2.3 after etching). It also consists of the primary Pr-rich phase (dark regions in the grain boundary) and a very diffuse eutectic mixture (dark and light regions in the grain boundary).

The localization of precise spots has been rather difficult due to the not very defined eutectic mixture. In addition, a needle like phase is found mainly in the areas where there is a greater concentration of the Pr-rich and eutectic phases.

As expected the matrix phase was found to be close to the composition $Pr_{11.8}Fe_{82.4}B_{5.8}$ ($Pr_2Fe_{14}B$: matrix phase) but some under estimation in the amount of boron was observed for the general area analysis.

The results for the $Pr_{17}Fe_{76.5}B_5Cu_{1.5}$ alloy can be seen in Table 8.3.2, and fig 8.3.2 gives the microstructure of all the regions analysed. The same ill-defined eutectic mixture is found in this alloy but an extra phase, identified by Kwon, Bowen and Harris (1991) as B-rich ($Pr_{1+\varepsilon}Fe_4B_4$), is also present.

Table 8.3.1. Analysis for $Pr_{20.5}Fe_{73.8}B_{3.7}Cu_2$ alloy. at% (see fig.8.3.1).

Phase/ Area	Phase Identification	Composition at% Pr	Fe	B	Cu
General Area	Spot=200 μm	20.6	75.6	1.4	2.4
Primary Pr-rich	Dark	98.2	0.8	0.1	0.9
Eutectic	Light +Dark	56.6	1.3	0.1	42
Matrix Φ	Gray	12.5	80.3	7.2	---
α Fe	Darker gray	5.6	91.4	3.0	---
Boride	Not present	----	----	----	----

(Error ± 1.0)

Fig.8.3.1 Details of the as-cast microstructure of the $Pr_{20.5}Fe_{73.8}B_{3.7}Cu_2$ alloy (3 cm mould, optical).

Table 8.3.2. Analysis for $Pr_{17}Fe_{76.5}B_5Cu_{1.5}$ alloy.(see fig.8.3.2)

Phase/ Area	Phase Identification	Composition at% Pr	Fe	B	Cu
General Area	Spot=200 μm	16.6	79.3	1.9	2.2
Primary Pr-rich	Dark	97.4	0.2	0.6	1.8
Eutectic	Light + Dark	91.9	1.9	0.3	5.9
Matrix Φ	Gray	12.6	81.4	6.0	---
α Fe	Darker gray	0.8	99.2	---	---
Boride	$Pr_{1+\varepsilon}Fe_4B_4$	Present, not analysed			

(Error ± 1.0)

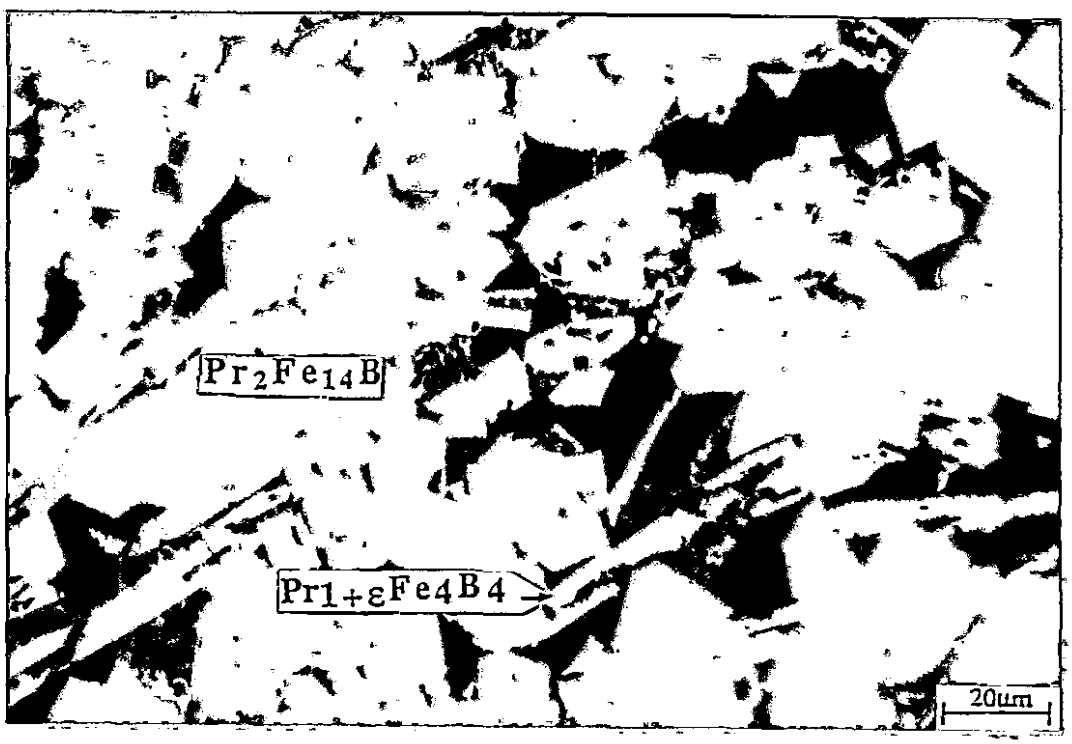

Fig 8.3.2 Details of the as-cast microstructure of the $Pr_{17}Fe_{76.5}B_5Cu_{1.5}$ alloy (3 cm mould, optical).

8.4 Heat Treatment

The microstructure of the $Pr_{20.5}Fe_{73.8}B_{3.7}Cu_2$ as-cast alloy, annealed at 1000°C for 24 hours and furnace cooled (3 cm mould), is shown in fig 8.4.1. The obvious changes during annealing are the reduction in the amount of grain boundary needle like phase and the appearance of a coarse grain boundary eutectic (see fig. 8.3.1 for comparison).

The effects of annealing at 1000°C and then furnace cooling was to remove the free Fe from the matrix phase and to change the nature of the grain boundary phase. After annealing the grain boundary region consists of a coarser and more defined eutectic mixture and also a sharper morphology of the Pr-rich phase.

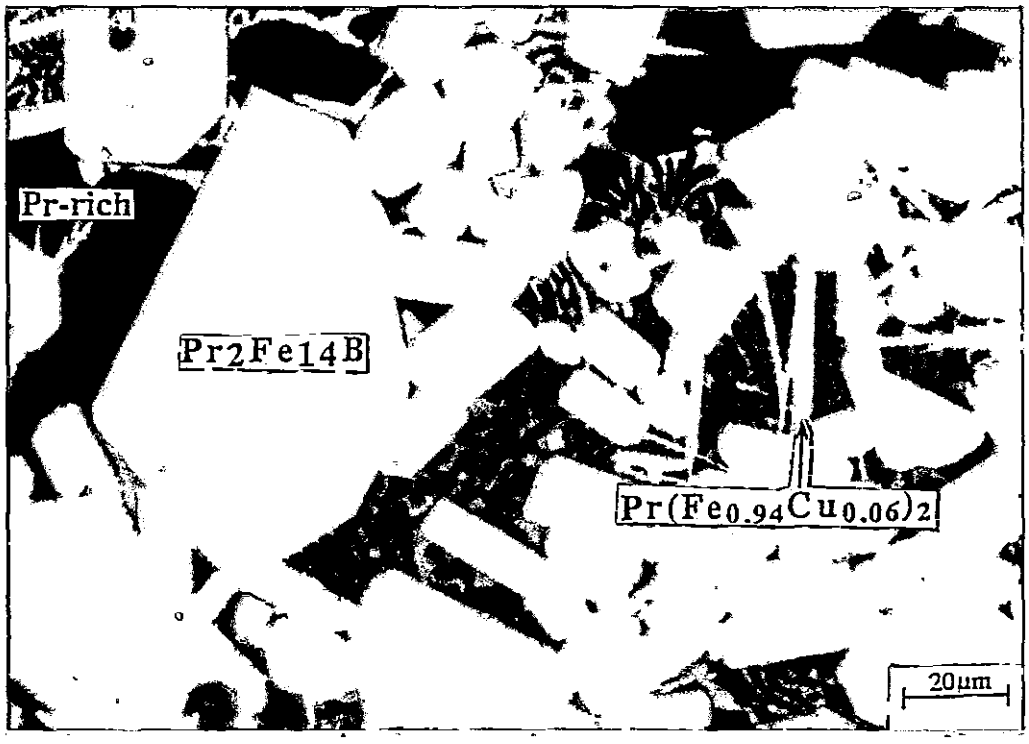

Fig 8.4.1 Microstructure of the as-cast annealed $Pr_{20.5}Fe_{73.8}B_{3.7}Cu_2$ alloy (3 cm mould).

In the $Pr_{17}Fe_{76.5}B_5Cu_{1.5}$ alloy, eutectic coexists with the Pr-rich and $PrFe_4B_4$ phases and also exhibits a more defined eutectic mixture, as can be clearly seen in fig.8.4.2. Microanalysis results from Kwon, Bowen and Harris (1991), in these annealed alloys, have shown that the eutectic phase region in both alloys is enriched in Cu atoms and the copper contents in the light and dark phases in the eutectic region are found to be around 34.0 at% and 4.0 at%, respectively. In addition the Cu content in the primary Pr-rich phase was found to be around 0.3 at%. The composition of this phase appeared to be essentially the same in both alloys.

Also in these studies an extra phase has been found in the $Pr_{20.5}Fe_{73.8}B_{3.7}Cu_2$ alloy (so called gray phase) with the ratio Pr to Fe being about 1:2, its presence is confirmed in this work in fig 8.4.1.

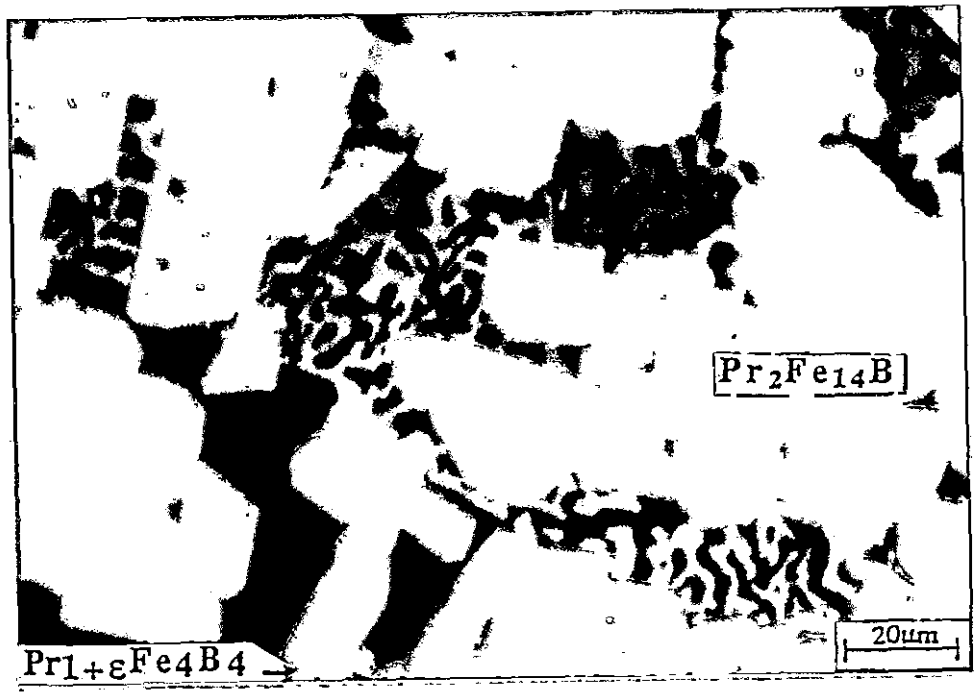

Fig 8.4.2 Microstructure of the as-cast annealed $Pr_{17}Fe_{76.5}B_5Cu_{1.5}$ alloy (3 cm mould).

8.5 Cast Magnets

Fig 8.5.1 shows the demagnetization curves for the annealed $Pr_{20.5}Fe_{73.8}B_{3.7}Cu_2$ alloy cast in 3 and 0.7 cm mould, measured parallel to the largest mould wall, i.e., perpendicular to the growth direction. Before annealing, this alloy exhibits very poor magnetic properties. As can be seen the solidification conditions have a dramatic effect on the Br and iHc.

Figure 8.5.2 shows the microstructure of the 0.7 cm annealed cast alloy, a comparison with fig.8.5.3 reveals the better grain alignment of this ingot.

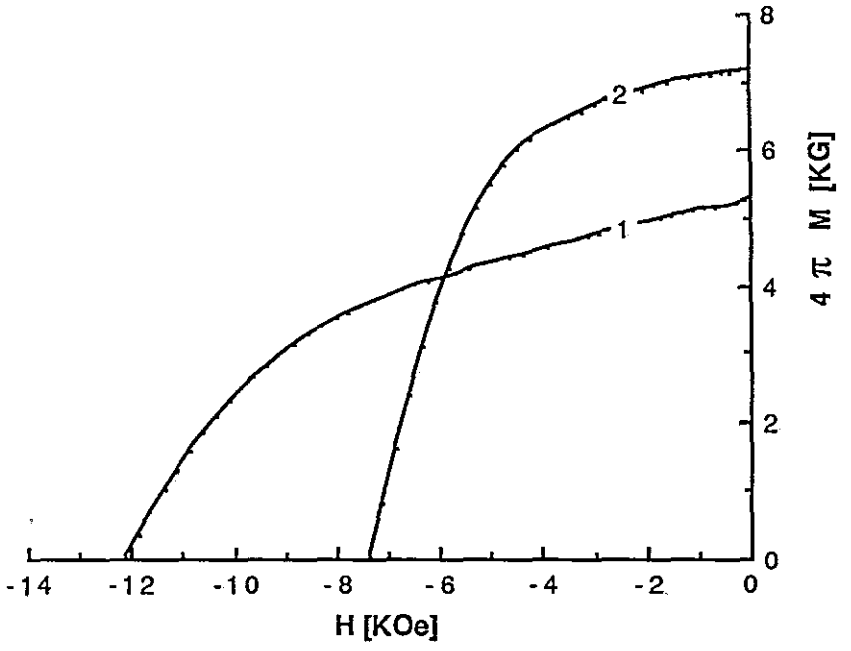

Fig.8.5.1 Demagnetization curves for $Pr_{20.5}Fe_{73.8}B_{3.7}Cu_2$ cast magnets (annealed 1000°C,24 hours). Curve 1 for alloy cast in the 3 cm mould and, Curve 2 for cast in the 0.7 cm mould.

The intrinsic coercivity of the sample cast in the 3 cm mould is much higher than that of the material cast in the 0.7 cm mould and the latter exhibits a square loop with enhanced values of the Br and $(BH)_{max}$. These observations are consistent with an increased c-axis alignment in the latter and the more isotropic nature of the former (Givord et al.1989).

The microstructure of the $Pr_{20.5}Fe_{73.8}B_{3.7}Cu_2$ alloy cast in the 0.7 cm mould seems to have a better distribution of the Pr-rich phase around the matrix grains which could also be a contributory factor in the better magnetic properties obtained with this mould.

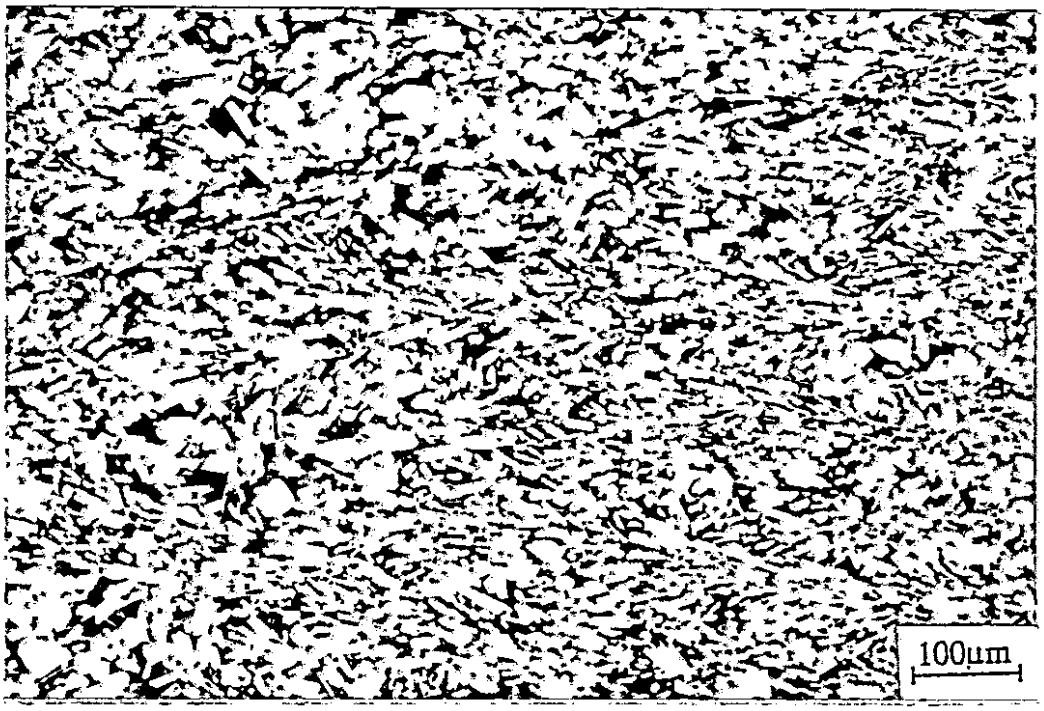

Fig.8.5.2 Microstructure of the as-cast annealed $Pr_{20.5}Fe_{73.8}B_{3.7}Cu_2$ alloy (0.7 cm mould).

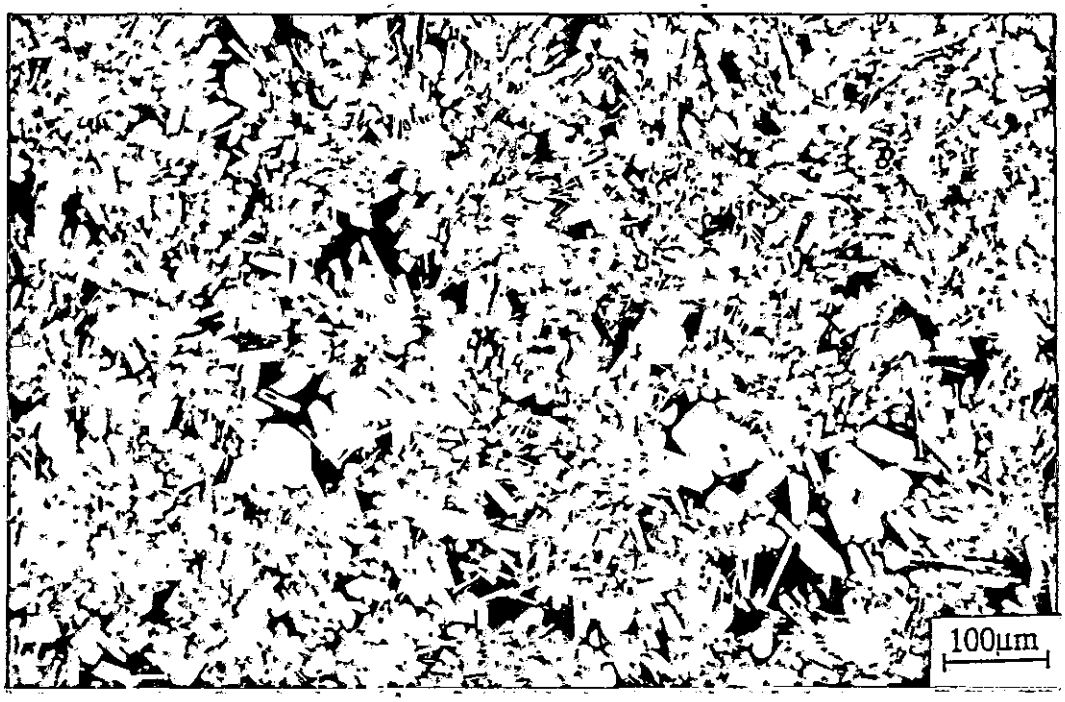

Fig 8.5.3 Microstructure of the as-cast annealed $Pr_{20.5}Fe_{73.8}B_{3.7}Cu_2$-alloy (3 cm mould).

The $Pr_{17}Fe_{76.5}B_5Cu_{1.5}$ alloy showed very poor magnetic properties (maximum values : Br ~3 kG , iHc~1.5 kOe , BHmax ~1 MGOe), before and after annealing and in both 0.7 and 3 cm moulds (results given in the next section). This can be attributed to the bigger grain size and the smaller amount of grain boundary phase in this alloy.

The matrix grains of the $Pr_{20.5}Fe_{73.8}B_{3.7}Cu_2$ alloy are well isolated from one another due to the presence of the greater amount of grain boundary phase, which reduces the magnetic coupling between the matrix grains and therefore enhances the intrinsic coercivity.

8.6 VFZ Trials

Table 8.6.1 shows a summary of the magnetic properties found in as-cast ingot and VFZ material for the $Pr_{20.5}Fe_{73.8}B_{3.7}Cu_2$ alloy, after annealing at 1000°C for 24 hours. Before annealing the as-cast alloy and VFZ material exhibit very poor magnetic properties. The remanence (0.7 cm mould) and intrinsic coercivity (3 cm mould) are substantially higher than the reported values for the Pr-Fe-B-Cu alloys (see table 5.3.1 for a comparison)

Table 8.6.1 Magnetic properties of as-cast and zoned $Pr_{20.5}Fe_{73.8}B_{3.7}Cu_2$ alloy after annealing at 1000 °C for 24 hours.

Growth rate(cm/h) Mould Thickness (cm)	Br (KG)	iHc (KOe)	BHmax (MGOe)
As-cast (0.7 cm)*	7.22	7.54	12.29
As-cast (3 cm)*	5.25	12.36	5.95
VFZ 38.10 cm/h	3.62	3.40	1.79
VFZ 6.35 cm/h	2.29	0.29	0.01
VFZ 2.54 cm/h	0.97	0.32	0.01

*(Demagnetization curves in fig. 8.5.1; Error: Br : ± 0.1, iHc : ± 0.5, BHmax : ± 0.9)

The cast alloy, which solidified under high values of growth rate R and thermal gradient G (small chill copper mould), exhibits the best magnetic properties and this suggests that, for the VFZ alloy, the zoning speed must be high in order to achieve good magnetic properties; at the growth rate of 38.1 cm/h the microstructure of the VFZ alloy shows large columnar-like grains (fig 8.6.1) whereas at rates of 6.35 and 2.54 cm/h the grains are large and equiaxed (fig 8.6.2).

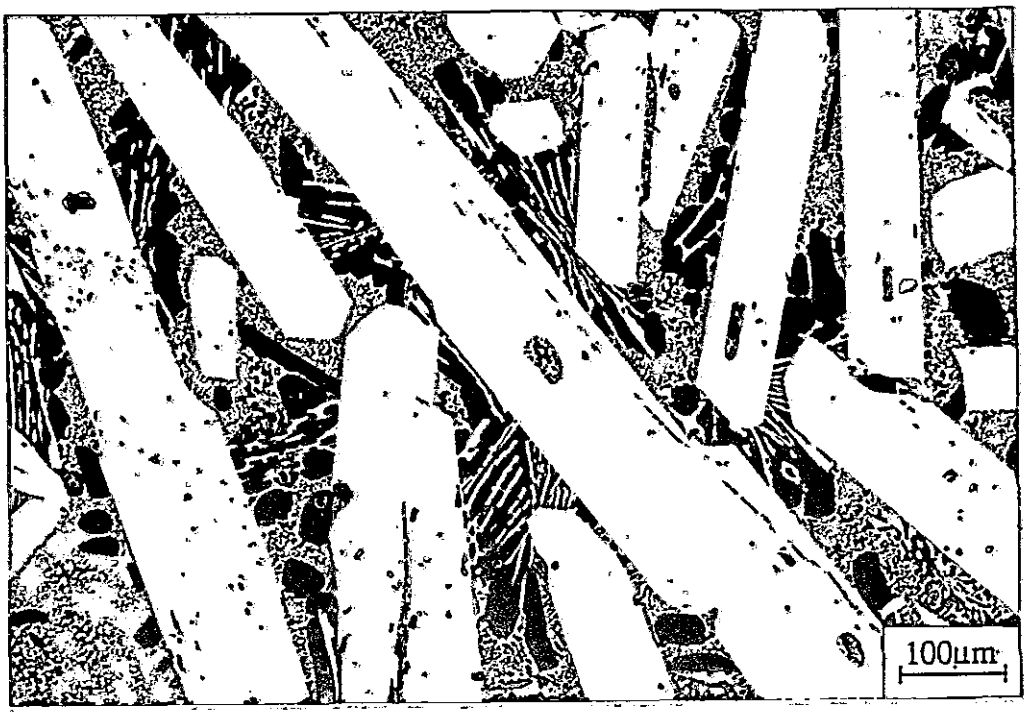

Fig 8.6.1 Microstructure of VFZ annealed alloy I (R=38.10 cm/h).

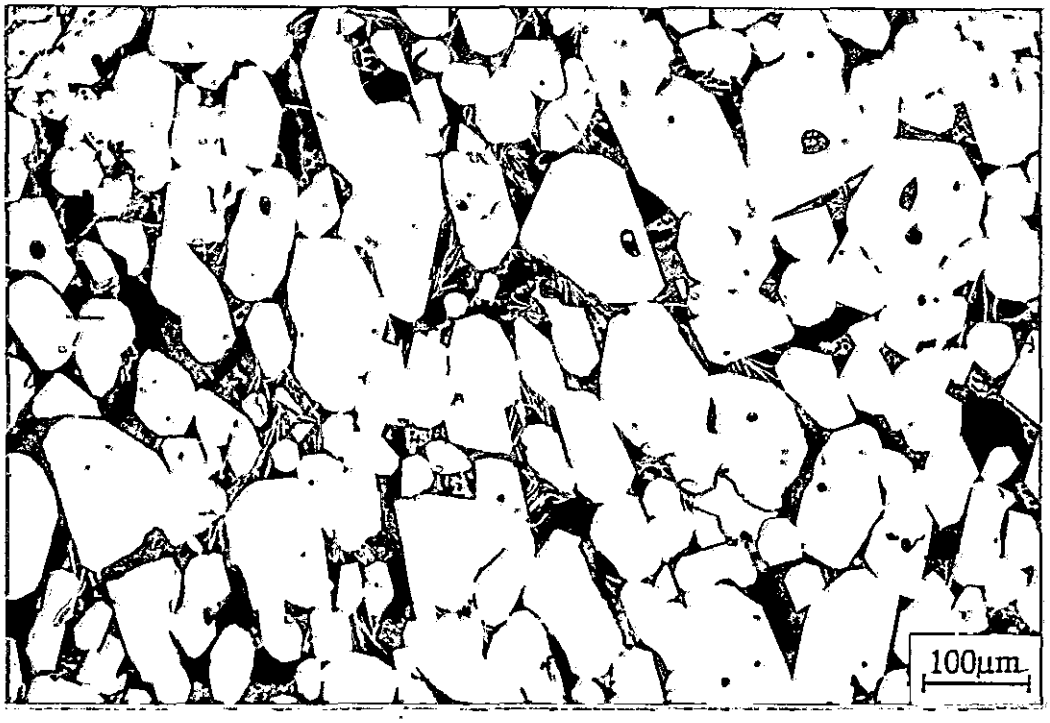

Fig 8.6.2 Microstructure of VFZ annealed alloy I (R=6.35 cm/h).

Table 8.6.2 shows the magnetic properties of the annealed $Pr_{17}Fe_{76.5}B_5Cu_{1.5}$ alloy both as-cast and zoned. As can be seen the remanence, intrinsic coercivity and energy product are inferior to those of the annealed $Pr_{20.5}Fe_{73.8}B_{3.7}Cu_2$ alloy. Increasing the zoning speed led to a finer microstructure but not sufficient to reproduce the as-cast ingot microstructure. Fig.8.6.3 and 4 show the microstructure of the $Pr_{17}Fe_{76.5}B_5Cu_{1.5}$ alloy zoned at growth rates of 25.4 and 63.5 cm/h. The microstructure of the former ($Pr_{17}Fe_{76.5}B_5Cu_{1.5}$, at 25.4 cm/h) is very similar to that of the $Pr_{20.5}Fe_{73.8}B_{3.7}Cu_2$ alloy at R= 38 cm/h, although the boride phase is present, but a finer microstructure is obtained with the latter ($Pr_{17}Fe_{76.5}B_5Cu_{1.5}$, at 63.5 cm/h), but not quite the same as that of the as-cast alloy (see fig. 8.2.2).

It can also be noticed from table 8.6.2 that increasing the growth rate R from 25.4 to 63.5 cm/h and changing the mould size from 30 to 7 mm led to a decrease in the magnetic properties in each case. The magnetic properties of the $Pr_{17}Fe_{76.5}B_5Cu_{1.5}$ alloy are rather inferior to those reported by Shimoda (1988) for this alloy (see table 4.3.1). Such differences may be attributed to the different casting condition.

Table 8.6.2 Magnetic properties of as-cast and zoned $Pr_{17}Fe_{76.5}B_5Cu_{1.5}$ alloy after annealing at 1000 °C for 24 hours.

Growth rate(cm/h) Mould Thickness (cm)	Br (KG)	iHc (KOe)	BHmax (MGOe)
As-cast (0.7 cm)	1.51	0.74	0.21
As-cast (3 cm)	2.98	1.44	1.01
VFZ 63.5 cm/h	1.30	0.29	0.04
VFZ 25.4 cm/h	1.85	1.15	0.32
VFZ 12.7 cm/h	1.03	0.25	0.01

(Average error: Br : ± 0.1, iHc : ± 0.5, BHmax : ± 0.9)

Fig 8.6.3 Microstructure of VFZ annealed alloy II(25.4 cm/h).

Fig 8.6.4 Microstructure of VFZ annealed alloy II(63.5 cm/h).

The magnetic properties reported by Kwon, Bowen and Harris (1991) for the $Pr_{17}Fe_{76.5}B_5Cu_{1.5}$ alloy after annealing (Br = 5.8KG, iHc = 3.9KOe, BHmax = 4.8MGOe) are somewhat superior and since the casting conditions were the same as the one in the present work (same batch), variations of solidification behaviour within the same ingot can be expected.

Increasing growth rates of vertical float zoning lead to increasingly finer microstructures, which should produce improved magnetic properties, but this also requires increasing rates of heat removal to maintain the high values of the G/R ratio. Heat must also be removed fast enough so that the solid-liquid interface remains within the RF coil; if this is not accomplished, solidification takes place radially inwards below the RF coil and the desired preferred orientation will not be obtained. Our observations indicate that the rate of heat removal on VFZ is the major limiting experimental factor.

Recently, Chen et al. (1992) using directional solidification with liquid metal cooling produced $Pr_{19}Fe_{74.5}B_5Cu_{1.5}$ permanent magnets with Br $\approx$ 7.2 KG and iHc $\approx$ 5.6 KOe. This technique, can provide a much higher rate of heat removal than the VFZ technique, yet it was not possible to obtain better remanence than that obtained with the present cast magnets. They concluded that to obtain further easy-axis alignment hot working should be employed.

A second VFZ limitation for the Pr-Fe-B-Cu alloys is that the Pr-rich phase, during the rod heating, is molten before the matrix phase. This phase is interconnected in the grain boundary and quite

often it accumulates in the rod borders and leaks out, changing significantly the alloy composition.

To summarize: By annealing the as-cast alloys and VFZ material at 1000°C for 24 hours, the magnetic properties increased substantially for the $Pr_{20.5}Fe_{73.8}B_{3.7}Cu_2$ alloy. VFZ growth rates up to 38.1 cm/h for the $Pr_{20.5}Fe_{73.8}B_{3.7}Cu_2$ alloy and 63.5 cm/h for the $Pr_{17}Fe_{76.5}B_5Cu_{1.5}$ alloy have not been sufficient to reproduce the as-cast ingot microstructure. Large and small chill moulds (3 and 0.7 cm thick) have been employed and the Br and (BH)max can be increased substantially by casting the $Pr_{20.5}Fe_{73.8}B_{3.7}Cu_2$ alloy in very small chill moulds. Cast magnets prepared in larger chill moulds showed the best intrinsic coercivity.

8.7. The c-axis in PrFeB Alloys

Figure 8.7.1 shows the domain patterns of the $Pr_{20.5}Fe_{73.8}B_{3.7}Cu_2$ alloy using polarised light (Kerr effect). These patterns show that the columnar grains grow with their major axis predominantly in the basal plane rather than along the c-axis. This is a major difference between Sm-Co cast magnets and Pr-Fe-B. Sm-Co magnets have the advantage that the c-axis is parallel to the crystals growth direction.

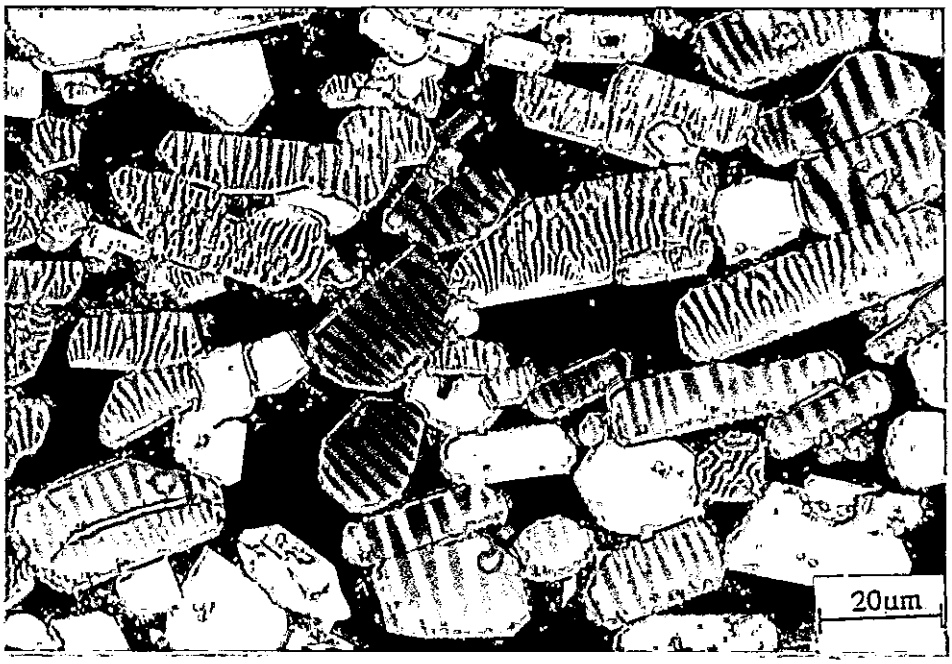

Fig 8.7.1 Domains revealed in a PrFeBCu alloy by polarized light.

CHAPTER NINE

THE PRODUCTION OF Pr-Fe-B-Cu HD MAGNETS

9.1 Introduction

This chapter describes the production of PrFeBCu sintered magnets using initial materials produced by a copper mould casting (3x10x20cm). Sintered magnets based on the compositions $Pr_{20.5}Fe_{73.8}B_{3.7}Cu_2$, $Pr_{17}Fe_{76.5}B_5Cu_{1.5}$ and $Pr_{16.9}Fe_{79.1}B_4$ have been prepared using the hydrogen decrepitation (HD) process and the powder metallurgy route. The effect of processing variables (milling time, sintering temperature and heat treatment) on the magnetic and physical properties (remanence, intrinsic coercivity, energy product and density) have been studied. As in the case of the cast magnets a heat treatment at 1000°C for 24 hours was also applied to the HD sintered magnets. The possibility of changing the easy direction of magnetization from the tetragonal c-axis to easy basal plane during hydrogen absorption has also been investigated as a means of producing radially anisotropic permanent magnets using the isostatic pressing method (IP).

9.2 Cast Alloys

The alloys investigated in this chapter have also been provided by Rare Earth Products Ltd. The chemical analyses of the alloys designated I, II and III, are given in the Table 9.2.1. The Cu-containing compositions were chosen because they exhibited good

magnetic properties in the cast state and the Cu-free alloy was chosen for comparison. The as-cast microstructures of the starting alloys with the familiar columnar grain structure are shown in Fig. 8.2.1 ($Pr_{20.5}Fe_{73.8}B_{3.7}Cu_2$) and Fig. 9.2.1 ($Pr_{16.9}Fe_{79.1}B_4$). Phase analyses reveals that the alloys are composed of the matrix phase $Pr_2Fe_{14}B$, Pr-rich material in the grain boundaries and free-iron inside the matrix phase. The $Pr_{17}Fe_{76.5}B_5Cu_{1.5}$ alloy was studied in section 8.2 (Alloy II, Seiko composition, Shimoda 1988).

Table 9.2.1. Chemical analyses of the as-cast alloys.

Alloy Description	Wt % Pr	Fe	B	Cu	Atomic %
(I) Pr-Rich	40.0	Bal.	0.60	1.60	$Pr_{20.5}Fe_{73.8}B_{3.7}Cu_2$
(II) Seiko	35.0	Bal.	0.80	1.30	$Pr_{17}Fe_{76.5}B_5Cu_{1.5}$
(III) Cu-Free	34.8	Bal.	0.63	----	$Pr_{16.9}Fe_{79.1}B_4$

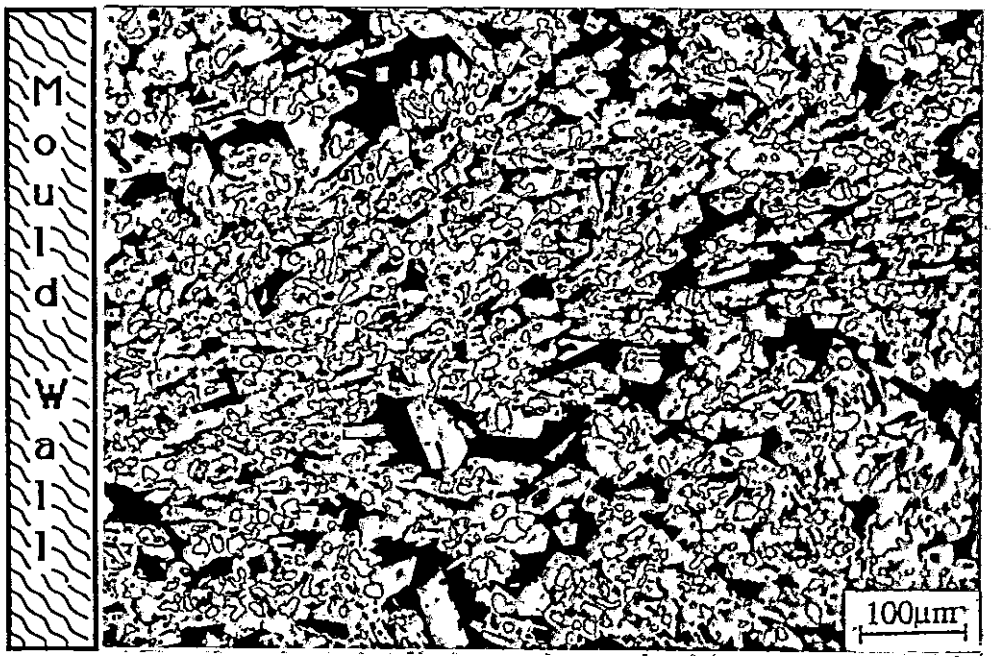

Fig. 9.2.1 Microstructure of the as-cast $Pr_{16.9}Fe_{79.1}B_4$ alloy (Etched with Nital).

9.3 The Effect of Milling Time and Annealing on iHc

The effects of milling time and annealing at 1000°C for 24 hours are shown in Fig.9.3.1 and 2. The most striking feature of these graphs is the variation of intrinsic coercivity with the milling time for the annealed samples. The $Pr_{20.5}Fe_{73.8}B_{3.7}Cu_2$ HD magnet exhibits a remarkable increase in iHc in the powder milled for 9 hours. In the same way, the $Pr_{16.9}Fe_{79.1}B_4$ HD magnet also exhibits a dramatic enhancement in iHc after annealing but at a significantly longer milling time (27 hours). For the former ($Pr_{20.5}Fe_{73.8}B_{3.7}Cu_2$) iHc stays high after the peak whereas for the latter ($Pr_{16.9}Fe_{79.1}B_4$) it falls to around the initial values.

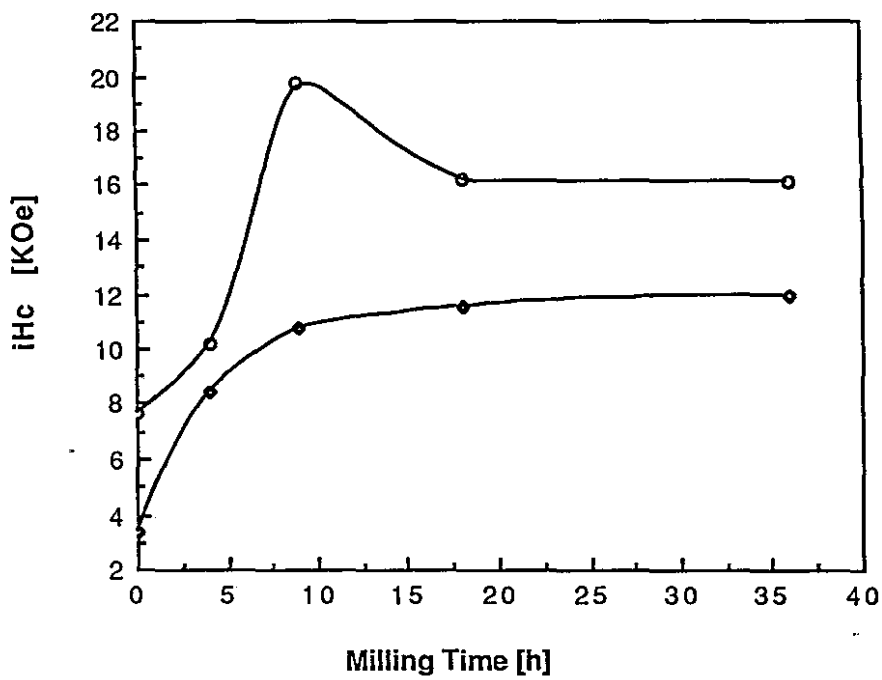

Fig.9.3.1 Variation of iHc with milling time for slowly cooled magnets of the $Pr_{20.5}Fe_{73.8}B_{3.7}Cu_2$ alloy. (◊:As-sintered, o : annealed 1000°C, 24h)

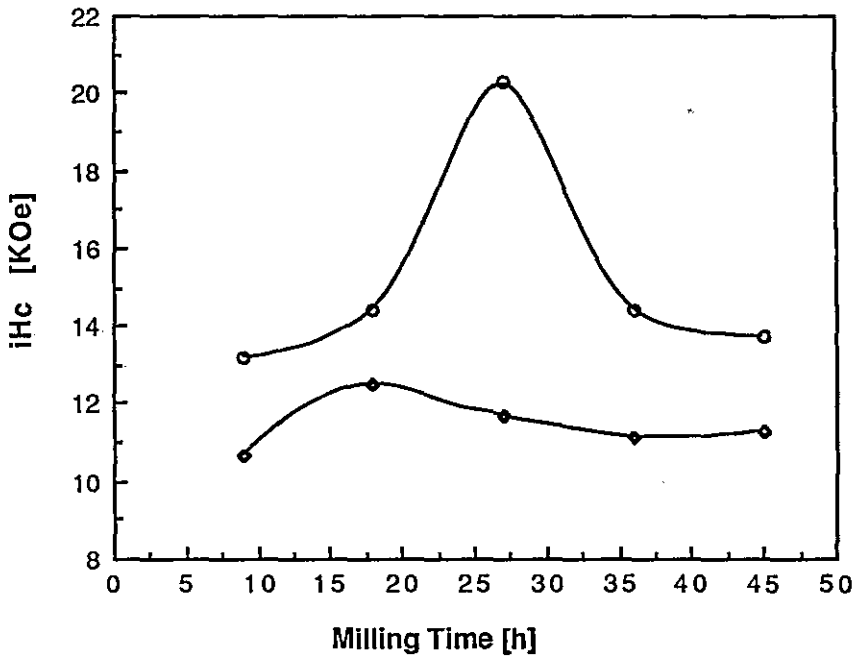

Fig.9.3.2 Variation of iHc with milling time for slowly cooled magnets of the $Pr_{16.9}Fe_{79.1}B_4$ alloy. (◊:As-sintered, o : annealed 1000°C,24 hours)

Another distinct feature of the $Pr_{20.5}Fe_{73.8}B_{3.7}Cu_2$ alloy is that, even for as-crushed material with a coarse particle size (zero milling time in Fig.9.3.1), the magnet exhibits appreciable coercivity and this can be attributed to the higher proportion of grain boundary phase in this material (better isolation).

It has been suggested, in the studies done by Kwon, Bowen and Harris (1991) on the cast alloys, that annealing at 1000°C increases iHc by eliminating free Fe and slow cooling further increases the magnetic properties by enhancing the smoothness of the grain boundaries. Contributions to iHc behaviour in the sintered magnets include (a) the milled particle size and hence the subsequent grain

size of the sintered magnet, (b) the coverage and thickness of the Pr-rich grain boundary material, (c) the smoothness of the grain boundaries and (d) the removal of any residual free iron. It is not clear at this juncture however, why there is a peak in the iHc behaviour for both alloys. A microstructural investigation carried out on these magnets is described in chapter 10, in an attempt to explain the coercivity behaviour observed in this section. Fig. 9.3.3 shows the respective remanence and energy product for both alloys and it can be seen that there is the same increase in these parameters for each case.

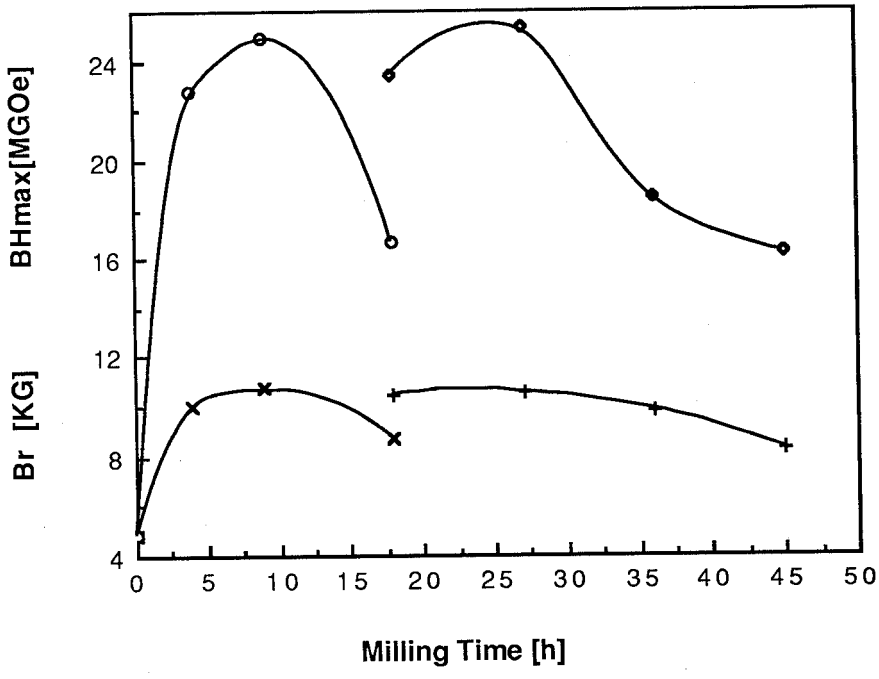

Fig. 9.3.3 Variation of Br and $(BH)_{max}$ with the milling time for slow cooled and annealed samples of alloy I ($Pr_{20.5}Fe_{73.8}B_{3.7}Cu_2$; o : $(BH)_{max}$, x:Br) and alloy III ($Pr_{16.9}Fe_{79.1}B_4$; ◊:$(BH)_{max}$, + : Br).

Demagnetization curves for the as-sintered and annealed magnets (24 hours, 1000°C) of alloys I ($Pr_{20.5}Fe_{73.8}B_{3.7}Cu_2$) and III ($Pr_{16.9}Fe_{79.1}B_4$) are shown in the fig. 9.3.4 and 5. The $Pr_{20.5}Fe_{73.8}B_{3.7}Cu_2$ magnet exhibits a slightly inferior squareness factor (loop shape) than the $Pr_{16.9}Fe_{79.1}B_4$ magnet, before and after annealing. The same investigation carried out for the corresponding Nd alloys showed no peak in iHc and a small increase in the general magnetic properties with annealing (details given in section 9.7).

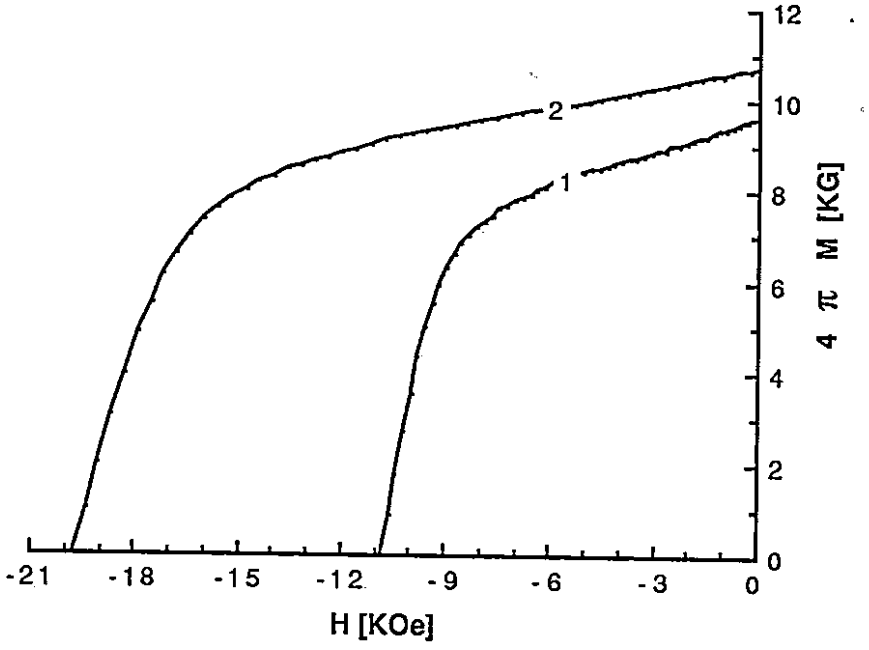

Fig.9.3.4 The demagnetization curves for slow cooled magnets of alloys I ($Pr_{20.5}Fe_{73.8}B_{3.7}Cu_2$), before (1) and after annealing (2) (milling time 9 h).

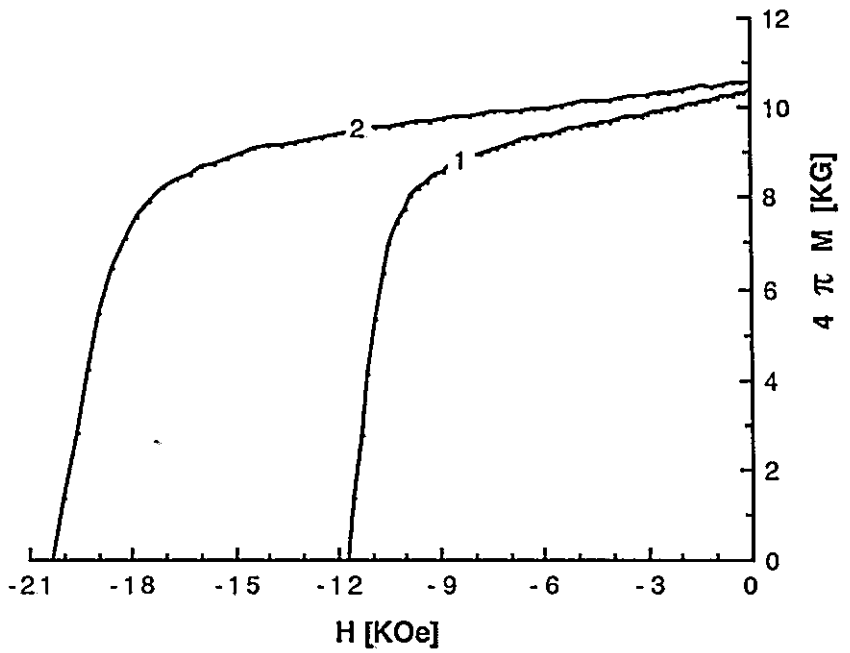

Fig.9.3.5 The demagnetization curves for slow cooled magnets of alloy III ($Pr_{16.9}Fe_{79.1}B_4$), before (1) and after annealing (2) (milling time 27 hours).

Similar coercivities (17.4 KOe; Br=5.8 KG and BHmax = 6.5 MGOe) have also been obtained in annealed $Pr_{15}Fe_{80}B_5$ magnets produced by mechanical grinding (Noh, Jeung and Kang 1991). With a copper containing $Pr_{15}Fe_{80}B_5$ alloy the coercivity increase to 19.7KOe (Br=7.0 KG and BHmax = 10.2 MGOe).

The effect of milling time and annealing at 1000°C for 24 hours for the $Pr_{17}Fe_{76.5}B_5Cu_{1.5}$ magnets are shown in Fig.9.3.6, and the demagnetisation curve for the best magnet is shown in fig. 9.3.7. Lower coercivity has been found with these magnets but a higher remanence and energy products have been achieved.

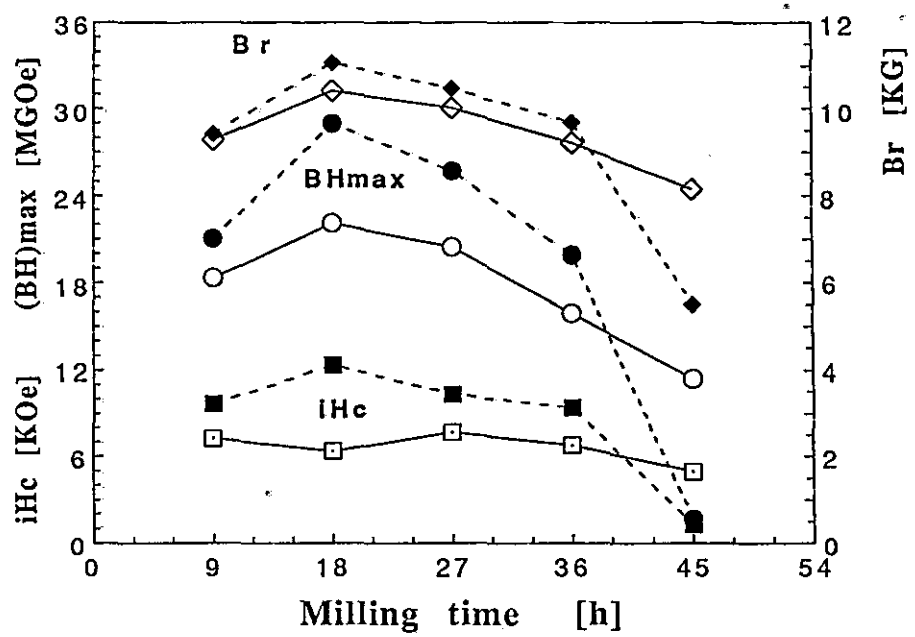

Fig.9.3.6 Variation of (BH)max (o) and iHc (▣) and Br (◊) with the milling time for slow cooled HD magnets of $Pr_{17}Fe_{76.5}B_5Cu_{1.5}$ alloy (Black/Dashed : annealed 1000°C, 24 hours).

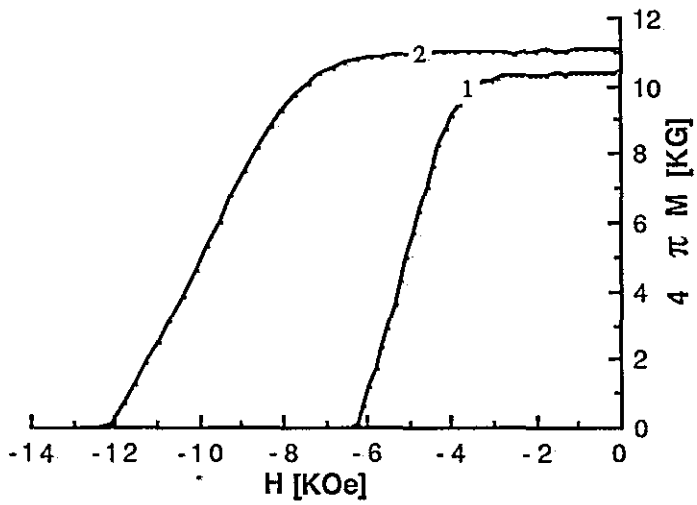

Fig.9.3.7 The demagnetization curves for slow cooled magnets of alloy II ($Pr_{17}Fe_{76.5}B_5Cu_{1.5}$), before (1) and after annealing (2) (milling time 18 hours).

A summary of the magnetic properties of the present magnets and a comparison with reported magnets is given in the Table 9.3.1. The higher remanence for the hot pressed magnets can be attributed to the "squeezing out" of the Pr-rich material during the hot pressing operation. The higher Br for the Tb containing magnets can be ascribed to the lower Pr content and the higher anisotropy field which should result in better c-axis alignment.

Table 9.3.1 Comparison of various HD sintered permanent magnets .

ALLOY TYPE Ref.	PROCESSING CONDITIONS	HEAT TREATMENT	Br KG	iHc KOe	BH MGO	d g/cc
$Pr_{20.5}Fe_{73.8}B_{3.7}Cu_2$*	HD=10 bar, I.P.	1000°C,24h,Furn.	10.7	19.8	24.9	7.33
$Pr_{17}Fe_{76.5}B_5Cu_{1.5}$*	HD=10 bar, I.P.	1000°C,24h,Furn.	11.1	12.4	29.0	7.30
$Pr_{16.9}Fe_{79.1}B_4$*	HD=10 bar, I.P.	1000°C,24h,Furn.	10.6	20.3	25.3	7.10
$Pr_{14}TbFe_{79}B_6$ (a)	HD=60atm,ArFlow	1100°C,1h,Quenc	11.3	10.4	28.6	6.93
$Pr_{17}Fe_{77.5}B_6Cu_{1.5}$+(b)	HD uniaxial press	----------	7.5	8.5	10.5	---
$Pr_{17}Fe_{79}B_4$ (c)	Powder Met.	----------	10.0	11.7	18.0	----
$Pr_{15}Fe_{79}B_6$ (a)	Powder Met.	1000°C,30min,Q.	12.9	12.4	39.4	7.50
$Pr_{14}TbFe_{79}B_6$ (a)	Powder Met.	1100°C,1h,Quen	12.3	16.6	33.5	7.34
$Pr_{17}Fe_{76.5}B_5Cu_{1.5}$*(d)	Hot Pressing	1000°C,24h,Furn.	12.6	10.0	36.2	---

(Average error: Br : ± 0.1, iHc : ± 0.5, BHmax : ± 0.9)

HD: hydrogen decrepitated, IP: isostatically pressed, +radial, *uniaxial orientation , Furn: furnace cooled, Q : quenched ; (a) Jiang et al. (1988-89), (b) Lin et al. (1990) , (c) : Paik et al. (1989), (d) Shimoda et al. (1988-89).

9.4 The Effect of Post Sintering Heat Treatment on iHc

Figure 9.4.1 and 2 show how the intrinsic coercivity, remanence and energy product of magnets made from alloy I and III are affected by the annealing time in the sequence shown in Fig.7.5.1. This heat treatment was chosen in order to diminish any influence of a low temperature eutectic reaction and hence to study the effect of annealing at 1000 °C.

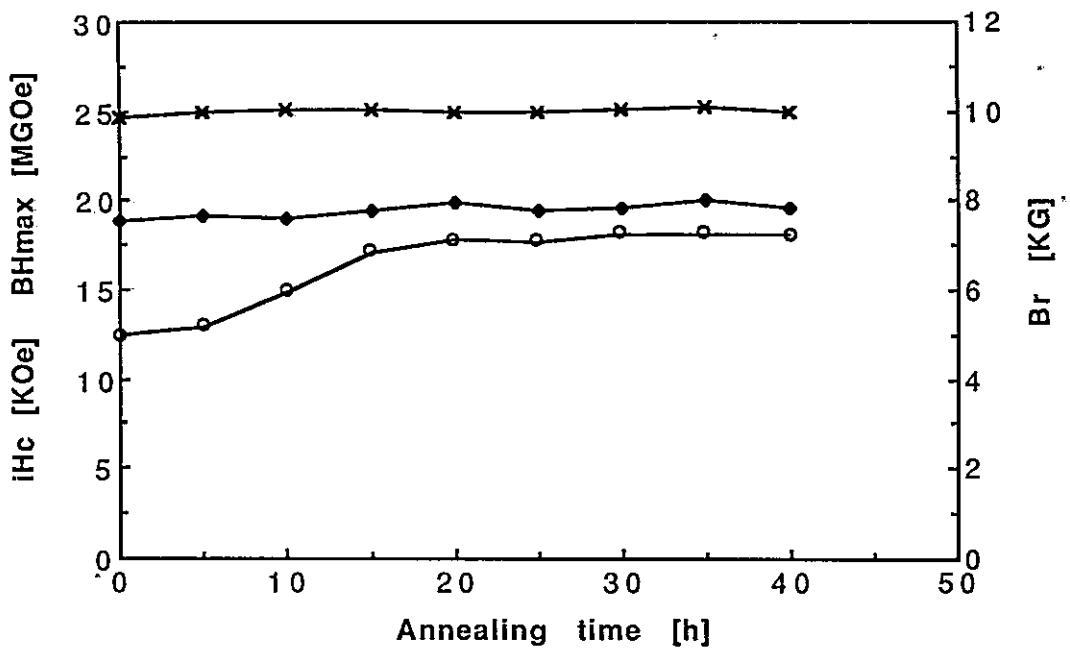

Fig. 9.4.1 Variation of Br, iHc and BHmax with annealing time for magnets of alloy I ($Pr_{20.5}Fe_{73.8}B_{3.7}Cu_2$), using the heat sequence of fig. 7.5.1. (◊: BHmax, x : Br, o : iHc)

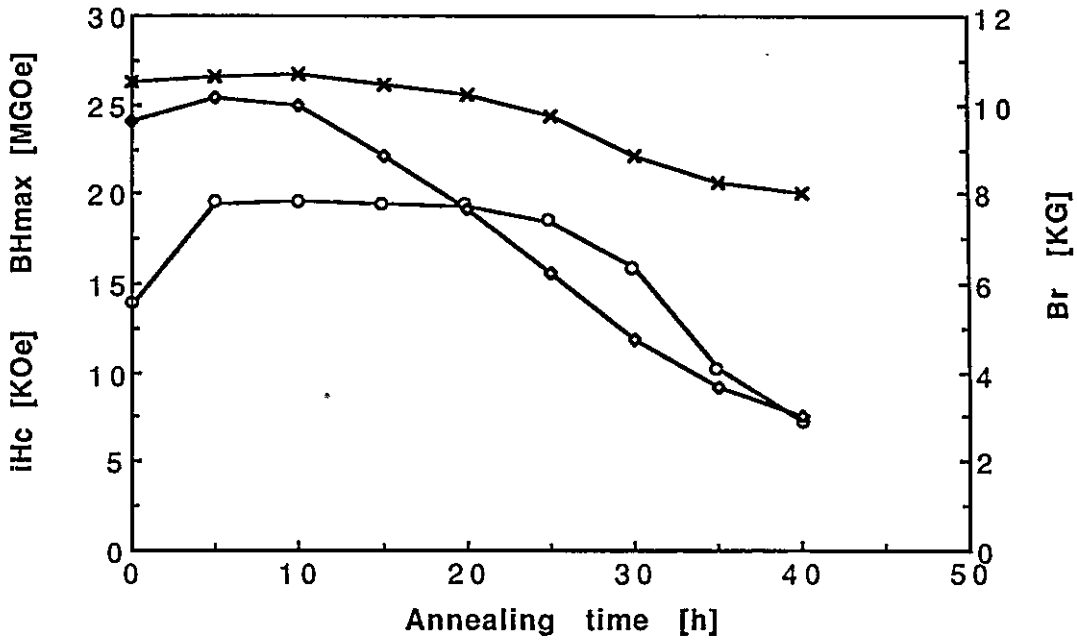

Fig. 9.4.2 Variation of Br, iHc and BHmax with annealing time for magnets of alloy III ($Pr_{16.9}Fe_{79.1}B_4$), using the heat sequence of fig. 7.5.1. (◊: BHmax, x : Br, o : iHc)

For the $Pr_{20.5}Fe_{73.8}B_{3.7}Cu_2$ alloy there is no significant further increase in iHc or BHmax after 15 hours and for the $Pr_{16.9}Fe_{79.1}B_4$ alloy the increase is more rapid but also deteriorates faster. The values, for both alloys, after 24 hours are inferior to those of the slow cooled samples. This is more pronounced for alloy III.

9.5 The Effect of Sintering Temperature on Br and Density

The influence of the sintering temperature on the Br values of magnets of the $Pr_{16.9}Fe_{79.1}B_4$ alloy is shown in Fig. 9.5.1. These values are rather lower than those obtained in the corresponding hot pressed magnets (Shimoda et al1989, 12.6 KG) . Jiang et al. (1989) have shown that Pr-Fe-B magnets prepared via HD and sintered in flowing Ar have a tendency to retain some residual hydrogen, leading to a decrease in the density due to lattice expansion and to the appearance of pores, resulting in reduced Br and consequently the energy product. This should not be the case with the present magnets which have been sintered in a vacuum.

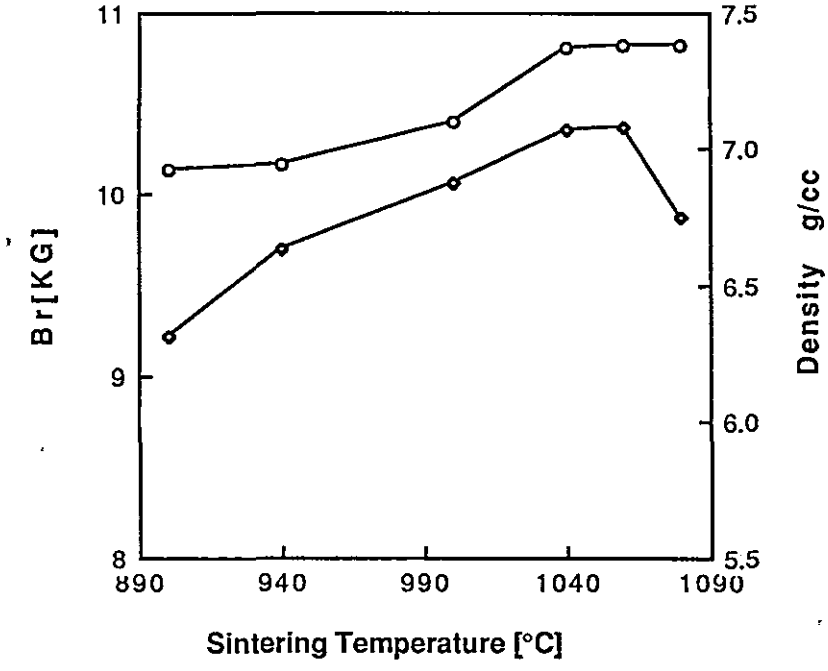

Fig. 9.5.1 Variation of remanence with the sintering temperature. Quenched samples of alloy III ($Pr_{16.9}Fe_{79.1}B_4$). (o:density, ◊: Br).

Although in this work the magnets were vacuum sintered and showed higher densities as can be seen in Fig 9.5.1 they still exhibit low remanence values compared with the hot pressed material but this can be attributed to the "squeezing out" of the Pr-rich material during the hot pressing operation.

9.6 The Effect of the HD process on the c-axis alignment

It has been reported by Pourarian, Huang and Wallace (1986), that $Pr_2Fe_{14}BH_5$ (HD pressure: 60 atm) exhibits planar anisotropy and Lin et al. (1990) demonstrated that the tetragonal c-axis of the HD powder lies in the plane perpendicular to the magnetic field direction during alignment and the subsequent dehydrogenation and sintering does not change this radial alignment. Their powder was uniaxially pressed with the field direction perpendicular to the press direction using hydrogen decrepitated and hammer milled material. In the present work, an isostatic pressing method has been used which removes the influence of pressing on the magnetic properties of the magnet.

Figure 9.6.1 shows the demagnetisation curve in the X,Y (radial) and Z (pulse alignment) direction for Hydrogen Decrepitated (Alloy I) magnets aligned and subsequently pressed in an isostatic press. All the magnets prepared via the HD process (alloy I and III) showed uniaxial anisotropy in the direction of alignment Z. The absence of radial alignment can be attributed to the lower hydrogenation pressure of 10 bar used in the present work giving a lower hydrogen content than that reported by Pourarian, Huang and Wallace (1986). Lattice parameter measurements using X-

ray diffraction (see Table 9.6.1) revealed that the alloy decrepitated at 10 bar had a formula unit of $Pr_2Fe_{14}BH$ assuming a linear variation of volume with H content.

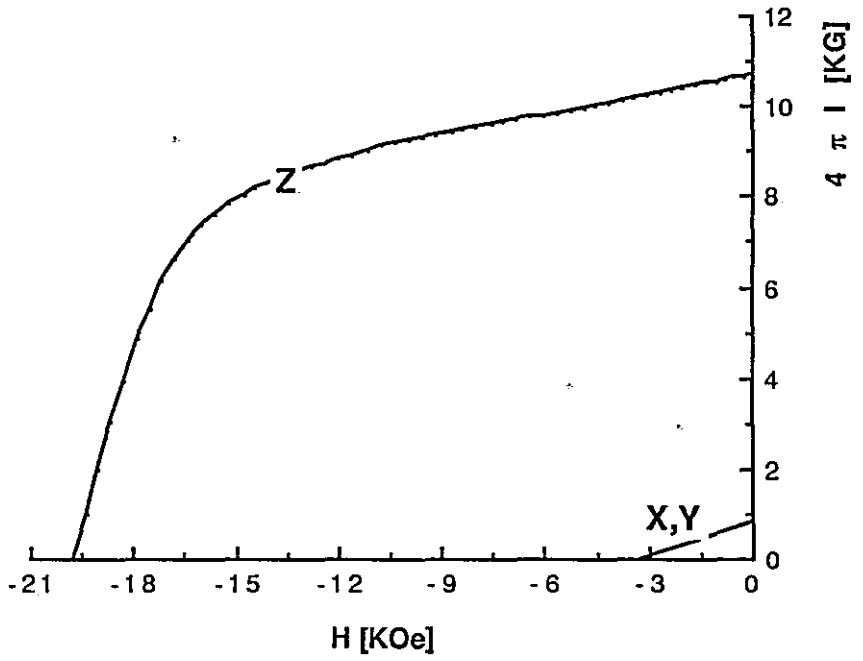

Fig. 9.6.1 Demagnetization curves for magnets of alloy I, X, Y=radial directions and Z = alignment pulse direction.

Table 9.6.1. Lattice parameters for alloy II (Debye-Scherrer film).

Compound	a (A)	c (A)
$Pr_2Fe_{14}BH_x$	8.943	12.46

The X-ray diffraction pattern shown in fig.9.6.2 (similar to those of Shimoda et al. 1989) indicates clearly that the c-axis of the $Pr_2Fe_{14}B$ lies in the direction of magnetic alignment of the HD sintered magnets which is consistent with the magnetic measurements. According to Zhou et al. (1988) well aligned samples show only three strong peaks: (004), (105) and (006), where the (004) and (006) are perpendicular to the easy direction [001] in the tetragonal crystal structure of the $Nd_2Fe_{14}B$ phase, the (105) is tilted by about 15° from the (00*n*) plane and the (006) reflection is the strongest reflection.

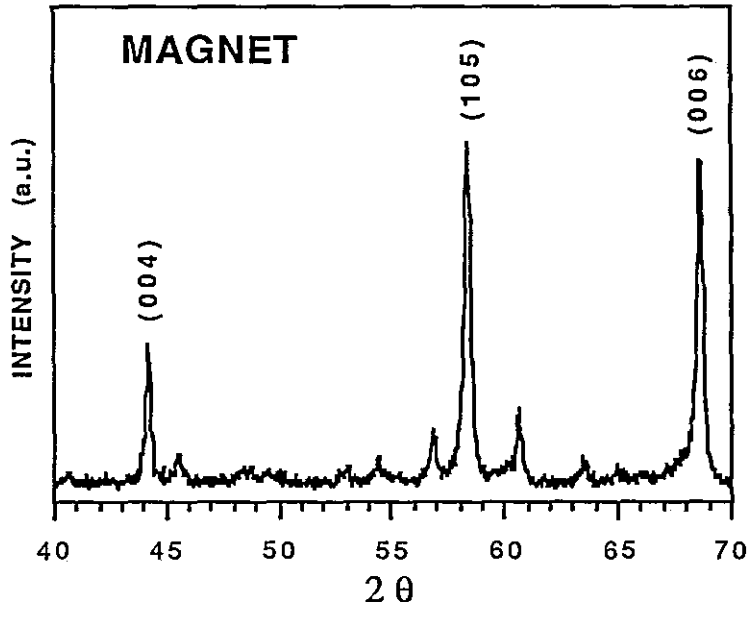

Fig.9.6.2 X-ray diffraction pattern of a $Pr_{17}Fe_{79}B_4$ magnet prepared using the HD process.

9.7 The Effect of Annealing at 1000°C on Nd-based Magnets

Figures 9.7.1, 2 and 3 show the variation of magnetic properties with milling time for slow cooled HD magnets of $Nd_{20.5}Fe_{73.8}B_{3.7}Cu_2$, $Nd_{17}Fe_{76.5}B_5Cu_{1.5}$ and $Nd_{16.9}Fe_{79.1}B_4$ alloy respectively, both as-sintered and annealed at 1000°C for 24 hours. As can be seen a small increase in the magnetic properties occurs with this post sintering heat treatment for these alloys, but no iHc peak, as in the case of the PrFeB(Cu) alloys, was found. The $Nd_{17}Fe_{79}B_4$ magnets exhibited very poor magnetic properties, in contrast with the $Pr_{16.9}Fe_{79.1}B_4$ magnets.

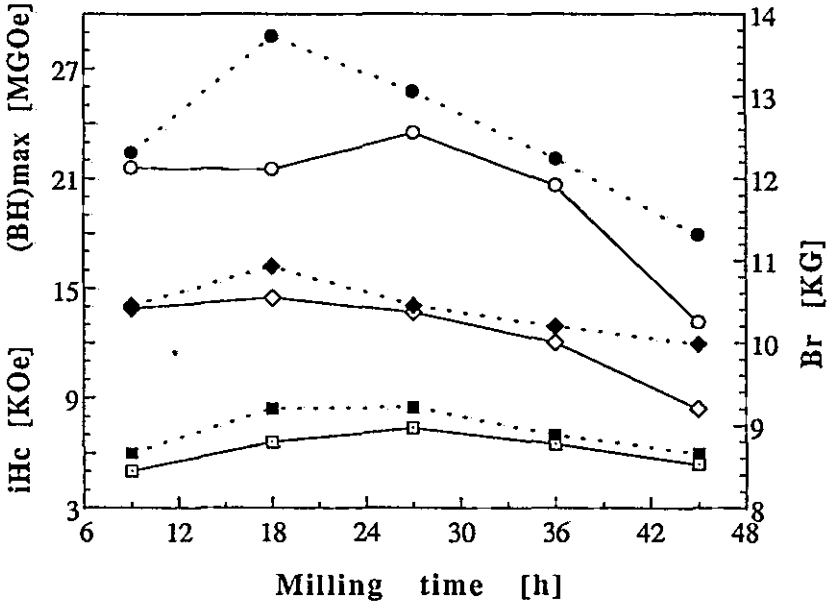

Fig. 9.7.1. Variation of (BH)max (o) and iHc (▣) and Br (◊) with the milling time for slow cooled HD magnets of $Nd_{20.5}Fe_{73.8}B_{3.7}Cu_2$ alloy (Black/dashed : annealed 1000°C, 24 hours)

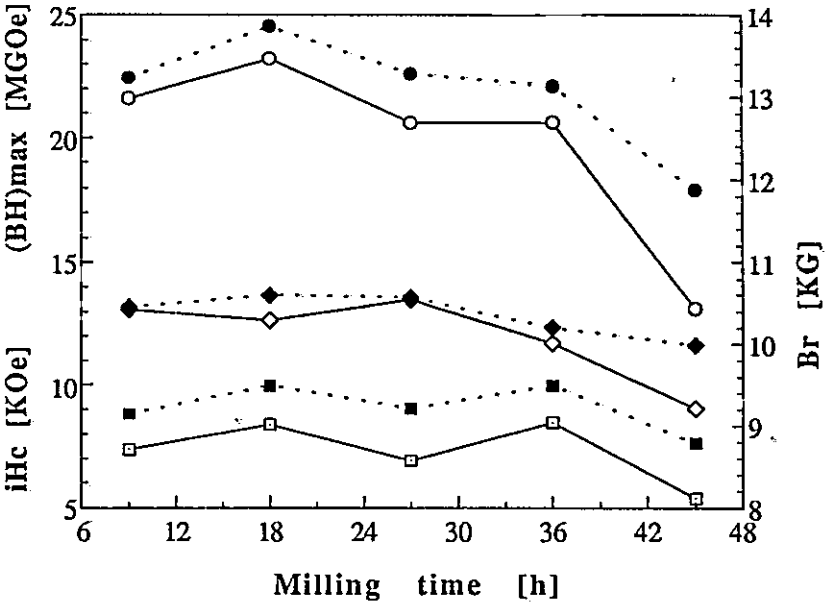

Fig.9.7.2. Variation of (BH)max (o) and iHc (⊡) and Br (◊) with the milling time for slow cooled HD magnets of $Nd_{17}Fe_{76.5}B_5Cu_{1.5}$ alloy (Black/dashed : annealed 1000°C, 24 hours).

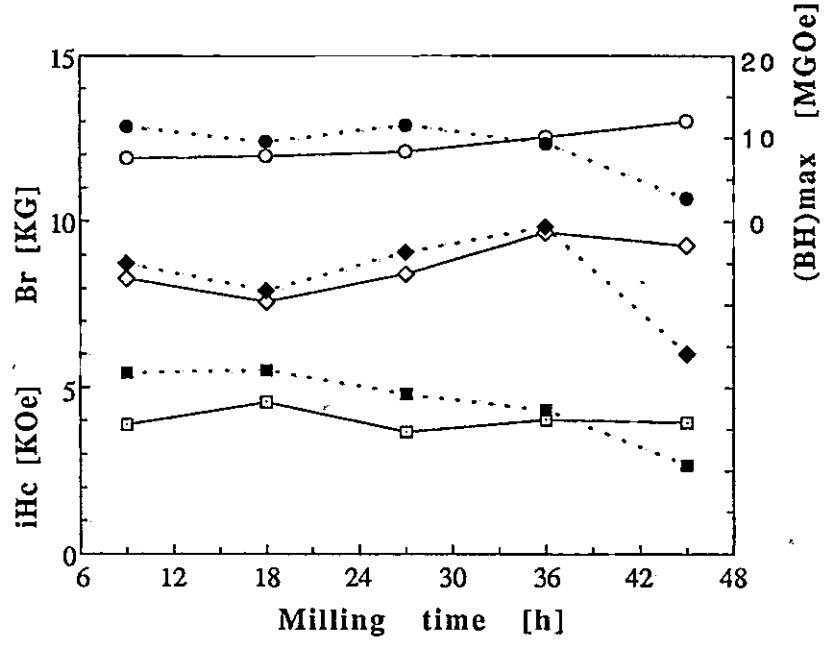

Fig. 9.7.3. Variation of (BH)max (o) and iHc (⊡) and Br (◊) with the milling time for slow cooled HD magnets of $Nd_{16.9}Fe_{79.1}B_4$ alloy (Black/dashed : annealed 1000°C, 24 hours).

CHAPTER TEN

MICROSTRUCTURAL STUDIES ON PrFeBCu HD SINTERED MAGNETS

10.1 Introduction

In the past, Pr-Fe-B sintered permanent magnets with high coercivity have only been produced with substitutions of Co,Al, Dy and Tb. It has been shown in the last chapter that magnets based on the compositions $Pr_{20.5}Fe_{73.8}B_{3.7}Cu_2$ and $Pr_{16.9}Fe_{79.1}B_4$ produced using the hydrogen decrepitation (HD) process achieve high coercivities after a post sintering heat treatment. Annealing the magnets at 1000°C, resulted in an increase in the intrinsic coercivity from ~11 kOe to around 20 kOe for both alloys.

In this chapter, the microstructure of HD sintered permanent magnets with a composition of $Pr_{20.5}Fe_{73.8}B_{3.7}Cu_2$ have been investigated using optical metallography, scanning electron microscopy (SEM) and transmission electron microscopy (TEM) in an attempt to reveal the reason for the increased coercivity on annealing. This study has been carried out on both as-sintered and high temperature annealed magnets. Thermomagnetic analysis (TMA) and differential thermal analysis (DTA) have also been employed in the present investigations. The present investigation has not been extended to the copper free magnets since this study has already been carried out by Paik et al. (1989) and was summarized in section 6.3.

10.2 Optical Microscopy Investigations

The microstructure of the as-sintered $Pr_{20.5}Fe_{73.8}B_{3.7}Cu_2$ HD magnet is shown in Fig.10.2.1a, and the microstructure of this magnet after annealing at 1000°C for 24 hours and then slow cooling is shown in fig 10.2.1b (demagnetization curves are shown in fig. 9.3.4). Both samples were etched since the contrast between the different phases and grain boundaries was more pronounced in this condition. In the as-sintered state, the magnet consists of the $Pr_2Fe_{14}B$ matrix phase, the Pr-rich material in the grain boundaries and a dark grey phase (Pr_2Fe_{17}) within the matrix phase (the chemical analysis is discussed later).

After the annealing treatment, the amount of the dark grey phase diminished and the grain boundaries became much more defined. This could indicate that the coverage of the matrix phase with a non ferro-magnetic Pr-rich material is improved after the post sintering heat treatment and this would enhance the intrinsic coercivity since better magnetic isolation of the $Pr_2Fe_{14}B$ grains would be achieved. In the annealed condition, as indicated by fig.10.2.1.b, the Pr_2Fe_{17} phase appears more as individual grains and in isolated regions. A comparison between these two microstructures also demonstrates that there has been no significant grain growth during the post sintering heat treatment. It has been suggested by Paik et al.(1989) that the Pr_2Fe_{17} phase retards the grain growth of the $Pr_2Fe_{14}B$ matrix phase. No clear evidence of a grain boundary eutectic has been found in the sintered magnets (Kwon, Bowen and Harris 1992a).

(a)

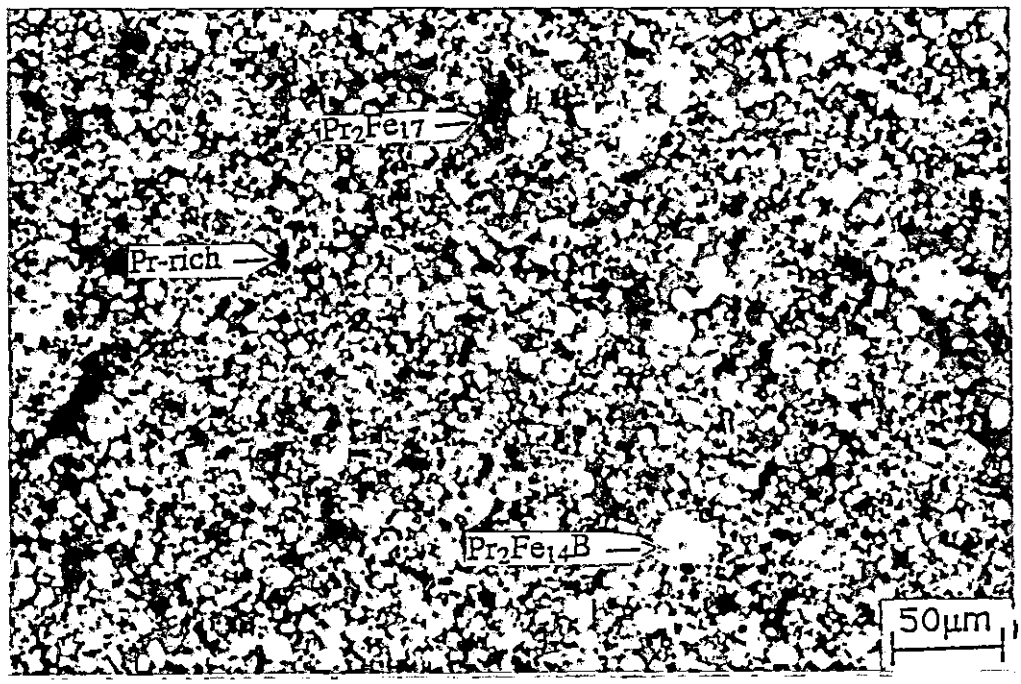

(b)

Fig.10.2.1 Optical micrograph showing a general view of the microstructure of the $Pr_{20.5}Fe_{73.8}B_{3.7}Cu_2$ HD magnet in the as-sintered (a) and annealed (b) condition (Black regions : grains pulled out on polishing or on etching with nital).

10.3 Scanning Electron Microscopy Studies (SEM)

Figures 10.3.1 and 2 show back scattered electron images of the as-sintered and annealed $Pr_{20.5}Fe_{73.8}B_{3.7}Cu_2$ HD magnets. The presence of the dark phase (Pr_2Fe_{17}) is also observed in both samples, although its occurrence is more pronounced in the as-sintered sample. Fig.10.3.2 also indicates that the magnetic isolation (white regions) of 2:14:1 grains is improved when compared with fig.10.3.1. This is consistent with the optical microscope results.

It can be seen in fig. 10.3.1 that the dark phase is distributed within the matrix phase (confirmed by higher magnification, see fig 10.3.3) and since backscattered electron images reveal the difference between the average atomic numbers of the phases, the differences in contrast show that the phases have different compositions. Fig.10.3.2 indicates that, after annealing, the dark phase is more concentrated in the form of isolated grains and this is consistent with the optical microscope examinations.

EDX microanalysis indicated that the dark phase is richer in iron than the matrix phase and the matrix phase showed a Fe:Pr at. ratio of about 7 and the dark phase a Fe : Pr at. ratio of approximately 8.2 indicating a 2 : 17 type phase. This is consistent with previous studies (Paik et al.1989) , which have shown that, in sintered magnets of the $Pr_{17}Fe_{83-x}B_x$-type, the magnetically soft Pr_2Fe_{17} phase always occurs when $x < 5$.

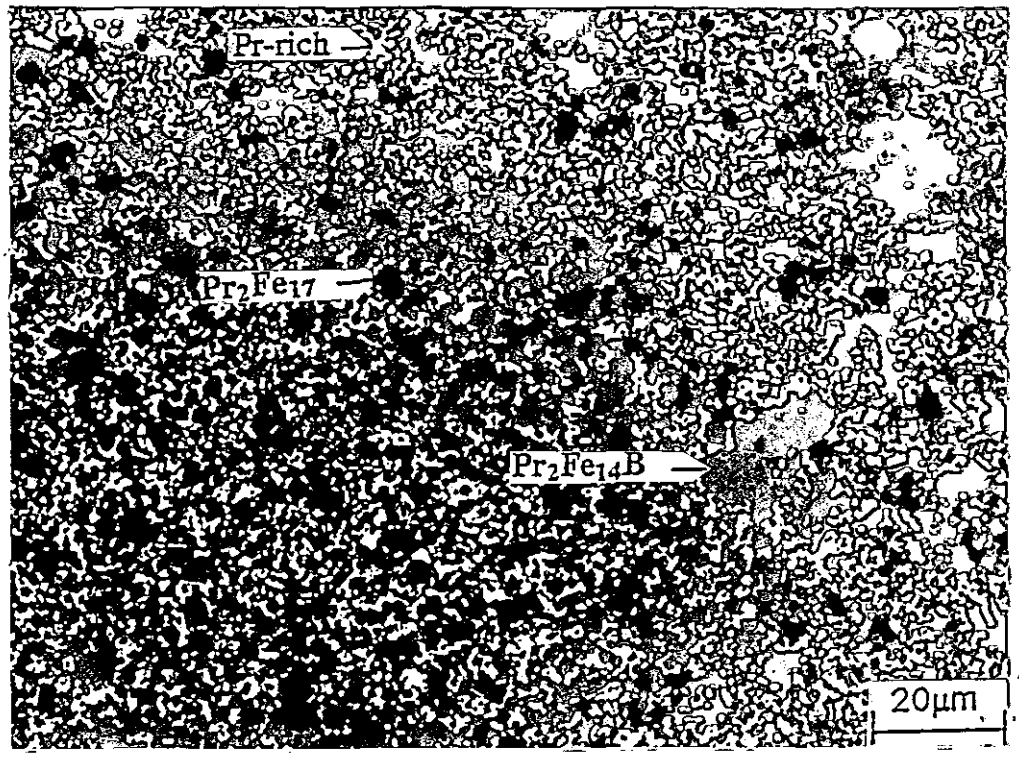

Fig. 10.3.1 Back scattered electron image of the $Pr_{20.5}Fe_{73.8}B_{3.7}Cu_2$ HD magnet in the as-sintered condition.

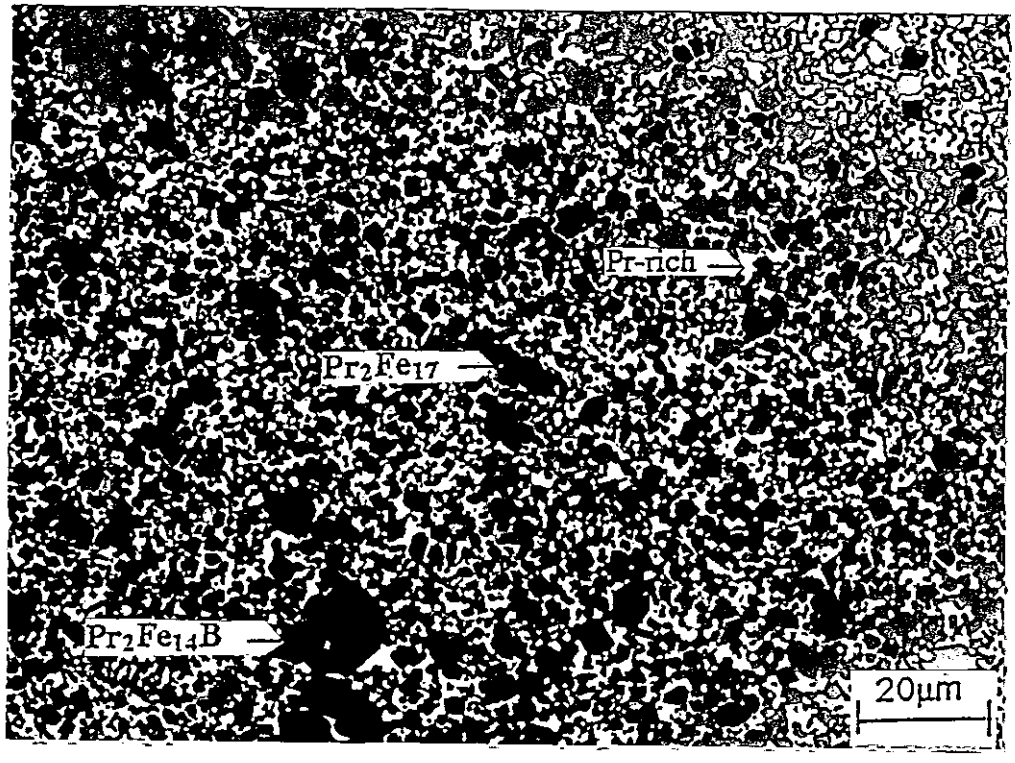

Fig.10.3.2 Back scattered electron image of the $Pr_{20.5}Fe_{73.8}B_{3.7}Cu_2$ HD magnet in the annealed condition.

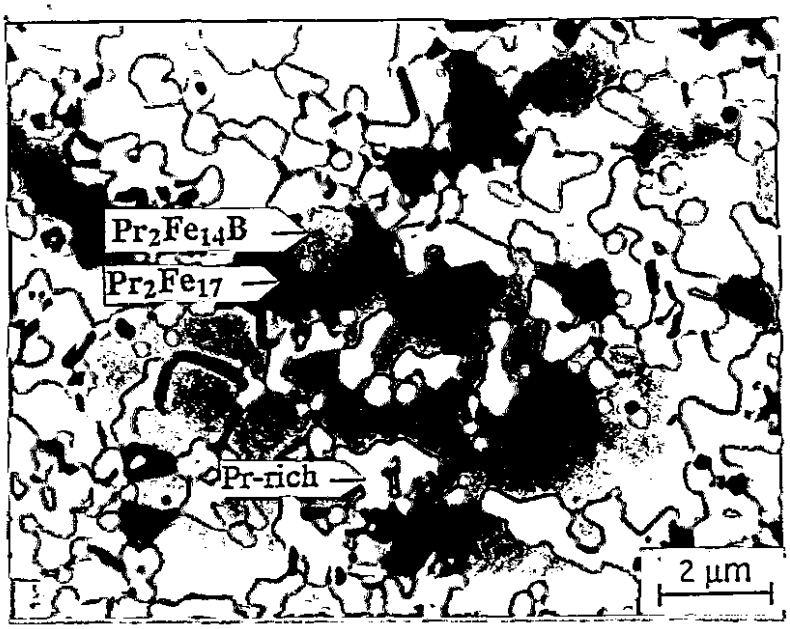

Fig.10.3.3 Back scattered electron image of details of the $Pr_{20.5}Fe_{73.8}B_{3.7}Cu_2$ HD magnet in the as-sintered condition.

Similarly a Nd_2Fe_{17} magnetically soft phase has also been found in Nd-based sintered magnets with similar compositions (Paik et al.1989, Kianvash and Harris 1992, and Yin 1992). It has been shown (Kianvash and Harris 1992) that the amount of this phase (Nd_2Fe_{17}) was reduced with a high temperature heat treatment. According to this work (Kianvash and Harris 1992), some of the 2 : 17-type phase was removed during the high temperature heat treatment and this is consistent with the present observations for the Pr-based magnets. No other phases could be detected by SEM.

10.4 Thermomagnetic Analysis (TMA) Studies

A thermomagnetic analysis curve of the as-sintered magnet is presented in fig.10.4.1. There was no significant change in the TMA curve after the post sintering heat treatment (Fig.10.4.2). The small magnetisation variation (increasing between the temperatures 70 to 230 °C) can be ascribed to the competing effects of increasing temperature on the degree of saturation of the sample (due to decreasing anisotropy of the misaligned sample) and the value of the saturation magnetisation.

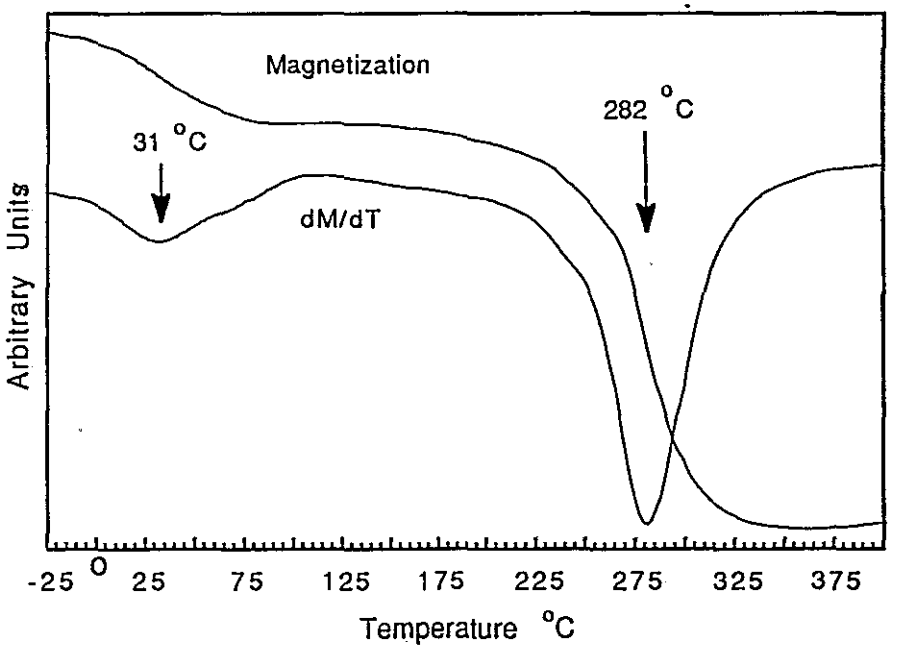

Fig. 10.4.1 Magnetisation (non-saturated) versus temperature for the $Pr_{20.5}Fe_{73.8}B_{3.7}Cu_2$ HD magnet in the as-sintered condition (error±5°C).

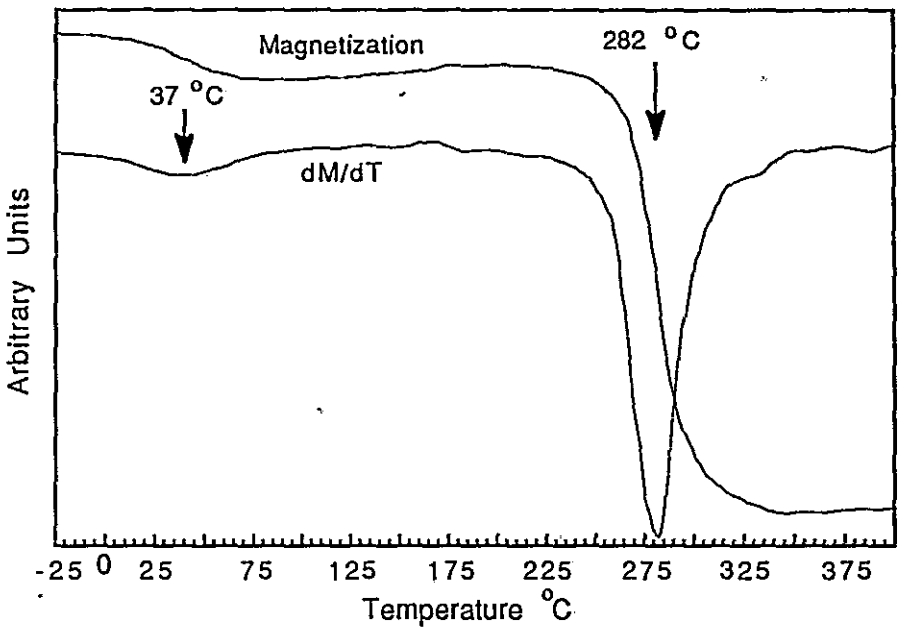

Fig. 10.4.2 Magnetisation (non-saturated) versus temperature for the $Pr_{20.5}Fe_{73.8}B_{3.7}Cu_2$ HD magnet in the annealed condition (error±5°C).

The TMA curves of both magnets showed that, in addition to the matrix phase (Tc = 282 °C), there was a lower Curie point ferromagnetic phase in both magnets with a Tc around 31 and 37°C, and this can be attributed to the presence of a 2 : 17 type phase in these magnets, consistent with the SEM observations. This phase (Pr_2Fe_{17}) has a reported Curie point as low as 10 °C (Strnat, Hoffer and Ray 1966) and 15 °C (Paik et al.1989), and as high as 28 °C (Rotenberg et al. 1985). It has also been reported (Rotenberg et al. 1985) that when free Fe is present the Curie point of this phase varies from 42 to 50 °C.

10.5 Differential Thermal Analysis (DTA) Studies

The Curie temperature of the matrix phase determined by DTA was around 290 °C (see fig. 10.5.1 and 2). This value is slightly higher than that determined by TMA. This phase also has various reported Curie temperatures such as 303 °C (Jiang et al. 1988), 290°C (Jinghua, Yiying and Jingkui 1991) and 284 °C (Takahashi et al. 1991).

At around 463 °C, a small peak, which could be related to the melting temperature of the Pr-rich eutectic grain boundary phase (Kwon, Bowen and Harris 1992a, and Takahashi et al. 1991), can also be observed in Fig. 10.5.1 and 2. This eutectic phase has been found in the grain boundaries of the as-cast alloy after annealing and the DTA studies showed an appreciable peak at 463°C, which was related to the melting point of this phase (Kwon, Bowen and Harris 1992a).

In the present studies on sintered magnets there is no clear evidence for the presence of the eutectic phase by optical metallography and SEM studies. This is believed to be due to the finer grain size of the sintered magnet and hence more evenly distributed grain boundary phases making it difficult to resolve the eutectic mixture (if present). Only a small peak was detected by DTA at 463 °C and it was assumed that the peak was much smaller than in the as-cast state due to the incorporation of oxygen in the grain boundaries during milling and subsequent processing steps.

In the "as-sintered" condition the DTA curve also shows a peak around 667 °C. This peak could be associated with the Pr_2Fe_{17} phase (Pr-Pr_2Fe_{17} eutectic isotherm : 667 °C : Jinghua, Yiying and Jingkui 1991; and 670 °C : Ray 1968) or with the $Pr_2Fe_{14}B$ phase ($Pr_2Fe_{14}B$-Pr eutectic isotherm : 676 °C : Jinghua, Yiying and Jingkui 1991; see section 5.4). As its presence is not observed in the annealed condition, it can be most likely related to the presence of the Pr_2Fe_{17} phase, since the occurrence of this phase has diminished after annealing.

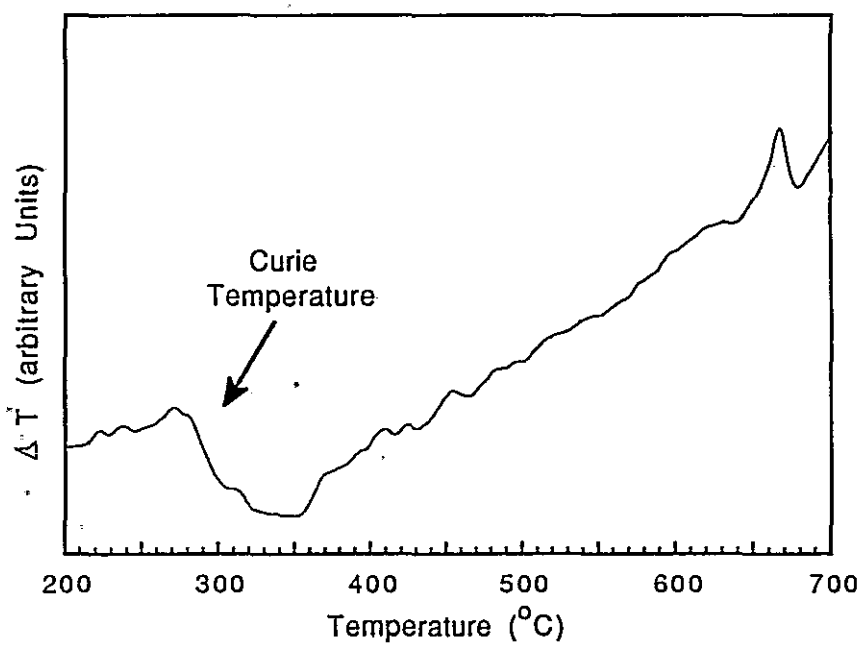

Fig.10.5.1 DTA heating curve for as-sintered $Pr_{20.5}Fe_{73.8}B_{3.7}Cu_2$ magnet prepared using the HD process (error±7°C).

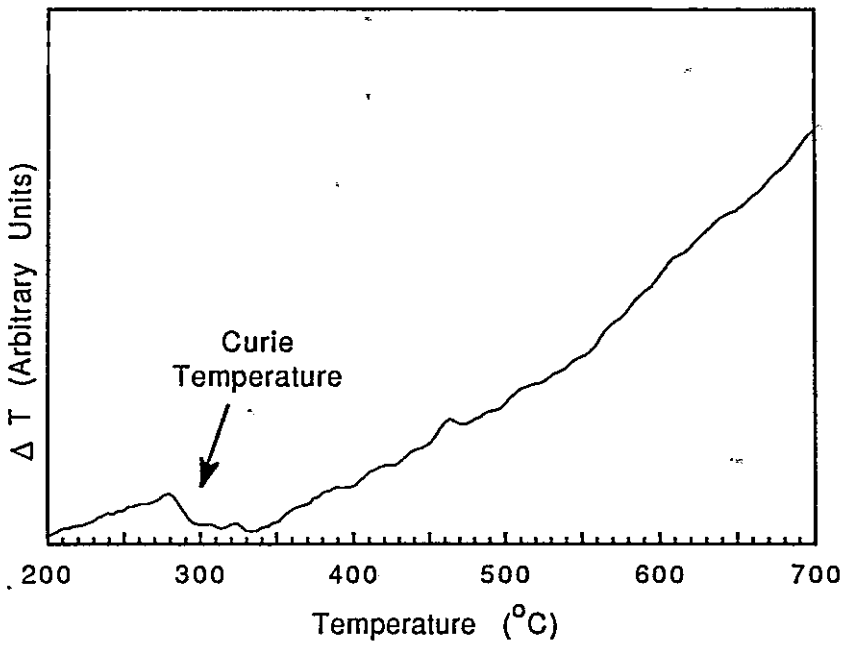

Fig.10.5.2 DTA heating curve for annealed $Pr_{20.5}Fe_{73.8}B_{3.7}Cu_2$ magnet prepared using the HD process (error ± 7 °C).

10.6 Transmission Electron Microscopy (TEM) Studies

Transmission electron microscopy studies confirmed that the annealed $Pr_{20.5}Fe_{73.8}B_{3.7}Cu_2$ HD magnets contain a phase with a Fe : Pr at. ratio of ~ 8.6 (2 : 17) and this is consistent with the SEM analysis (Fig. 10.6.1 shows the analysed region). TEM observations also showed the presence of a $Pr_{34}Fe_{62}Cu_4$ phase in the annealed sample and Fig. 10.6.2 shows the TEM analysed region of this phase. This phase has been found in the cast alloy after annealing (Kwon, Bowen and Harris 1992 and 1992a) and has been reported

(Kajitani, Nagayama and Umeda 1992) recently by some Japanese workers.

A similar Cu containing phase has also been found in $Nd_{17}Fe_{76.5}B_5Cu_{1.5}$ sintered HD magnets (Kianvash and Harris 1992). Although the occurrence of such a Cu-containing phase at the grain boundaries could improve the coercivity by developing better magnetic isolation, it was assumed in the present work that this phase does not play an important role in the coercivity of the HD sintered magnets since Cu-free Pr-Fe-B HD sintered magnets also exhibited a similar increase in coercivity on annealing.

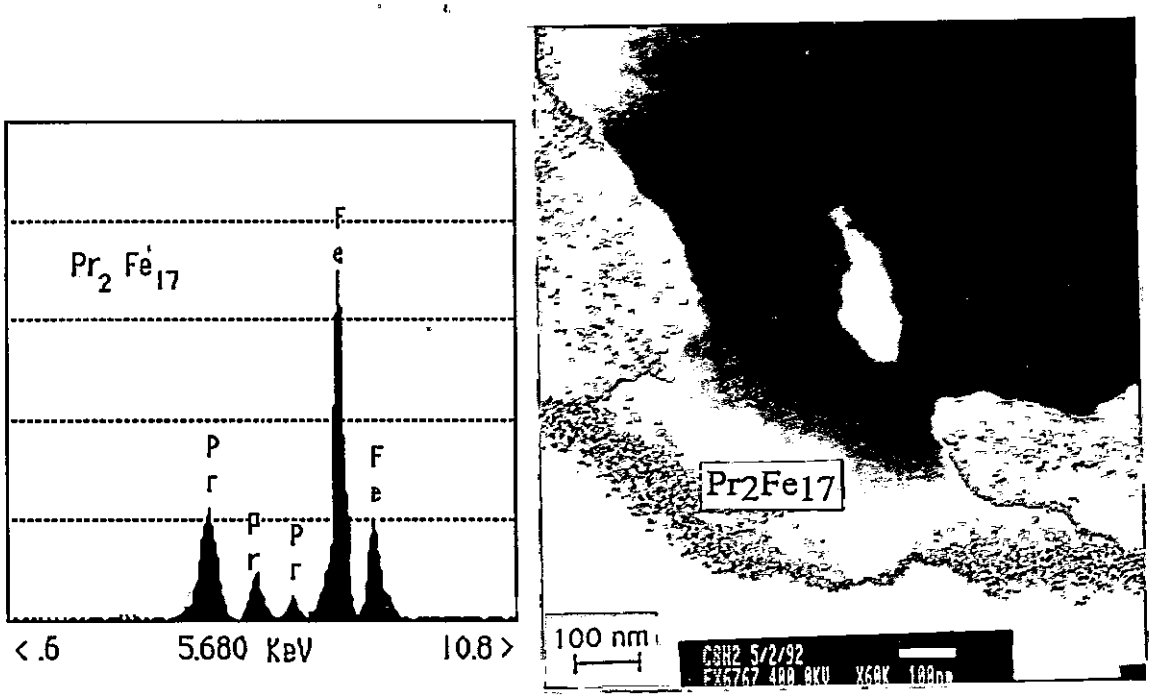

Fig. 10.6.1 Transmission electron micrograph and X-ray spectrum of a Pr_2Fe_{17} phase (annealed magnet).

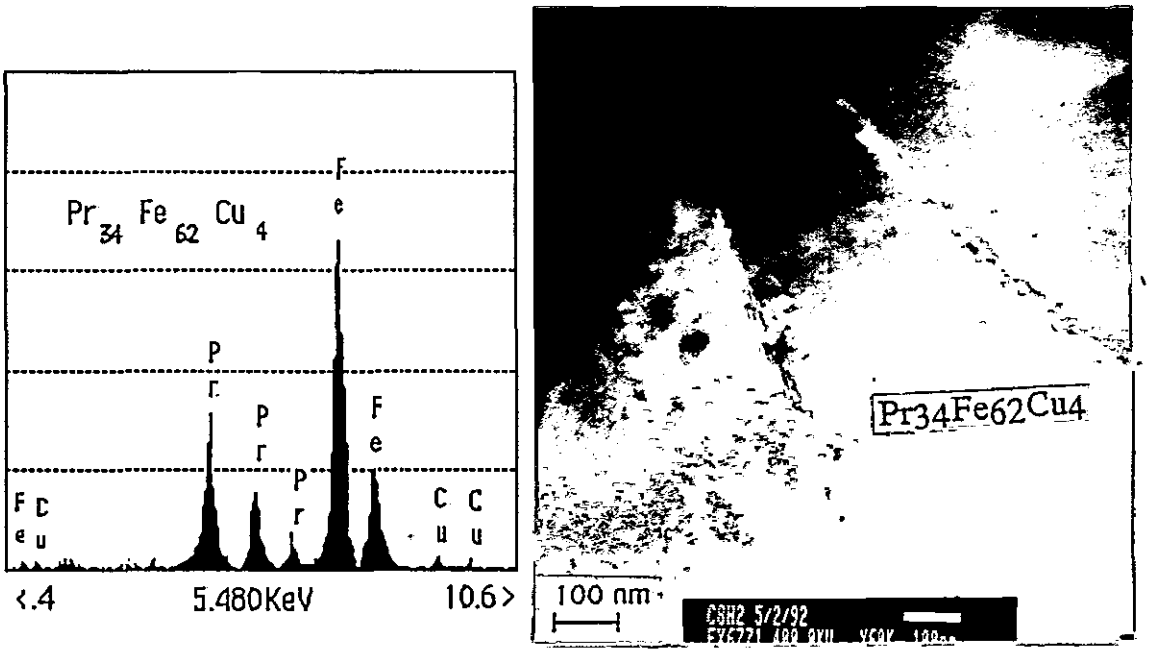

Fig. 10.6.2 Transmission electron micrograph and X-ray spectrum of a $Pr_{34}Fe_{62}Cu_4$ phase (annealed magnet).

To Summarize : the increase in the coercivity of $Pr_{20.5}Fe_{73.8}B_{3.7}Cu_2$ HD sintered magnets with a high temperature heat treatment can be attributed to the better magnetic isolation of the $Pr_2Fe_{14}B$ grains obtained with this treatment. The amount of the Pr_2Fe_{17} phase decreased after the post sintering heat treatment which could also be responsible for the enhanced coercivity in this magnet. In the as-sintered condition this phase is closely associated with the matrix phase whereas after annealing it occurs as individual grains. A $Pr_{34}Fe_{62}Cu_4$ phase has been identified in a magnet annealed at 1000 °C for 24 hours.

CHAPTER ELEVEN

THE EFFECT OF THE ALLOY STATE ON THE MAGNETIC PROPERTIES OF VARIOUS HD SINTERED MAGNETS

11.1 Introduction

The starting microstructure of $Nd_{15}Fe_{77}B_8$ as-cast ingots has been found to play a role in the final magnetic properties of sintered magnets (Ward and Taylor 1989). In this investigation the microstructures were modified by changing the cooling rate of the ingot and the sintered magnets were prepared using a standard milling time. It has been shown by Lemaire et al. (1990) and also by Morros et al. (1991) that the Nd-Fe-B bulk ingot is composed of regions with different microstructures and it has been suggested by the former authors that this could affect the magnetic properties of the sintered magnet. It has also been proposed by them that, for Nd-Fe-B-type alloys, the powder metallurgy route might have a tendency to rehomogeneize the material through the milling and sintering steps, and if this were the case then the magnet-processing steps would cause a progressive attenuation of the influence of the ingot microstructure on the magnetic properties of the sintered magnet.

It has been assumed in the present work that any rehomogenizing effects would be determined mostly by the milling stage and that a greater influence of the initial microstructure would be expected at lower milling times. It has been shown in chapter 9 that even for as-crushed material with a coarse particle

size, HD sintered magnets based on the alloy $Pr_{20.5}Fe_{73.8}B_{3.7}Cu_2$ exhibited appreciable magnetic properties even in the cast and annealed condition. Therefore, in order to investigate the detailed effect of milling time, this alloy was considered to be the most suitable candidate since the effects at low milling times can be observed. This is not possible for Nd-Fe-B alloys since they exhibit virtually no permanent magnetic properties without appreciable milling (Weizhong et al. 1991). Thus the $Pr_{20.5}Fe_{73.8}B_{3.7}Cu_2$ alloy has been selected for this work instead of the previously studied alloy, in order to make possible an investigation of a wider range of milling times.

An initial heat treatment for homogenization, usually at elevated temperature and for a few days, has been applied to Nd-Fe-B alloys by McGuiness and Harris (1988) to eliminate free iron and composition gradients, by accelerating the solid-state diffusion and consequently yielding a more homogeneous alloy. Thus, homogenization by annealing the as-cast ingot was used as a controlled means of modifying the alloy microstructure prior to magnet processing. The magnetic behaviours of magnets prepared from this homogenized alloy were compared with those of samples prepared from the standard as-cast ingot alloy. In this chapter the possibility that the ingot homogenization heat treatment and milling time influence the final magnetic properties of HD sintered magnets of a $Pr_{20.5}Fe_{73.8}B_{3.7}Cu_2$ alloy has been investigated.

A study of the influence of the HD material degassing on the final magnetic properties of HD sintered magnets prepared from a $Pr_{16}Fe_{76}B_8$ alloy (IV) have also been carried out. For all the magnets

studied in this chapter a systematic milling time study has been carried out.

Finally, the influence of the initial microstructure on the final magnetic properties of $Nd_{16}Fe_{76}B_8$ HD sintered magnets has also been studied to provide a comparison with the Pr-based alloys. For this study, rods of this alloy were directionally solidified using VFZ equipment under controlled conditions for a fixed value of the temperature gradient/growth rate ratio (G/R). Sintered permanent magnets using the hydrogen decrepitation process were prepared from the VFZ material in order to try and relate the final magnetic properties with the initial state of the alloy.

11.2 The effect of ingot heat treatment on the magnetic properties of $Pr_{20.5}Fe_{73.8}B_{3.7}Cu_2$ HD sintered magnets

The as-cast state of the $Pr_{20.5}Fe_{73.8}B_{3.7}Cu_2$ alloy was shown in chapter 8 (fig.8.2.1 and 3) and is very heterogeneous. Phase analysis indicates that the alloy is composed of the matrix phase $Pr_2Fe_{14}B$ (plate-like white crystals), copper and praseodymium-rich phases in the intergranular regions and free-iron inside the matrix phase (consistent with the peritectic nature of this phase, see section 5.4). The $Pr_{1+\varepsilon}Fe_4B_4$ boride phase has not been observed. The microstructure of the homogenized $Pr_{20.5}Fe_{73.8}B_{3.7}Cu_2$ alloy is shown in Fig.11.2.1. A comparison with the as-cast microstructure in fig.8.2.1 demonstrates that there is no significant grain growth during the homogenization heat treatment, which is consistent with previous work by Kwon, Bowen and Harris (1991a). The most

obvious change during the heat treatment is the elimination of free iron, which can be seen in fig.8.2.1 but not in fig.11.2.1.

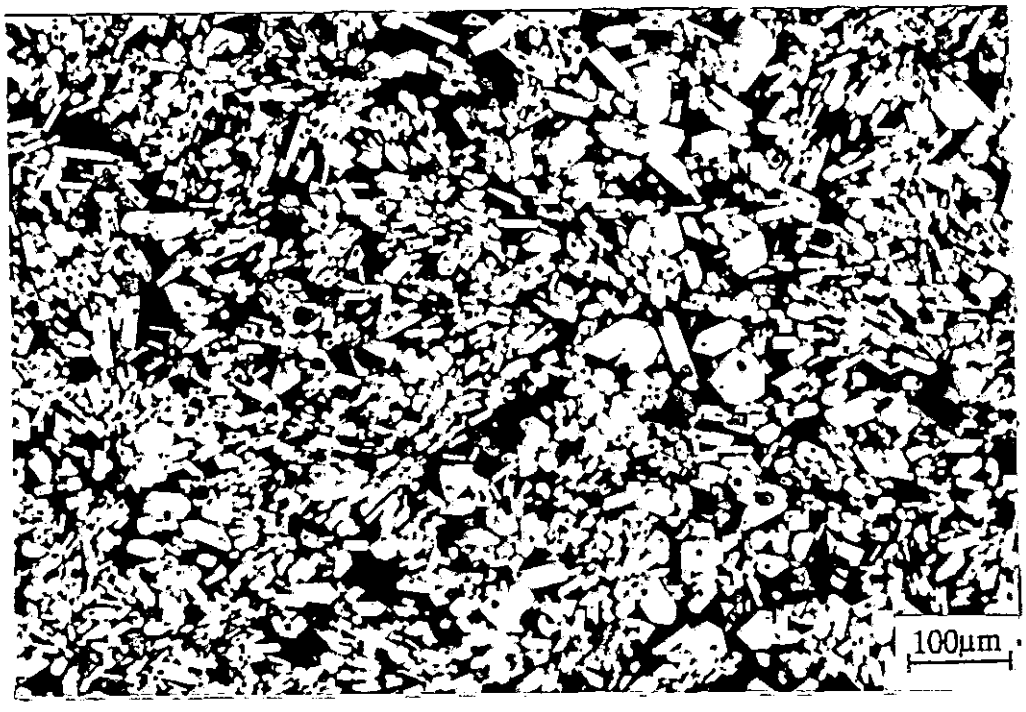

Fig.11.2.1. Optical micrograph showing a general view of the microstructure of the homogenized $Pr_{20.5}Fe_{73.8}B_{3.7}Cu_2$ alloy (Etched with Nital). There is now no evidence of free iron within the $Pr_2Fe_{14}B$ crystals.

Due to a reaction between the Pr-rich phase and Cu a second change observed is the reduction in the amount of grain boundary needle like phase and the appearance of a coarse grain boundary eutectic (see section 8.4). It has been shown by Kwon, Bowen and Harris (1991a) that a minimum of 5 hours is required for this homogenization heat treatment to occur, but 24 hours was used in the present work to avoid any possible variations due to the homogenization procedure.

Figure 11.2.2 shows the demagnetization curves for HD magnets prepared using the as-cast and homogenized alloy crushed with a pestle and mortar and then sintered. There is a dramatic increase in remanence and consequently in energy product for the magnets made from the homogenized alloy. This can be attributed to the better density (see Table 11.2.1) and to the better loop shape, which can be attributed to the elimination of the free iron (magnetically soft phase) from the ingot material and to improved alignment.

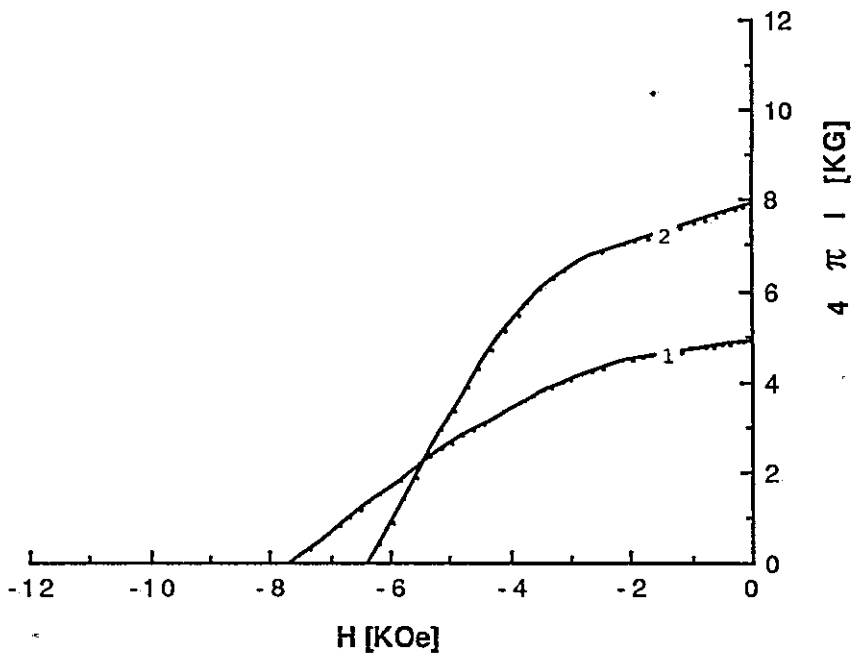

Fig.11.2.2. Demagnetization curves for $Pr_{20.5}Fe_{73.8}B_{3.7}Cu_2$ magnets prepared using the crushed alloy. As-cast : 1, Homogenized : 2.

These magnets exhibit appreciable magnetic properties, whereas $Nd_{16}Fe_{77.5}B_{6.5}$ magnets prepared under the same conditions (Weizhong et al. 1991) exhibit virtually no magnetic

properties. This difference in behaviour can be attributed to (a) the much finer microstructure of the $Pr_{20.5}Fe_{73.8}B_{3.7}Cu_2$ alloy in the as-cast state (achieved with the reduced boron content and copper substitution, Shimoda et al. 1989), (b) the extensive amount of the Pr-rich material surrounding each $Pr_2Fe_{14}B$ crystal and (c) the enhanced anisotropy field of the matrix $Pr_2Fe_{14}B$ phase (Hirosawa et al. 1986) compared with that of $Nd_2Fe_{14}B$.

Table 11.2.1 Density and magnetic properties of magnets prepared from as-cast and homogenized alloy. (*homogenized value).

Density and Mag. Prop.	Milling time		
	Crushed	4 h	9 h
ρ^* / ρ	7.14 / 6.48	7.37 / 7.32	7.32 / 7.33
$BH_{max}{}^*/BH_{max}$	11.0 / 4.9	27.6 / 22.7	25.4 / 24.9
$B_r{}^*$ / B_r	7.8 / 4.9	10.9 / 10.0	10.1 / 10.7
$_iH_c{}^*$ / $_iH_c$	6.4 / 7.7	9.1 / 10.2	20.2 / 19.7
SF* / SF	0.33 / 0.30	0.73 / 0.60	0.59 / 0.39

ρ [g cm^{-3}], $(BH)_{max}$ [MGOe], Br [KG], iHc [KOe], SF [Ratio]

(Average error: Br : ± 0.1, iHc : ± 0.5, BHmax : ± 0.9)

The demagnetization curves for magnets produced using the as-cast and homogenized alloy ball milled for 4 hours are shown in Figure 11.2.3. The improvement in energy product for the magnet prepared from the homogenized alloy is still very significant. It can also be noticed that the intrinsic coercivity of the magnet made from the as-cast alloy is again higher than that of the magnet made from the homogenized alloy and the latter exhibits a squarer loop with enhanced values of the remanence. Recent studies on Pr-Fe-B sintered magnets (Martinek, Kohler and Kronmuller 1991), have shown that an improved grain alignment leads to a reduction of coercivity due to an increase of internal demagnetizing fields, which

is consistent with the present observations. The same behaviour has also been reported for the Nd-Fe-B sintered magnets (Martinek and Kronmuller 1990). Full density has been achieved for both magnets with this milling time (see Table 11.2.1).

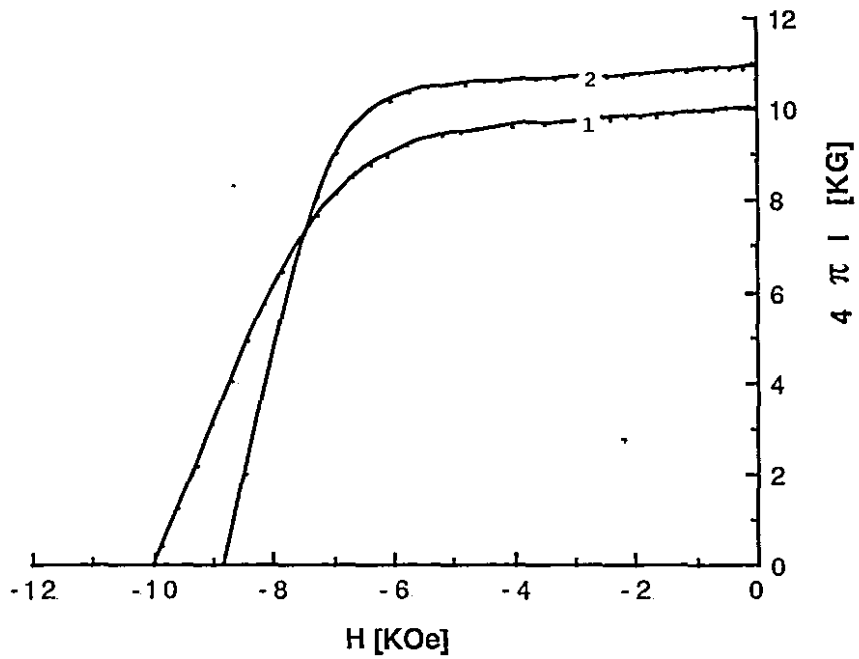

Fig.11.2.3. Demagnetization curves for $Pr_{20.5}Fe_{73.8}B_{3.7}Cu_2$ magnets produced using the alloy milled for 4 hours. As-cast : 1, Homogenized :2.

Figures 11.2.4 and 5 show the typical microstructures of the magnets prepared from the as-cast and homogenized alloys milled for 4 hours. The uniform distribution of the Pr-rich material can be seen in both magnets. The magnet prepared from the homogenized alloy exhibits a slightly larger grain size, which could be another contributory factor to the decrease in coercivity for the magnets prepared from the homogenized alloy.

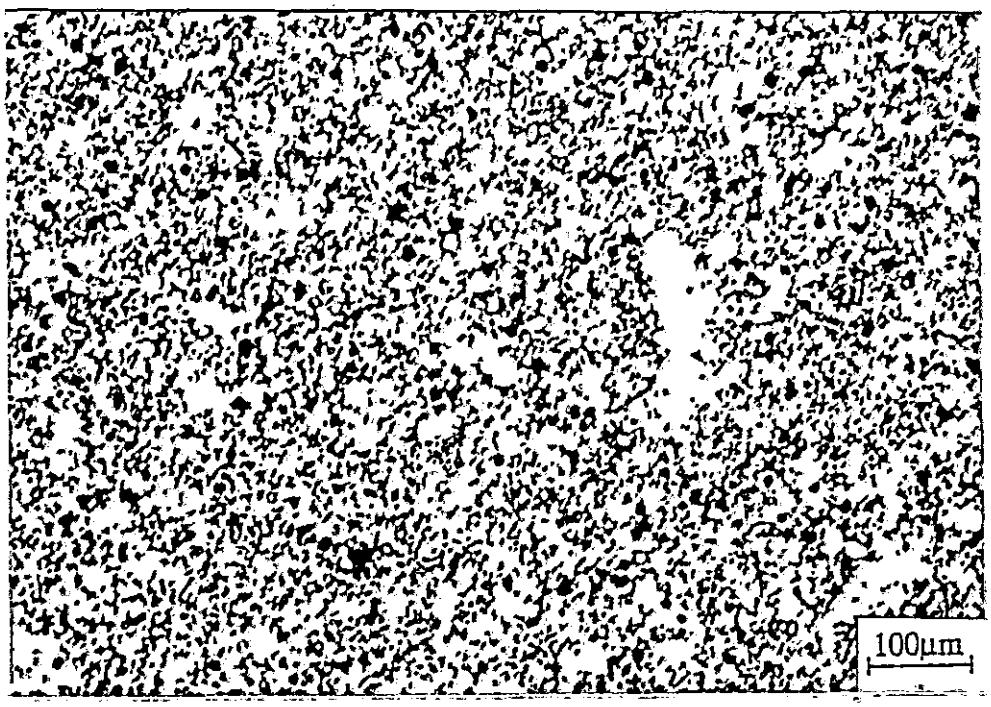

Fig.11.2.4. Optical micrograph showing the microstructure of the magnet prepared from as-cast $Pr_{20.5}Fe_{73.8}B_{3.7}Cu_2$ alloy milled for 4 hours.

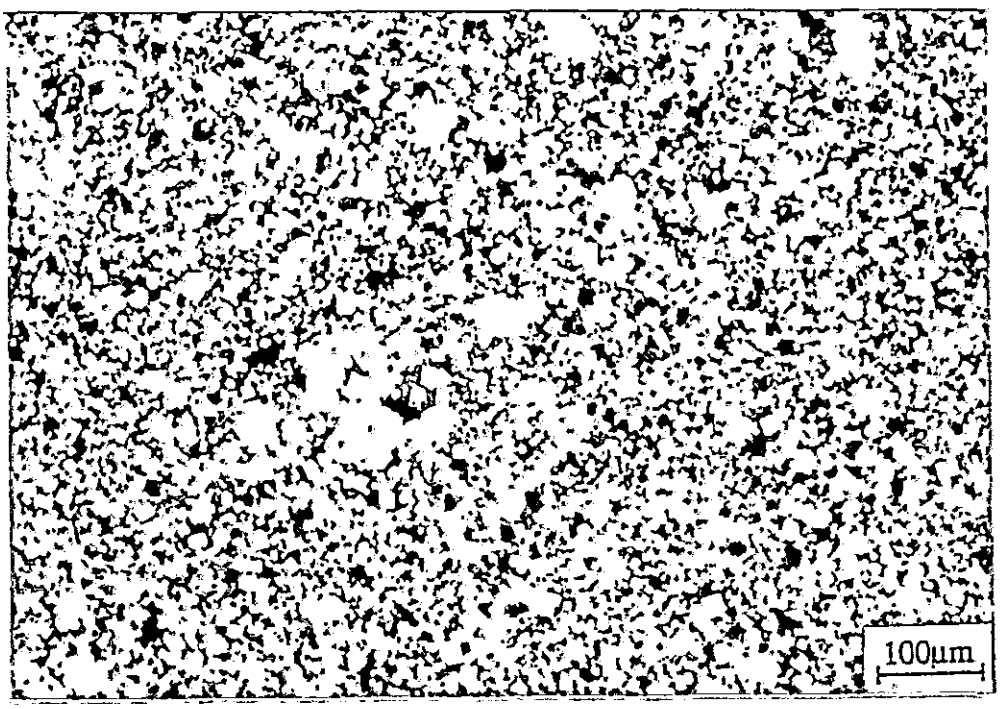

Fig.11.2.5. Optical micrograph showing the microstructure of the magnet prepared from homogenized $Pr_{20.5}Fe_{73.8}B_{3.7}Cu_2$ alloy milled for 4 hours.

The demagnetization curves for magnets produced using the as-cast and homogenized alloy ball milled for 9 hours are shown in Figure 11.2.6. High coercivity was achieved with this milling time after the post sintering heat treatment for the magnets prepared from both the as-cast and homogenized alloy, which is consistent with the results of chapter 9.

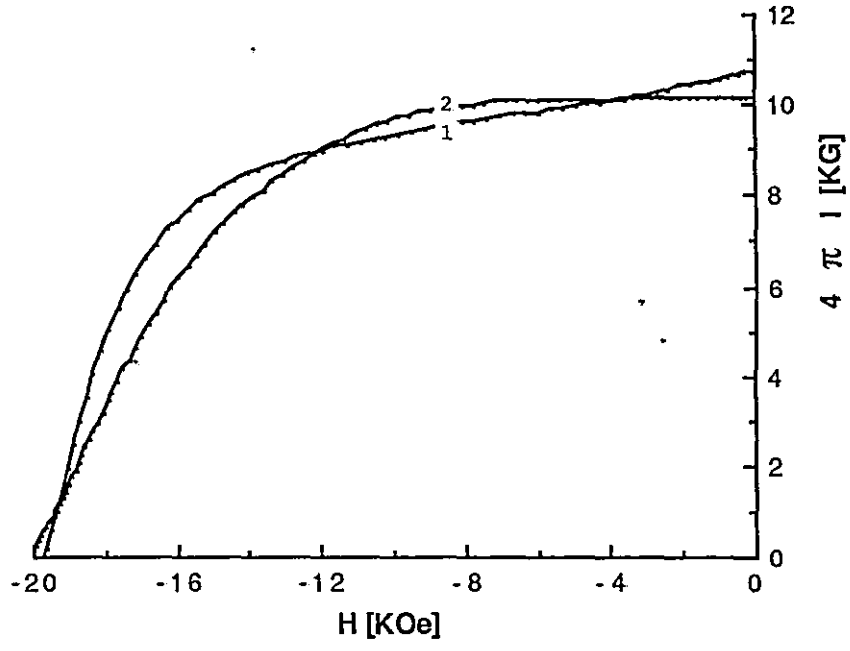

Fig.11.2.6. Demagnetization curves for $Pr_{20.5}Fe_{73.8}B_{3.7}Cu_2$ H D magnets prepared using alloys milled for 9 hours. As-cast : 1, Homogenized :2.

The homogenization heat treatment improves the squareness factor, which enhances the energy product but the remanence and density are slightly reduced. The two curves are much closer to each other than in the previous case. This behaviour indicates that full magnetic properties are obtained in both types of magnets with

this milling time. It has been shown (McGuiness 1989) for $Nd_{16}Fe_{76}B_8$ HD magnets that full magnetic properties are achieved using milling times of 18~24 hours (roller ball milling). Much shorter milling times (9hours) are required for the $Pr_{20.5}Fe_{73.8}B_{3.7}Cu_2$ alloy and this can be attributed to the greater amount of rare earth rich material in this alloy and to the higher anisotropy field of $Pr_2Fe_{14}B$ (Hirosawa et al. 1986).

Table 11.2.2 Percentage variation in the magnetic properties of magnets prepared from as-cast and homogenized alloy. (Percentage variation equation : $\Delta x(\%)=[(x^*/x)-1]X100$, where x^* is the value for the homogenized material. A positive value of Δx corresponds to an increase in the magnetic property with the homogenization heat treatment, and negative corresponds to a decrease)

Percentage Variation	Milling time		
	Crushed	4 h	9 h
ΔBH_{max} (%)	124.5	21.6	2.0
ΔB_r (%)	59.2	9.0	-5.6
$\Delta {}_iH_c$ (%)	-16.9	-10.8	2.5
Δ SF (%)	10.0	21.7	51.3

The above observations are summarised in the percentage change in the magnetic properties achieved by the homogenization heat treatment given in table 11.2.2. The largest influence of the initial state of the ingot material is observed for the magnets prepared using the alloy in the crushed state, where a very appreciable increase in energy product and remanence occurred

with homogenization. However, this influence became less significant with progressive milling time and the percentage change in energy product, remanence and intrisic coercivity becomes very small around 9 hours of milling time. Thus, the present observations on the alloy $Pr_{20.5}Fe_{73.8}B_{3.7}Cu_2$ indicate that a rehomogenization of the initial cast material occurs as a result of the progressive milling and subsequent sintering and annealing treatment. This can be ascribed to the progressively finer particle size of the green compacts which then results in more rapid diffusion during liquid phase sintering and subsequent post sintering heat treatment. This results in the progressive diminution in the influence of the initial cast structure and phase distribution on the magnetic properties of the sintered magnets.

To summarize: The as-cast ingot microstructure of the alloy $Pr_{20.5}Fe_{73.8}B_{3.7}Cu_2$ has been modified by an homogenization heat treatment at 1000°C for 24 hours. For particular processing conditions, sintered magnets prepared from the homogenized alloy using the hydrogen decrepitation (HD) process exhibit superior remanence and energy product to those prepared from the as-cast ingot. The squareness factor has also been improved considerably in the magnets prepared from the homogenized alloys. It was also shown that the influence of the initial microstructure on the intrinsic coercivity of Pr-Fe-B-Cu HD sintered permanent magnets diminishes rapidly with increasing milling time and is a minimum when the coercivity reaches the maximum value of ~20 kOe.

11.3 The effect of HD material desorption on the magnetic properties of $Pr_{16}Fe_{76}B_8$ HD sintered magnets

The effect of milling time and annealing (post sintering heat treatment) at 1000°C for 24 hours are shown in Fig.11.3.1. The $Pr_{16}Fe_{76}B_8$ HD magnet exhibits a substantial increase in iHc in the powder milled for 18 hours. The intrinsic coercivity reaches around 17.5 kOe on annealing. The demagnetisation curve for this annealed $Pr_{16}Fe_{76}B_8$ HD magnet is shown in fig. 11.3.2 (curve 1). The remanence and energy product are improved as the alloy is milled for longer time with no significant change on annealing.

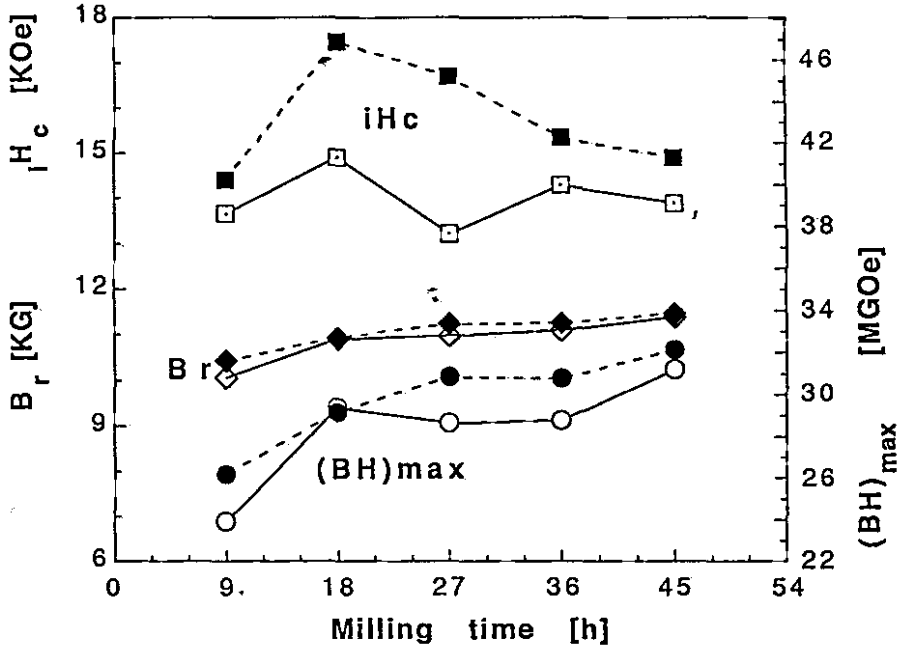

Fig. 11.3.1 Variation of (BH)max (o) and iHc (▣) and Br (◊) with the milling time for sintered (1060°C, 1 hour) and slow cooled magnets of $Pr_{16}Fe_{76}B_8$ alloy (Black/dashed : annealed 1000°C, 24 hours, slow cooled : post sintering heat treatment).

The effect of complete desorption (at 600 °C for 5 hours) of the HD alloy prior to magnetic processing was to increase the remanence and decrease the intrinsic coercivity. The demagnetisation curve of an annealed magnet prepared with a desorbed HD alloy milled for 18 hours is shown in fig. 11.3.2 (curve 2). In this case an energy product of 36 MGOe has been reached. The maximum value for annealed $Pr_{16}Fe_{76}B_8$ magnets prepared using HD alloy was for the 45 hours of milling time (BHmax=32.1 MGOe, Br=11.5 kG, iHc=14.9 kOe). These results also show that the alloy state has a dramatic influence in the magnetic properties of $Pr_{16}Fe_{76}B_8$ sintered magnets.

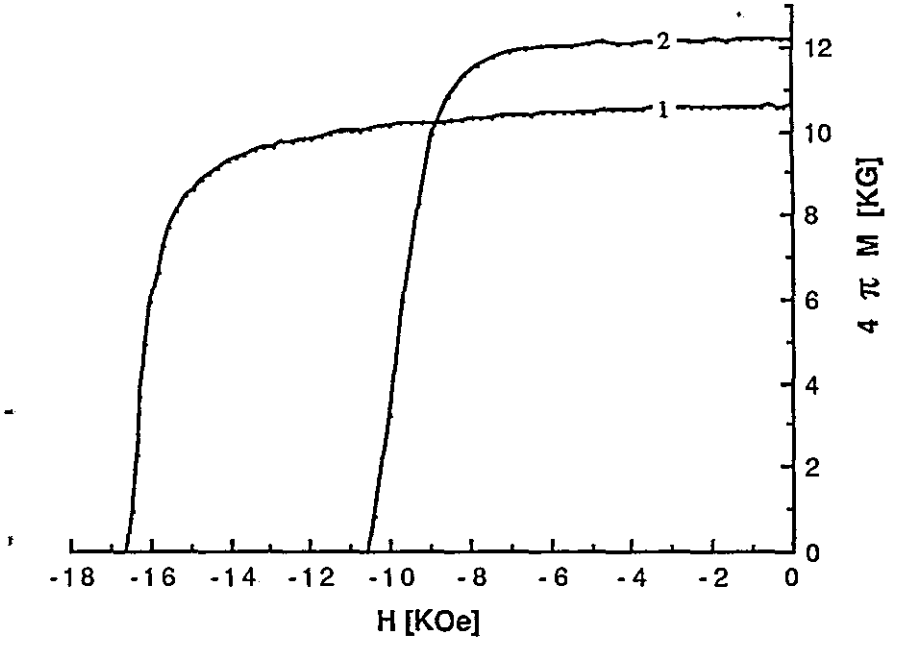

Fig.11.3.2. Demagnetization curves for annealed (post sintering heat treatment,1000°C for 24 hours) $Pr_{16}Fe_{76}B_8$ magnets produced using the alloy milled for 18 hours. HD alloy : 1, desorbed alloy at 600 °C for 5 hours : 2.

11.4 The effect of ingot VFZ on the magnetic properties of $Nd_{16}Fe_{76}B_8$ HD sintered magnets

The effects of milling time and annealing at 1000°C for 24 hours (post sintering heat treatment) are shown in Fig.11.4.1. There is an overall decrease in the magnetic properties of the $Nd_{16}Fe_{76}B_8$ HD magnets with this heat treatment. The best magnetic properties are achieved without annealing and with 18 hours of milling time.

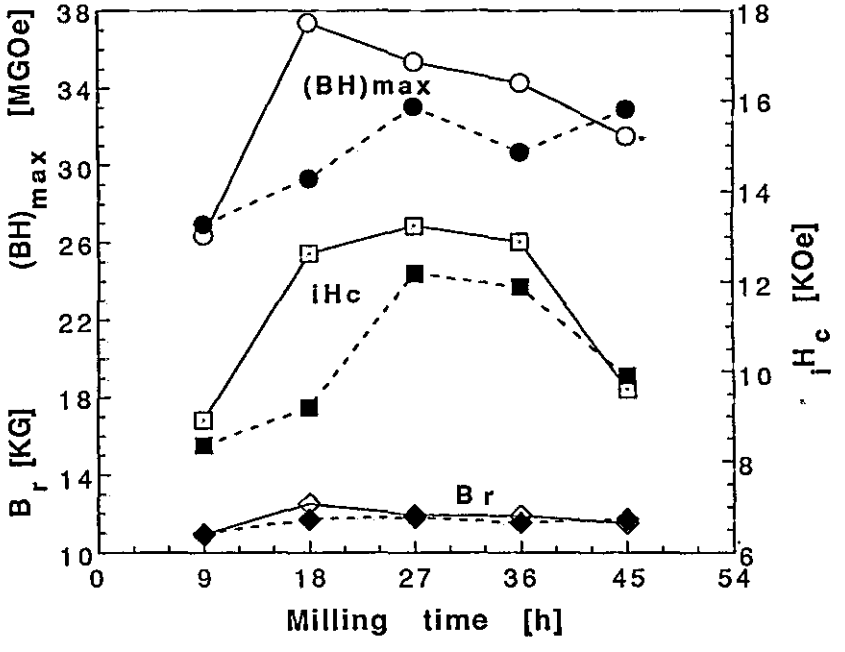

Fig. 11.4.1 Variation of (BH)max (o) and iHc (⊡) and Br (◊) with the milling time for sintered and slow cooled magnets of $Nd_{16}Fe_{76}B_8$ alloy (Black/dashed : annealed 1000°C, 24 hours, slow cooled).

Figure 11.4.2 shows the demagnetization curves of $Nd_{16}Fe_{76}B_8$ HD sintered magnets prepared from the as-cast ingot (20x10x3cm mould) and VFZ materials (2.54 cm h^{-1}) and Fig.11.4.3 and 4 show

the respective microstructures of the start materials. Somewhat inferior magnetic properties are obtained in the case of the VFZ material which could be due to the change in the amount and distribution of the Nd-rich material. The shape of the curve (squareness factor) seems to be the most affected. The X-ray analysis (EDX) in the VFZ alloy confirmed that the Nd-rich phase is concentrated in large regions. This is clearly seen in the X-ray spectra in fig.11.4.4 A and B. Taylor and Ward (1989) have reported similar behaviour in $Nd_{15}Fe_{77}B_8$ magnets by changing the cooling rate of the ingots and consequently the grain size.

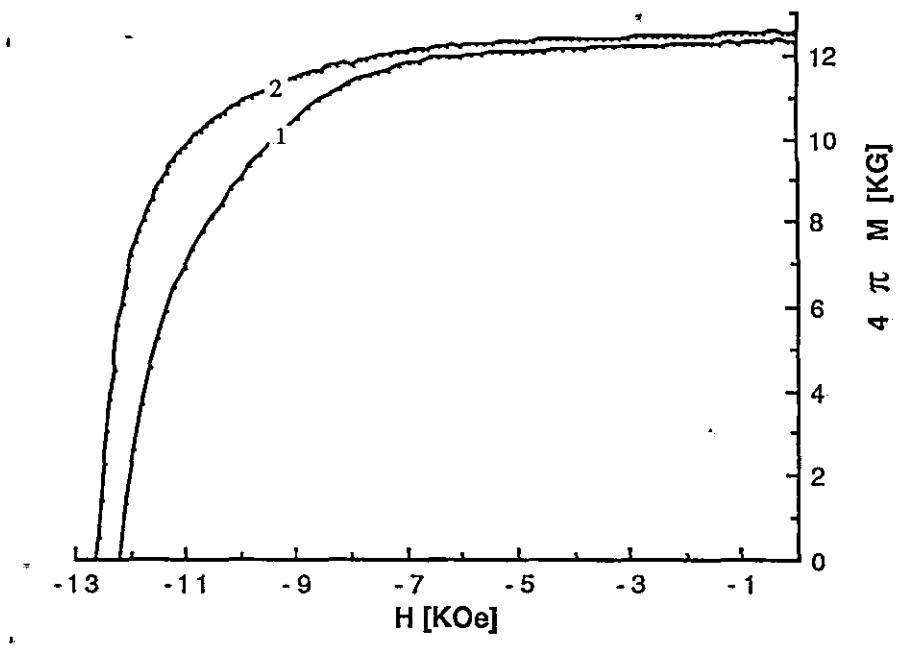

Fig.11.4.2 Demagnetization curves for $Nd_{16}Fe_{76}B_8$ HD sintered magnets prepared from as-cast alloy (2) and VFZ material (1) milled for 18 hours.

a)

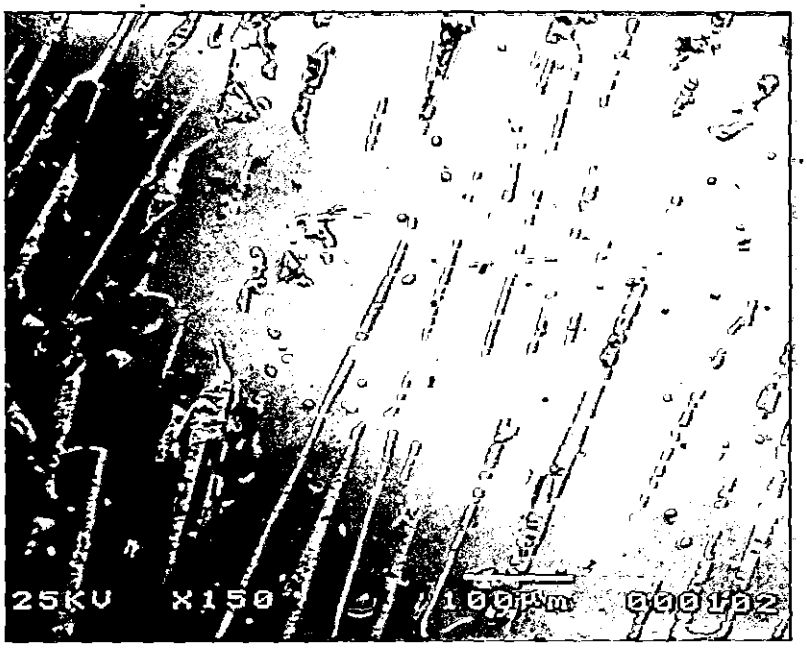

b)

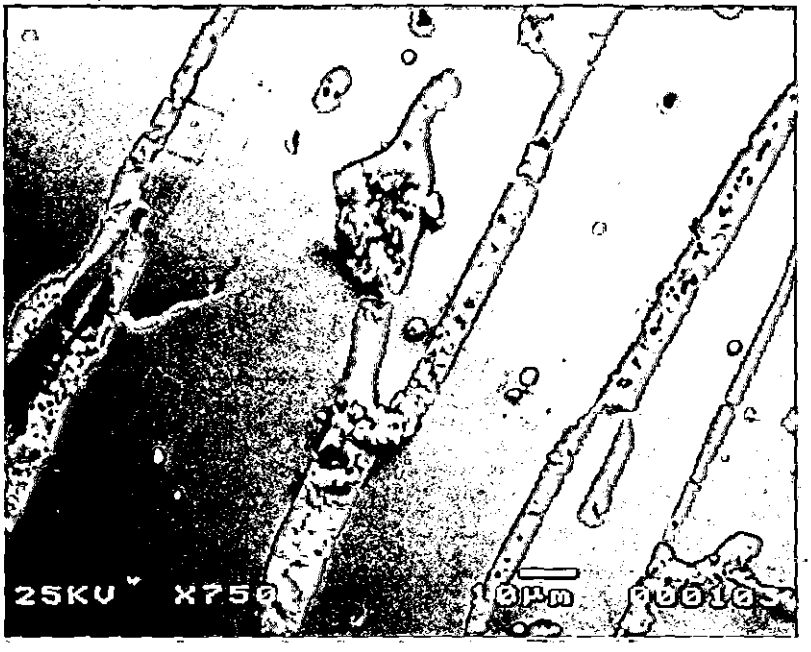

Fig.11.4.3 Microstructure of the as-cast ingot of the $Nd_{16}Fe_{76}B_8$ alloy: (a) general view and (b) details.

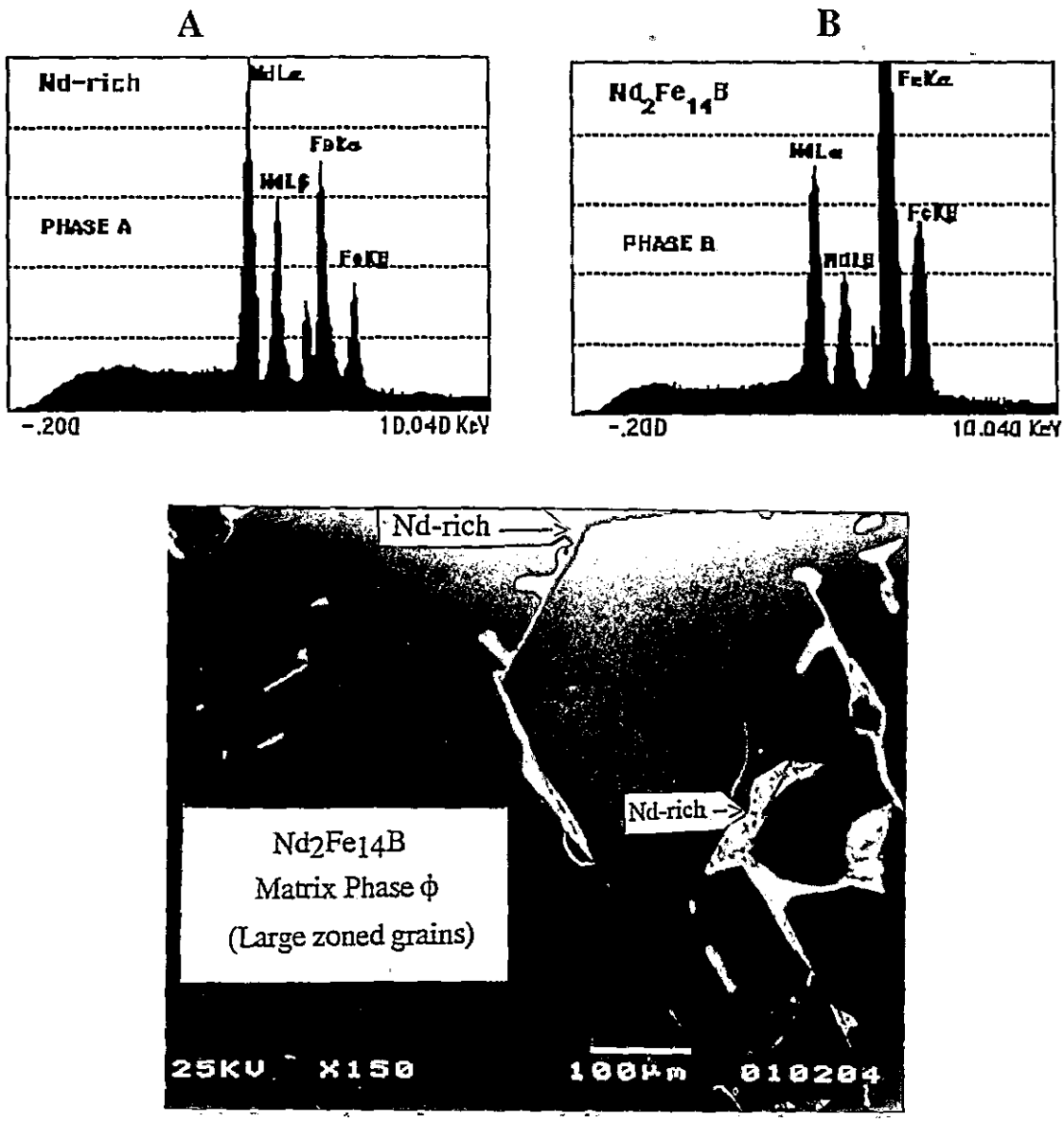

Fig.11.4.4 Microstructure of the VFZ $Nd_{16}Fe_{76}B_8$ alloy and X-ray spectra.

Lemaire et al (1990) characterized the inhomogeneities of macrostructure of different parts from one ingot and reported that, although the milling step could have an homogenization effect, such differences could affect the final magnetic properties of the sintered magnet. Fig.11.4.2 confirms that these differences can have some effect on the magnetic properties of sintered magnets.

The magnetic domain pattern in the $Nd_{16}Fe_{76}B_8$ alloy, shown in fig. 11.4.5, demonstrated that the columnar grains grow with their major axis predominantly in the basal plane rather than along the c-axis, in the same way as the Pr-Fe-B alloys.

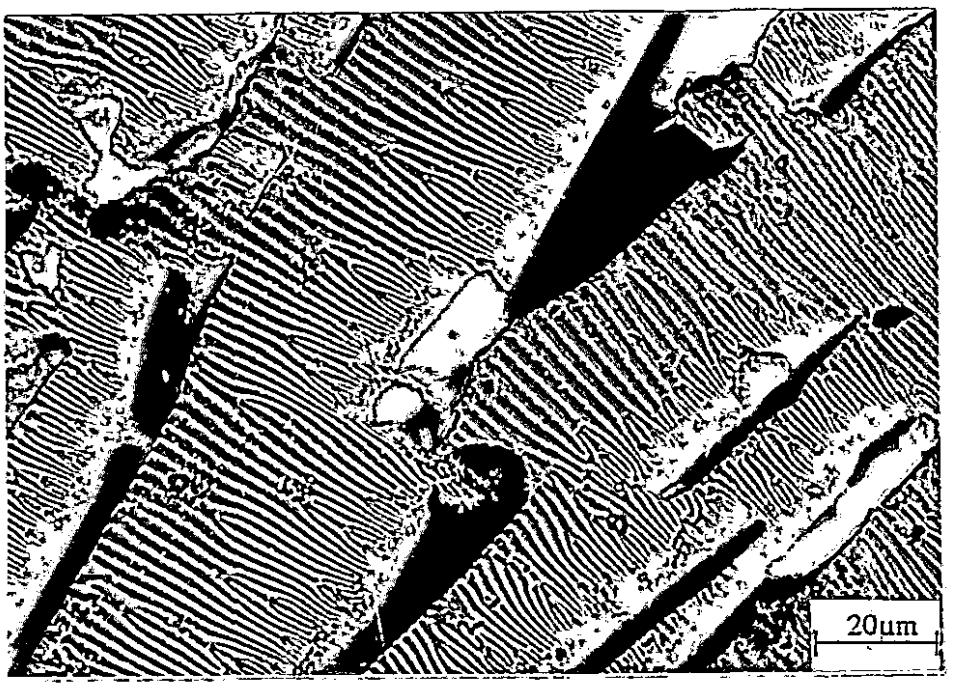

Fig.11.4.5 Microstructure of the VFZ $Nd_{16}Fe_{76}B_8$ alloy (ferrofluid).

CHAPTER TWELVE

CONCLUSIONS

12.1 Cast and VFZ magnets

1. The Pr-Fe-B-Cu alloy in the cast condition exhibits some coercivity which is significantly enhanced by annealing at 1000°C for 24 hours and slow cooling. The annealing effect was attributed to a combination of the enhancing of the magnetic isolation, the elimination of free iron and the smoothing of the grain boundaries.

2. Cast permanent magnets based on $Pr_{20.5}Fe_{73.8}B_{3.7}Cu_2$ exhibit higher magnetic properties than those of cast $Pr_{17}Fe_{76.5}B_5Cu_{1.5}$ magnets. This was attributed to the smaller particle size and better magnetic isolation in the former.

3. Large and small chill moulds have been employed and the Br and $(BH)_{max}$ can be increased substantially by casting the alloy in very small chill moulds (and subsequent annealing). The better magnetic properties obtained in the magnets which were cast in very small moulds was found to be due to the better grain alignment in these moulds.

4. VFZ growth rates up to 38 cm/h have not been sufficient to reproduce the as-cast ingot microstructure of $Pr_{20.5}Fe_{73.8}B_{3.7}Cu_2$ alloy. Cast magnets prepared in a very small chill mould showed

the best magnetic properties, with $(BH)_{max}$=12.3 MGOe, Br=7.2 kG and iHc=7.5 kOe.

5. Domain patterns showed that the Pr-Fe-B columnar grains grow with their major axis predominantly in the basal plane rather than along the c-axis.

12.2 HD Sintered permanent magnets

1. The intrinsic coercivity of Pr-Fe-B and Pr-Fe-B-Cu HD sintered permanent magnets can be increased substantially by annealing.

2. HD sintered permanent magnets based on $Pr_{20.5}Fe_{73.8}B_{3.7}Cu_2$ when annealed exhibit a iHc peak at lower milling times than $Pr_{16.9}Fe_{79.1}B_4$ magnets. This can be attributed to the grain refinement obtained with Cu-additions and the higher proportion of grain boundary material. $Pr_{17}Fe_{76.5}B_5Cu_{1.5}$ HD sintered permanent magnets showed higher energy products.

3. HD Pr-Fe-B-Cu sintered permanent magnets exhibit higher iHc and lower Br than hot pressed magnets. The higher intrinsic coercivity can be due to the smaller grain size of the sintered magnets and the lower remanence can be attributed to the higher Pr contents in the sintered magnets, bearing in mind that some Pr is squeezed out during the hot pressing process.

4. Isostatically pressed sintered magnets of Pr-Fe-B-Cu alloys produced by the HD process at 10 bar of H_2 are shown to exhibit uniaxial anisotropy. It seems that higher hydrogen pressures are necessary to change the alignment.

5. The microstructures of both as-sintered and annealed magnets have been investigated by scanning electron microscopy (SEM) and transmission electron microscopy (TEM) in an attempt to reveal the reason for the increase in iHc . Backscattered electron images on SEM and energy dispersive X-ray analysis (EDX) indicated the presence of Pr_2Fe_{17} (Fe : Pr (at.%) $\sim$ 8.2) in both magnets. The presence of this phase has been confirmed by subsequent thermomagnetic analysis and TEM investigations. The amount of this phase diminished after the heat treatment. A $Pr_{34}Fe_{62}Cu_4$ phase has been observed by TEM. The increase in the coercivity on annealing has been attributed to the improved magnetic isolation of the $Pr_2Fe_{14}B$ grains and to the diminution of the amount of Pr_2Fe_{17} phase obtained with the heat treatment.

6. $Pr_{20.5}Fe_{73.8}B_{3.7}Cu_2$ HD sintered magnets prepared from powder of as-cast ingot and homogenized alloy obtained after low milling times exhibit different magnetic properties but their magnetic properties converge when prepared from powder obtained after milling for nine hours. This behaviour can be attributed to the rehomogenization of the cast structure after milling for the extended period and then sintering.

7. Nd-based HD magnets do not respond to the annealing at 1000°C for 24 hours in the same manner as the PrFeB(Cu) HD magnets.

8. Sintered magnets prepared using the hydrogen decrepitation (HD) process from the large grained Nd-Fe-B zoned alloys exhibit inferior squareness factors to those prepared from the as-cast ingot.

9. Sintered magnets prepared using the hydrogen decrepitation (HD) process from desorbed $Pr_{16}Fe_{76}B_8$ HD alloy exhibit superior Br and inferior iHc to those prepared from the HD material.

10. The magnetic properties of HD sintered magnets of Pr/Nd-Fe-B-(Cu) respond differently to milling time and annealing as is shown in table 12.2.1.

Table 12.2.1 Comparison of various HD sintered permanent magnets produced in the present work (post sintering heat treatment: 1000°C for 24 hours, except *).

ALLOY TYPE	Milling time [hours]	Br KG	iHc KOe	BH MGO	S.F
$Pr_{20.5}Fe_{73.8}B_{3.7}Cu_2$	09	10.7	19.8	24.9	0.4
$Pr_{17}Fe_{76.5}B_5Cu_{1.5}$	18	11.1	12.4	29.0	0.6
$Pr_{16.9}Fe_{79.1}B_4$	27	10.6	20.3	25.3	0.5
$Pr_{16}Fe_{76}B_8$	18	10.9	17.5	29.2	0.8
$Pr_{16}Fe_{76}B_8$ (desorbed)	18	12.2	10.6	36.0	0.8
$Pr_{16}Fe_{76}B_8$	45	11.5	14.9	32.1	0.9
$Nd_{20.5}Fe_{73.8}B_{3.7}Cu_2$	36	11.5	7.3	30.7	0.8
$Nd_{17}Fe_{76.5}B_5Cu_{1.5}$	18	10.6	10.0	24.5	0.6
$Nd_{16.9}Fe_{79.1}B_4$	27	9.1	4.8	11.5	0.2
$Nd_{16}Fe_{76}B_8$ *	18	12.5	12.6	37.4	0.75

(Average error: Br : ± 0.1, iHc : ± 0.5, BHmax : ± 0.9)

12.3 Sugestions for future work

1. Mould casting in a magnetic field Pr-Fe-B-Cu alloys with Co substitutions in which the Curie temperature is higher than the alloys without substitution. The influence of the magnetic field might be to enhance and align the forming crystals with the c-axis parallel to the field. The Curie temperature of the $Pr_2Fe_{(14-x)}Co_xB$ system when x= 3 is about 474°C and for x=5, Tc= 558°C. The maximum is when x=14 and Tc is 713°C.

2. Annealing the Pr-Fe-B-Cu alloy in a magnetic field could also produce some effect, such as grain growth in the c-axis parallel to the magnetic field, and consequently some improvements in the magnetic properties of the cast magnet.

3. Sintering the HD magnets under uniaxial mechanical pressure could improve the alignment of the particles and improve the remanence.

4. A study of Nd substitutions in the Pr-Fe-B-Cu system for HD magnets also seems appropriate as far as costs are concerned.

REFERENCES

Abell J.S., and Harris I.R., IEEE Trans. Magn. Mag 24 (1988) 1620

Albright D. L., Conard G. P. and Kraft R. W., J.Appl. Phys. 38 (1967) 7

Bozorth R. M., Ferromagnetism, New York (1959), D. Van Nostrand Co.

Braun J H, Pellin R A., J.Electrochem. Soc., 108 (10) (1961) 969

Cahn J. W., and Hilliard J. E., J. Chem. Phys. 28 (1958) 258

Cahn J. W., and Hilliard J. E., J. Chem. Phys. 31 (1959) 688

Chalmers B., Principles of Solidification, John Wiley & Sons, Inc. (1964)

Chalmers B., Solidification, American Society for Metals, Metals Park, Ohio(1969)

Chang.W.C., Paik C.R., Nakamura H., Takahasi N., Sugimoto S., Okada M. and Homma M., IEEE Trans. Magn. MAG 26 (5) (1990) 2604

Chen Z., Shi Z., Wang L. and Fu H., J. Alloys and Compounds, 179 (1992) 61

Christodoulou C. N., and Schlup, J., J. Appl. Phys. 61 (8) (1987) 3760

Cole G. S.,American Society for Metals, Metals Park, Ohio(1969)

Colin M. and Racek R., Third Eur.Conf.Hard Mag.Mat.,Amsterdan, Sept. 17-19, (1974) 145

Colling D. A., and Kossowsky R. , Metallurgical Transations 2 (1971) 1523

Cullen T. J., J. Appl. Phys.42 (4) (1971)

Cullity B.D.,Introduction to Magnetic Materials, Addison-Wesley Pub. Co. (1972)

Draper P. H., Paper no XI-3 at the Fourth International Workshop on Rare Earth-Cobalt Permanent Magnets and their Applications, Hakone National Park, Japan, May 22-24 (1979)

Durst K. D., and Kronmuller H., J. Magn. Magn. Mat. 68 (1987) 63

Durand-Charre M., Bronner C., and Lagarde J., IEEE Trans. Magn. MAG 14 (5) (1978) 797

Faria R. N., Abell J. S., and Harris I. R., (1991) paper presented in the 5th Joint MMM Intermag Conference, Pittsburgh, Pennsylvania, June 18-21, 1991, J. Appl. Phys., 70 (10) (1991) 6471

Faria R. N., Abell J. S., and Harris I. R., J. Alloys and Compounds, 177 (1991a) 311

Faria R. N., Abell J. S., and Harris I. R., J. Alloys and Compounds, 185 (1992) 81

Fisher H.J. and Walter J.L. , Trans of the Metal Soc of Aime 224 (1962) 1271

Flemings M.C., Solidification Processing , MacGraw-Hill (1974)

Fort D. and Jones D.W., J. Less-Common Metals 81 (1981) 292

Fort D., J. Crystal Growth 94 (1989) 85

Gilbert Y.Chin, Green M. L., Nesbitt E. A., Sherwood R. C., and Wernick J. H., IEEE Trans. Magn. MAG 8, (1), (1972) 29

Givord D., Tenaud P., and Viadieu T., Concerted European Action on Magnets. Ed. Mitchell, Coey, Givord, Harris and Hanitsch. Elsevier Appl. Science (1989).381

Givord D., Tenaud P., and Viadieu T., IEEE Trans. Mag. Vol. 24 (2) (1988) 1921

Glardon R.and Kurz W , Paper No. VII at the 3th International Workshop on Rare-Earth Magnets and Their Applications, California, San Diego, (1978) 504

Glardon R., and Kurz W , J. Crystal Growth 51 (1981) 283

Gould J. E., Cobalt, 23 (1964) 82

Hadjipanayis G. C., Zhang M., and Chuan G., Appl. Phys. Lett. 54,(18), (1989) 1812

Harris I. R., J. Less-Common Metals 131 (1987) 245

Harris I.R., McGuinness.P.J., Jones D.G.R., and Abell J.S., Scripta Physica T19 (1987) 435

Harris I.R., McGuinness.P.J, Paper No. W1.3 at the 11th International Workshop on Rare-Earth Magnets and Their Applications, Pittsburgh, PA, 21-24 October 1990 p.29

Heng-zhi Fu, Xin-cai Liu, Zheng-xing Shi, Le-yi Wang, Wei Tang, Chang-gui Li and Hou-ding Song, IEEE Trans Magn MAG 25 (5) (1989) 3797

Higuchi A. and Miyamoto T., IEEE Trans Magn MAG 6 (2) (1970) 218

Hirosawa S., Matsuura Y., Yamamoto H., Fujimura S., and Sagawa M., J. Appl. Phys. 59 (3) (1986) 873

Hirosawa S., and Tsubokawa Y., J. Mag. Mag. Mat. 84 (1990) 309

Hoffmann A. and Stablein H., Tech. Mitt. Krupp, Forsch. Ber. 24 (1966) 113

Hoselitz K., and McCaig M., Proc. Phys. Soc. Lond. B 62 (1949) 163

Jacobs J.S. and Bean C.P., Phys. Rev. 102 (1956) 1413

Jiang S.Y., Chen H. Y., Cheng S. F., Boltich E. B., Sankar S. G., Laughlin D. E., and Wallace W. E., J. Appl. Phys. 64 (10) (1988) 5510

Jiang S.Y., Yan J.X., Li F.S. and Yang C.L., Paper No. 18P0103 at the 10th International Workshop on Rare-Earth Magnets and Their Applications, Kyoto, Japan, 16-19 May, (1989) 409

Jiang S.Y., Yan J.X., Ma B.M., Sankar S.G. and Wallace W.E., Paper No. 18P0202 at the 10th International Workshop on- Rare-Earth Magnets and Their Applications, Kyoto, Japan, 16-19 May, (1989) 457

Jiles D., Introduction to Magnetism and Magnetic Materials, Chapman and Hall, London , New York, Tokyo, Melbourne , Madras(1991)

Jinghua T., Yiying H. and Jingkui L., Scientia Sinica (Series A) V-XXX (6) (1987) 607

Kajitani T., Nagayama K. and Umeda T., Proceedings of the 12th Int. Workshop on RE Magnets and their Applications Canberra, July 1992, 574

Keller W. and Muhlbauer A., Floating-Zone Silicon , Marcel Dekker,Inc, New York and Basel (1981) 136

Kianvash A.and Harris I. R., J. Alloys and Compounds, 178 (1992) 325

Kimura Y. and Kamino K., Trans. JIM 11 (1970) 132

Kwon H.W., Bowen P., Harris I.R., Presented in the 5th Joint MMM Intermag Conference, Pittsburgh, Pennsylvania, June 18-21, 1991, J. Appl. Phys., 70 (10) (1991) 6357

Kwon H.W., Bowen P., Harris I.R., Proceedings of the 12th Int. Workshop on RE Magnets and their Applications Canberra, July 1992, 705

Kwon H.W., Bowen P., Harris I.R., J. Alloys and Compounds, 182 (1992b) 233

Kurz W. and Fisher D. J., Trans Tech Publications Ltd, Switzerland, 1989

Lemaire H., Tenaud P., Vial F. and Labulle B., J. Magn. Magn. Mat. 83 (1990) 234

Lin C.H., Chen C.J., Wu C.D. and Chang W.C., IEEE Trans. Magn. MAG 26 (5) (1990) 2607

Livingston J. D., J. Appl. Phys., 41 (1) (1970)J

Luborsky F. E., J. Appl. Phys. Suppl. 32(1961) 171S

Ma B. M., and Bounds C. O., (1991) paper presented in the 5th Joint MMM Intermag Conference, Pittsburgh, Pennsylvania, June 18-21, 1991, J. Appl. Phys., 70 (10) (1991) 6471

Martinek G., Kohler D., and Kronmuller H., CEAM 2 Report , september(1991), unpublished work

Martinek G., and Kronmuller H.., J. Mag. Mag. Mater 86 (1990) 177

Makino N. and Kimura Y.,.J. Appl. Phys. V-36 (3) (1965) 1185

McCaig M., Permanent Magnets in Theory and Practice, (1st edition) Pentech Press, London (1977)

McGuiness P.J., and Harris I.R., J. Appl. Phys. 64 (10) (1988) 5308

McGuiness P.J., Devlin E.,.Harris I.R., Rozendaal E. and Ormerod J., J. Mater. Sci. 24 (1989) 2541

McGuiness P.J., PhD Thesis, University of Birmingham, (1989) 161

McLean M. , Directionally Solidified Materials for High Temperature Service, The Metals Society, J. W. Arrowsmith Ltd, Bristol (1983)

Mikelson A.E., and Karkin Ya.Kh , J.Crystal Growth 52 (1981) 524

Morando R., Biloni H., Cole G. S., and Bolling G. F., Metall. Trans. 1 (1970) 1407

Morros J., Bounds C. O, Maestro P. and Pere D., CEAM 2 Report , September(1991), unpublished work

Muller A.,and Wilhelm M., Z. Naturf. 22a (1967) 264

Neel L., Comptes Rendus Acad. Sci. (Paris) 224 (1947) 1550

Nesbit E. A., and Wernick J. H. , ,Rare-Earth Permanent Magnets, Academic Press , New York (1973)

Noh T. H., Jeung W. Y., and Kang I. K., J. Appl. Phys. 70 (10) (1991) 6591

Noothoven van Goor J.M. and Zijlstra H., J. Appl. Phys. V-30 (12) (1968) 5471

Notis M.R., Shah D. M. , Young S. P., and Graham C. D. IEEE Trans. Magn. MAG 15 (2) (1979) 957

Notis M.R., and Sahm D., Grahm C. D. , and Stanley R. T. , J. Appl. Phys. 49 (3) (1978) 2043

Ogilvy A.J.W., Gregan G.P., and Davies H.A., Proc. Nd Permanent Magnets Workshop, Mitchell, Ed. Brussels, Belgium, CEE, (1984) 93

Ormerod J., Proc. Nd Permanent Magnets Workshop, Mitchell, Ed. Brussels, Belgium, CEE, (1984) 69

Paik C. R., Nakamura H., Okada M., and Homma M. Paper No. 18P0226 at the 10th International Workshop on Rare-Earth Magnets and Their Applications, Kyoto, Japan, 16-19 May, (1989) 631

Parker R. J., and Studders R. J. Permanent Magnets and Their Applications, Wiley, New York, London (1962)

Pfann W. G. , Zone Melting, Wiley , New York , London (1958)

Pirich R.G., Metallurgical Transactions A - 17A (1986) 1149

Pirich R.G. and Larson D.J,Jr., J. Appl.Phys. 50 (3) (1979) 2425

Pourarian F., Huang M.Q. and Wallace W.E., J. Less-Common Metals 120 (1986) 63

Ray A. E., Proc. 7th Rare Earth Res. Conf. , Editor J. F. Nachmann , (1968) 473

Rotenberg L. R. K., Oliveira R. F., Rechenberg H. R., and Missil F. P., J. Appl. Phys. 57 (1) (1985) 4127

Sagawa M., Fujimura S., Togawa N., Yamamoto H., and Matsuura Y., J. Appl.Phys. 55 (6) (1984) 2088

Sagawa M., and Hirosawa S., Journal de Physique , C8 No.12 T49 (1988) 617

Sagawa M., and Hirosawa S., J. Mater. Res. 3 (1) (1988) 45

Sahm P.R., J.Crystal Growth 6 (1969) 101

Sahm P.R., J.Crystal Growth 8 (1971) 109

Sahm P.R. and Hofer F., Z.angew. Physik (1970) 95

Savitsky E. M., Torchinova R. S., and Turanov S. A., J. Crystal Growth 52 (1981) 519

Sergeyev V. and Larichkina R.Y., IEEE Trans. Magn. MAG 6 (2) (1970) 239

Shimoda T., Akioka K., Kobayashi O., and Yamagami T., J. Appl.Phys. 64 (10) (1988a) 5290

Shimoda T., Akioka K., Kobayashi O., and Yamagami T., Journal de .Physique, C8, N12, T 49 (1988b) 631

Shimoda T., High Energy Cast PrFeB Magnets, presented at The Global Business and Technical Outlook for NdFeB Magnets Markets, February 26-28 , (1989a)

Shimoda T., Akioka K., Kobayashi O. and Yamagami T., Paper No. 18P0101 at the 10th International Workshop on Rare-Earth Magnets and Their Applications, Kyoto, Japan, 16-19 May, (1989b) 389

Shimoda T., Akioka K., Kobayashi O. and Yamagami T., IEEE Trans. Magn. MAG 25 (5) (1989c) 4099

Shimoda T., Akioka K., Kobayashi O. and Yamagami T., Paper No. 18P0101 at the 10th International Workshop on Rare-Earth Magnets and Their Applications, Kyoto, Japan, 16-19 May, 1989c, p. 389

Shimoda T., Akioka K., Kobayashi O. and Yamagami T., and Arai A., Paper No. W1.2 at the 11th International Workshop on Rare-Earth Magnets and Their Applications, Pittsburgh, PA, 21-24 October 1990 p.17

Sinnema S. et al, J.Crystal Growth 85 (1987) 248

Stoner E. C., and Wohlfarth E. P. , Phil. Trans. Roy. Soc. (Lond.) A240 (1948) 599

Strnat K., Hoffer G., and Ray A. E., IEEE Trans. Magn. MAG-2, (1966) 489

Subramanian P. R., and Laughlin D. E., Bulletin of Alloy Phase Diagrams, Vol. 9 No. 3a (1988) 424

Swets D.E., J.Crystal Growth 75 (1986) 277

Takahashi N., Nakamura H., Paik C, R., Sugimoto S., Okada M., Homma M., Materials Trans. JIM, Vol. 32, No. 1 (1991) 90

Verhoeven J.D. et al , Metallurgical Transactions A - 21A (1990) 2249

Ward M., and Taylor J.S., CEAM Report , I.V.Mitchell, J.M.D. Coey, D. Givord, I. R. Harris and R. Hanitsch, Elsevier Science Publishers LTD, (1989)

Weizhong T., Shouzeng Z., and Bing H., J. Mag. Mag. Mater 94 (1991) 67

Winegard W. C., Solidification of Metals, Inst. of Metals 29 (Lond.) (1964)

Wojciechowski S., and Chalmers B., Trans. Metall. Soc. AIME 242(1968) 690

Yin X. J., PhD Thesis , University of Birmingham, (1992)

Zijlstra H., Ferromagnetic Materials, Vol. III, North Holland, Amsterdam (1982). E.P. Wohlfarth. Ed.

Zhou S.Z., Zhou Y.X , and Graham Jr C.D., J. Appl. Phys. 63 (8) (1988) 3534

PUBLICATIONS

1) **High Coercivity Sintered Pr-Fe-B-Cu Magnets Using the Hydrogen Decrepitation Process**, R. N. Faria, J. S. Abell and I. R. Harris, *Journal of Alloys and Compounds*, 177 (1991) 311

2) **Controlled Solidification and Magnetic Properties of Pr-Fe-B-Cu and Nd-Fe-B Alloys**, R. N. Faria, J. S. Abell and I. R. Harris, *Journal of Applied Physics*, 70 (10) (1991) 6104, ("5th Joint MMM-Intermag Conference")

3) **The Effect of Ingot Heat Treatment on the Magnetic Properties of Pr-Fe-B-Cu Hydrogen Decrepitation Sintered Magnets** , R. N. Faria, J. S. Abell and I. R. Harris, *Journal of Alloys and Compounds*, 185 (1992) 81

4) **Developments in Cast and Hot Worked PrFeB Magnets**, H. W. Kwon, G. Mycock, R. N. Faria, P. Bowen and I. R. Harris, *Magnews - Newsletter*, (Summer - 1992) 5

5) **The Microstructural Characterization of Nd-Fe-B Alloys. I : Light Element Microanalysis**, X. J. Yin, M. G. Hall, I. P. Jones, R. N. Faria and I.R. Harris, *J. Magn. Magn. Mater*, To be published (Proofs stage)

6) **The Microstructure and Magnetic Properties of Some Cast and Annealed Pr-Fe-B-Cu Alloys**, G. J. Mycock, R. N. Faria and I. R. Harris, *Journal of Alloys and Compounds*, Accepted to be published

7) **Microstructural and Magnetic Studies of Pr-Fe-B-Cu HD Sintered Magnets**, R. N. Faria, X. J. Yin, J. S. Abell and I. R. Harris, *J. Magn. Magn. Mater*, To be published

8) **High Coercivity Pr-Fe-B-Cu Magnets Produced By Upset Forging of Cast Ingot**, P. V. P. Marcondes, R. N. Faria, P. Bowen and I. R. Harris, *Journal of Alloys and Compounds*, To be published

9) **Microstructural Studies on High Coercivity Pr-Fe-B-Cu Magnets Produced by Upset Forging of Cast Ingot**, P. V. P. Marcondes, R. N. Faria, P. Bowen and I. R. Harris, *Journal of Alloys and Compounds*, To be published

10) **Magnetic Properties of Pr-Fe-B Sintered Magnets Produced from Hydride Powder and from Partially and Totally Desorbed Hydride Powder**, R. N. Faria, A. J. Williams, J. S. Abell and I. R. Harris, *Journal of Alloys and Compounds*, To be published